PERFORMANCE OF PLATE ANCHORS

A Thesis

by

DHANVI VENGRE RAGHAVENDRA

Submitted to the Office of Graduate and Professional Studies of
Texas A&M University
in partial fulfillment of the requirements for the degree of

MASTER OF SCIENCE

Chair of Committee,	Charles Aubeny
Committee Members,	Marcelo Sanchez
	Jerome Schubert
Head of Department,	Robin Autenreith

December 2016

Major Subject: Civil Engineering

ABSTRACT

Suction Embedded Plate Anchors (SEPLA) are vertically loaded anchors which are installed by using a suction caisson to the required embedment depth. The cost effectiveness, ease of installation and the accuracy of the installation makes it an attractive choice for deep to ultra-deep waters. After installation, SEPLAs are tensioned by mooring lines which will cause the anchor to move from its initial vertical orientation to its final orientation perpendicular to the loading direction. The keying process results in the loss of embedment which reduces the holding capacity of the plate anchors. A plasticity model was created to predict the keying trajectory, tension capacity and the embedment loss for a plate anchor. The soil is assumed to be normally consolidated undrained clay that obeys associated flow rule. The interaction of the anchor with the surrounding soil, interaction of the anchor chain and the interaction of the anchor chain with the soil is also considered in the model to predict the keying trajectory of the anchor.

The results obtained from the model are compared to existing centrifuge tests and finite element models. The model was found to have very good agreement with the finite element data and it had reasonable agreement with the centrifuge test results. A parametric study was performed to better understand the behavior of the anchor during the keying process. The effect of anchor geometry, thickness of the anchor, eccentricity at the padeye, the pullout angle on the surface of the water, type of anchor line, soil strength and sensitivity on the behavior of the anchor were studied. The effects of these

parameters on the embedment loss, keying trajectory and capacity of the anchors have been calculated.

ACKNOWLEDGEMENTS

I would firstly like to thank my committee chair, Dr. Charles Aubeny, for his continual support and direction throughout the course of this research. He has always made himself available to answer numerous questions and explain several concepts in his extremely busy schedule. His guidance and teaching has allowed me to gain invaluable knowledge on slope stability, foundations and theories of plasticity.

I would like to thank my committee members Dr. Marcelo Sanchez and Dr. Jerome Schubert for their guidance and support. Dr. Sanchez's course offered me a good foundation on the theory of plasticity which played an important part in my thesis.

Lastly and probably most importantly, I would like to thank my parents who have always provided moral and emotional support throughout the course of this degree program. They have always me their highest priority, helped me and offered me advice whenever necessary.

TABLE OF CONTENTS

Page

LIST OF FIGURES

Page

LIST OF TABLES

Page

CHAPTER I

INTRODUCTION

1.1 General

The search for sustainable source of oil and gas has extended the offshore hydrocarbon fields to deep and ultra-deep waters which has resulted in remarkable progress in mooring systems and foundations of the offshore drilling units (MODUs)(Chi, 2010). Several types of MODUs are being used depending on the depth of the water: jack up rigs are used for very shallow waters, semi submersibles are used for mid water and deep waters and drill ships are used for ultra-deep waters.

The jack up unit is generally used for shallow water depths of about 400 ft. This unit provides a relatively stable platform at the drilling location. There are two types of jack up units, the Independent Leg type and the Mat type as shown in Figure 1.1 and Figure 1.2 respectively. The Independent Leg type jack up is preloaded to prevent the hull from completely jacking out of the water before its legs are driven into the bottom of the ocean. The preload sequence is not necessary for the mat type because of the low bearing pressure of the mat. Mat type jack ups are suitable for very soft soils as it prevents very high settlements. However, these can be used effectively only on even surfaces and can be damaged by objects on the sea beds. Spudcan footings are generally utilized to overcome this problem. Spudcans are inverted cones with a sloping top and are used to hold the legs in place as shown in Figure1.3. Spudcans can be used in hard and soft soils and on sloping beds.

Figure 1.1 Independent Leg Type Jackup Rig (Courtesy Maersk Group)

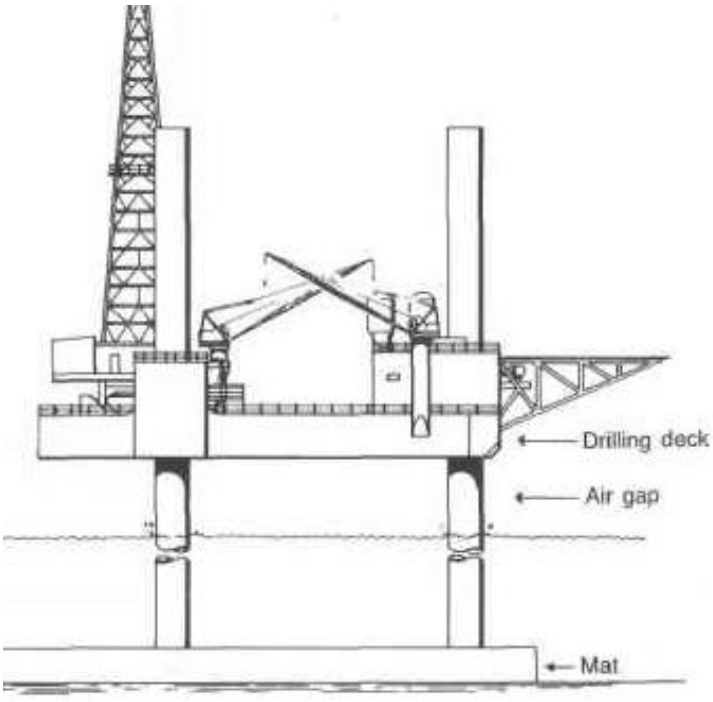

Figure 1.2 Mat Type Jackup rig (Courtesy Netwas Group)

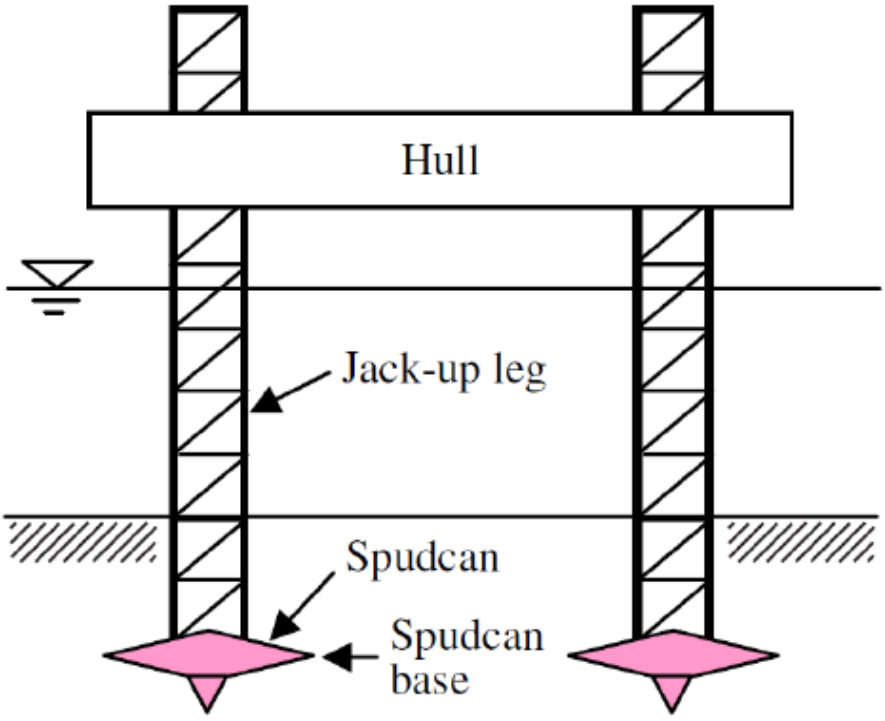

Figure 1.3 Spudcan Foundation for a Jackup Rig (Courtesy Lee and Randolph 2011)

Semi-submersibles can be used in water depths of less than 100 ft to several thousand feet. Semi-submersibles are supported by pontoon type columns that are submerged in water and are moored by anchors. Figure 1.4 shows a semi-submersible in the Gulf of Mexico.

Drill ships are generally used for ultra-deep waters of over 7000 ft to about 12,000 ft. Drill ships also use anchor mooring systems if they are not equipped with dynamic positioning systems. Figure 1.5 shows a typical drill ship used in

Figure 1.4 Maersk Semi-Submersible Rig (Courtesy Maersk)

Figure 1.5 Chevron Drilling Ship (Courtesy Pacific Drilling)

1.2 Plate Anchors and Mooring Systems

Plate anchors can be installed by drag embedment with wire rope or chain, or by direct embedment using suction, driving, or dynamic installation. Details of the various methods of installation are described later in this section.

Plate anchors consist of a flat plate (fluke) with shank generally at the center of the fluke and a padeye to attach the mooring line to the anchor. Sometimes, a plate anchor also has a flap attached to it in an attempt to reduce embedment loss. Figures 1.6 and 1.7 show plate anchors with and without flap.

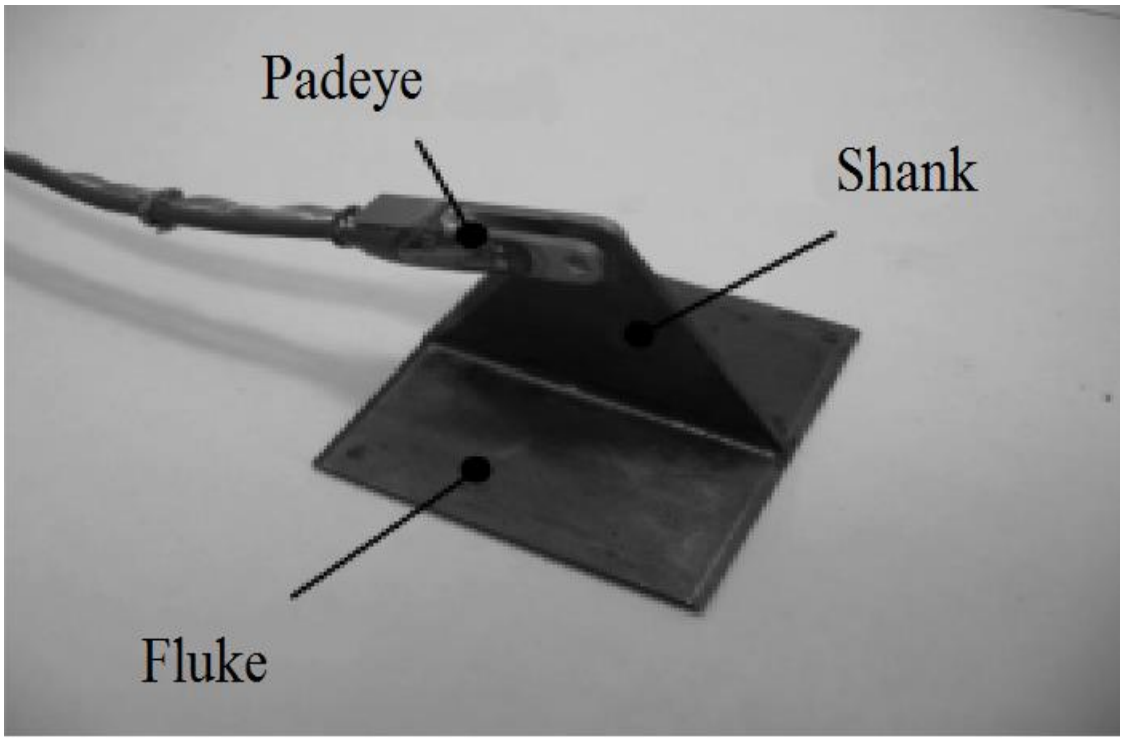

Figure 1.6 Plate Anchor (Courtesy Gaudin, et al, 2006)

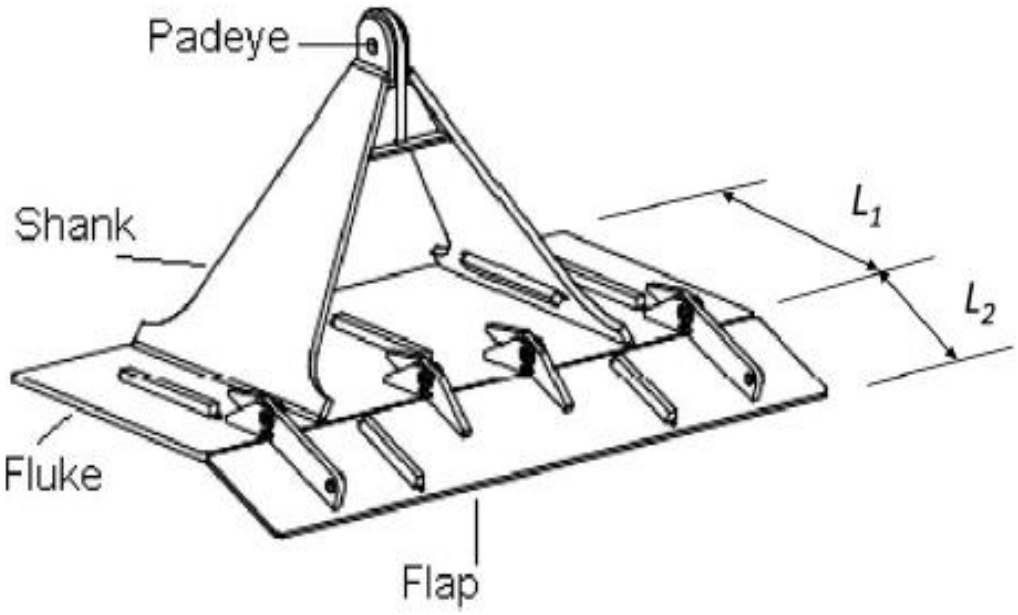

Figure 1.7 Plate Anchor with Flap (Courtesy Yang, Aubeny and Murff 2012)

The forces which are acting on the platforms of the MODUs are transferred to through the mooring lines to the anchor which helps in resisting these forces and keeps the MODUs stable. There are different types of mooring and anchor systems. The mooring system can broadly be classified as: Catenary Mooring and Taut leg mooring.

Catenary mooring is generally used in shallow to deep waters for temporary mooring. In this type of mooring a significant amount of chain rests on the sea bed and since the system of mooring consists of heavy chains, it is not suitable for ultra-deep depths as the weight of the mooring chain becomes a significant factor in the design of the floating platforms (Ruinen, 2000). The chain occupies the general shape of a concave curve in water (Aubeny, et al, 2010a) and it occupies an inverse catenary curve shape in

the soil (Neubecker, et al, 1995). Since the mooring lines are resting on the floor, the anchor is generally only subjected to horizontal forces and the self-weight of the mooring line provides most of the restoring force. Figure 1.8 shows a typical catenary system of mooring.

Taut leg mooring generally consists of polyester mooring lines and are very light compared to the catenary mooring system and hence system can be used for ultra-deep water. In this system the mooring lines are embedded in the ocean floor at an angle rather than lying on the seabed as occurs in a catenary system. Since the mooring lines are inclined the anchor must be able to resist both vertical and horizontal forces. The elasticity of the mooring line generally produces most of the restoring forces. The sea bed footprint (the radius of the mooring system) is lesser than that of the catenary system. Figure 1.9 shows a typical Taut led mooring system.

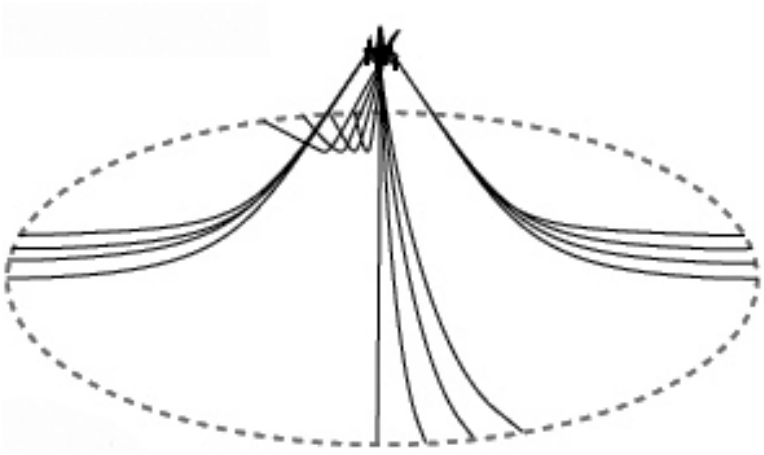

Figure 1.8 Catenary Mooring System

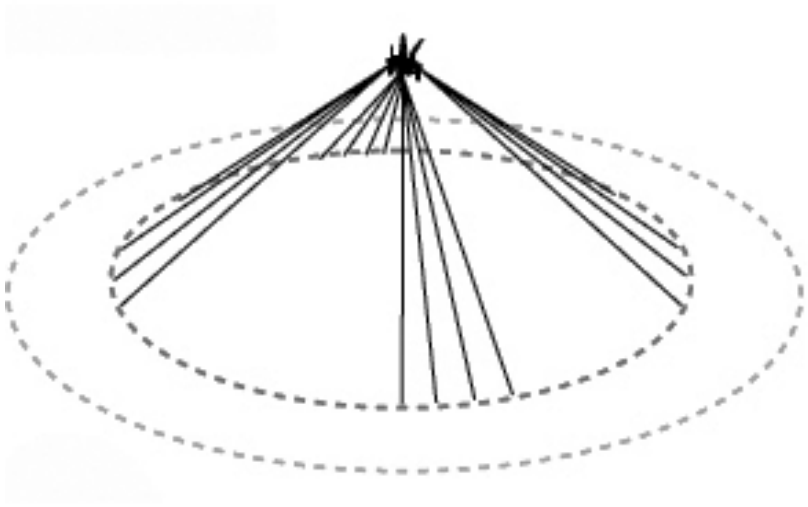

Figure 1.9 Taut-Leg Mooring System

1.3 Vertically Loaded Anchors (VLA)

The progression of oil and gas explorations to ultra-deep waters has paved way for a new type of anchorage as the traditional platforms are not practical at these depths (Aubeny et al, 2001). This has led to the replacement of static platforms by semisubmersibles and drill ships and they are held in place by connecting anchors in the sea bed through mooring lines. The uncertainty in the embedment depth and exact location of anchors after the drag embedment process resulted in the need for a more precise method of anchorage than drag anchors. This led to the development of Suction Embedded Plate Anchors (SEPLA), Dynamically Embedded Plate Anchors (DEPLA) and Pile Driven Plate Anchors (PDPA) over the past two decades. SEPLAs, DEPLAs, and PDPAs are Vertically Loaded Anchors where the plate anchors are placed precisely at the required depth by the application of vertical load during the installation process. The cost of

installation and the time required for installation is also low for these anchor systems which make it a very attractive option for deep and ultra-deep waters.

1.3.1 Installation of Plate Anchors

A SEPLA is one of the plate anchor systems where a suction caisson, called a follower, is used to place a plate anchor connected to its base at a required depth. The bottom of the suction caissons used for a SEPLA will generally have two vertical slots cut into it to mount the plate anchors. Mooring lines and Recovery bridles are used to hold the plate anchor and prevent excessive movement of the anchor. The caisson with the plate anchor attached is allowed to reach the ocean floor by the virtue of its own weight. Once the caisson is at rest on the ocean surface, a Remotely Operated Vehicle (ROV) is used to apply the required pressure to achieve the required embedment depth. Suction pressure is developed inside the caisson by turning on the ROV which will drive the caisson down into the ocean floor. When the caisson reaches the desired depth, the pump is turned off, the plate anchor and the mooring chain are separated from the suction caisson with the help of the ROV. The caisson is retrieved back by reversing the flow of water by pumping it back into the follower by the help of the pump and is recovered for future installations. After completely retrieving the caisson the anchor chain is tensioned this will cause the plate anchor oriented normally after installation to rotate or ‘key’ and move upwards and orient itself perpendicular to the angle of loading on the anchor chain. This orientation results in maximum bearing resistance as the maximum area of the plate is projected towards the applied force. Figure 1.10 shows the key steps involved in the installation of SEPLAs.

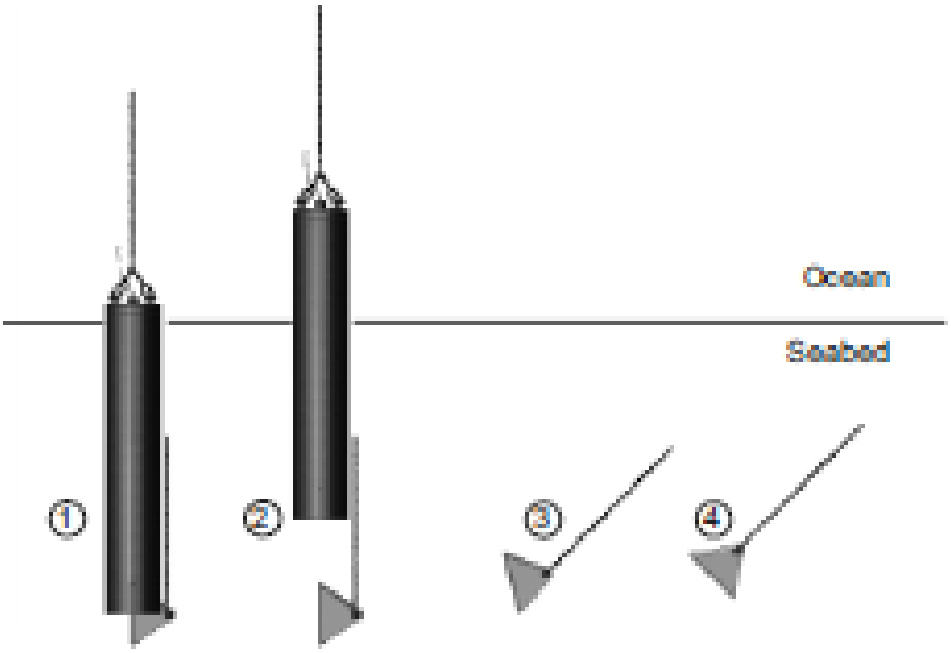

Figure 1.10 1. Installation 2. Retrieval 3. Keying 4. Mobilization (Courtesy Gaudin, et al, 2006)

PDPAs are similar to SEPLAs, except that a driven pile is used as the follower. The plate anchor is attached to a follower which is allowed to fall on its own weight to the sea bed through a template to the side of the barge to ensure that a straight path is taken. The follower after settling in the sea floor is driven to the desired depth using a vibratory or an impact hammer that has the required capacity. Once the anchor is in position, the follower is retrieved using a vibratory hammer. The anchor chain is tensioned and the plate anchor keys and orients itself perpendicular to the force applied. The detailed procedure of installation of PDPAs has been provided by the Design Guide for Pile Driven Plate Anchors by Forrest, et al, (1995). Figure 1.11 is a simplified diagram which shows the installation and the keying process of a PDPA.

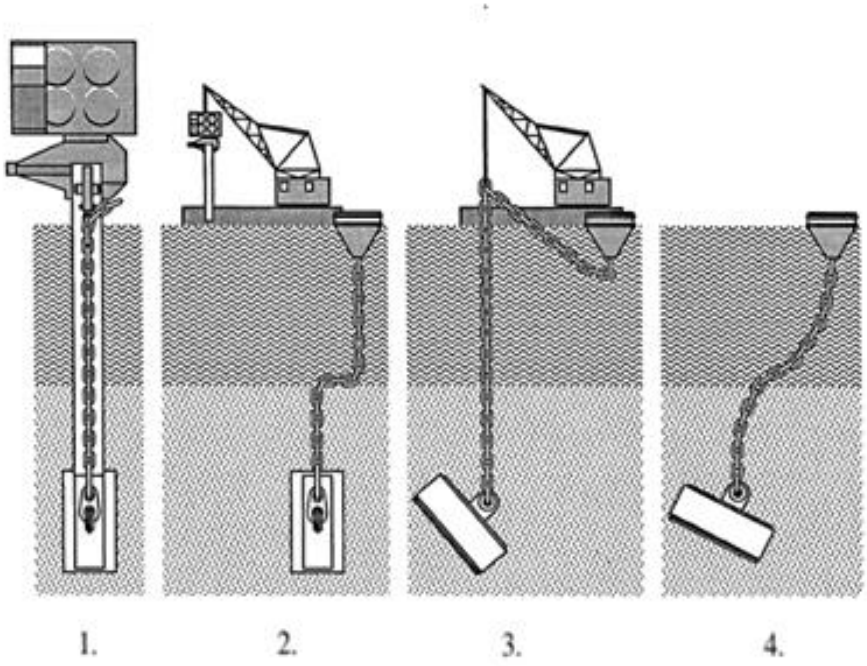

Figure 1.11 1.Installation 2. Retrieval 3. Keying 4. Mobilization (Courtesy Forrest Taylor and Bowman 1995)

In DEPLAs, a rocket or torpedo shaped shaft which acts as the follower and a set of four flukes are attached to this shaft is allowed to free fall in the water body. The depth at which the anchors are installed is calculated based on the kinetic energy of the DEPLA in water. The shaft is retrieved after the anchor is in place and the anchor chain is tensioned to key the anchor which results in anchor being perpendicular to the applied force on the anchor chain. Figure 1.12 shows the installation, keying process and the final position of the anchor where the applied load is perpendicular to the anchor.

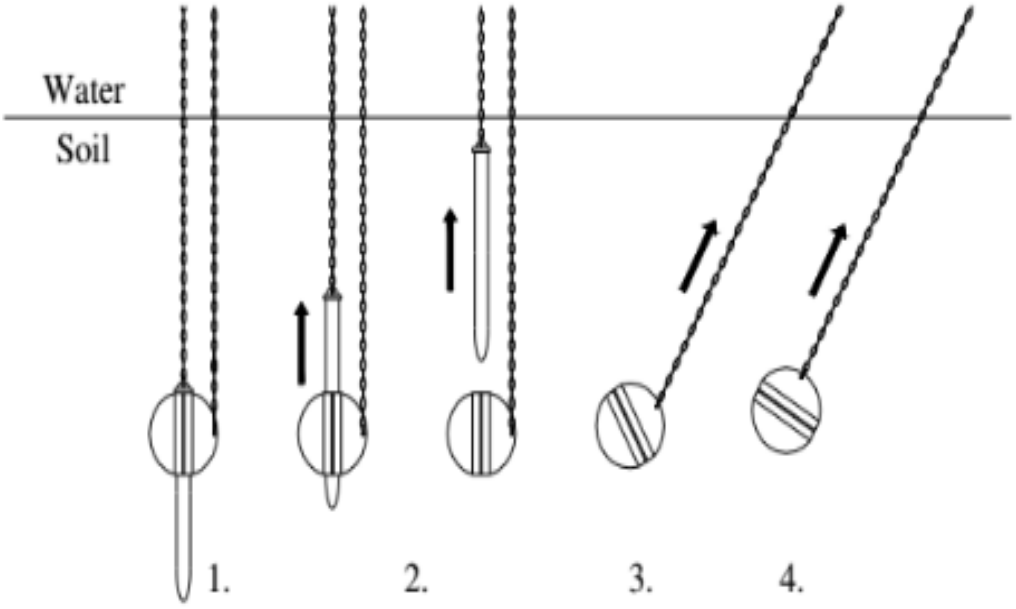

Figure 1.12 1. Installation 2. Retrieval 3. Keying 4. Mobilization (Courtesy O'Laughlin, et al, 2014)

1.4 Objective of Research

1.4.1 Problem Statement

Suction embedded plate anchors (SEPLA) are a relatively new type of anchorage system which offer a significant advantage over generally used anchors like gravity anchors, suction caissons, anchor piles, drag anchors. They overcome the short comings of suction caissons and drag anchors as they are extremely cost effective, possess high holding capacity and also can also be installed very accurately. Even with all the advantages, there is very little research done in this area. Generally either Finite Element Models (F.E.M) are developed or centrifuge tests are performed to assess the performance of SEPLAs. This study develops a simple Matlab code to calculate the strength, trajectory

and the embedment loss of the anchor using Plasticity Theory and also perform a parametric study to optimize the design of the plate anchor.

1.4.2 Outline

There is a considerable loss of embedment when the anchor is tensioned after installation. Calculation of this embedment loss becomes critical as the strength of the anchor greatly depends on the embedment depth of the anchor. The main criterion of this research is to use plasticity theory to develop a relatively effortless program to predict the trajectory, strength and embedment loss of plate anchors after installation. The research involves the interaction of the plate anchors with soil, the interaction of mooring chain with soil and the interaction of anchor and the chain. A parametric study is carried out by varying fluke length, fluke breadth, thickness of the fluke, length of the shank, eccentricity of the applied force, roughness of the soil, interaction coefficients, and angle of force application. The obtained results are compared with the available F.E.M and centrifuge test results.

CHAPTER II

BACKGROUND AND LITERATURE REVIEW

2.1 Concepts of Plasticity Theory

The earliest work on soil plasticity can be traced back to Coulomb's yield criterion in 1773 where he established the concept of limiting plastic equilibrium to calculate the pressure on a retaining wall due to fill. The only other significant work came by Rankine in 1857 where he introduced the concept of slip surfaces. The renowned book on soil mechanics by Terzaghi (1943) summarized most of the work on theory of plasticity done till date. Over the past few decades, theory of plasticity has evolved from being a tool to estimate the failure condition to the most sophisticated numerical analysis practiced in field today(Murff, 2006). The main concepts of theory of plasticity like yield criterion, flow rule and hardening law have been discussed in this section.

2.1.1 Yield Criterion

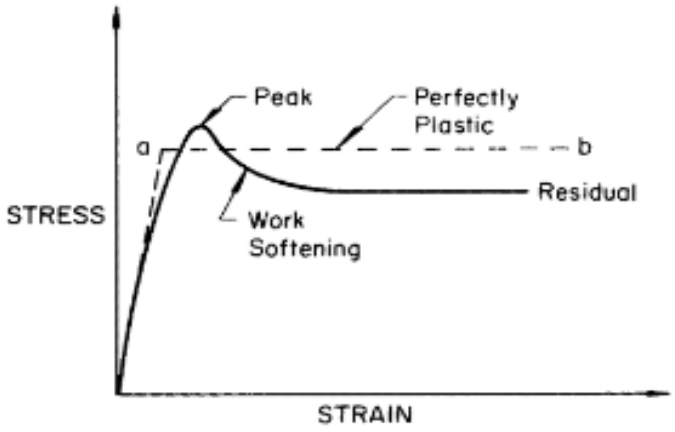

Figure 2.1 Stress-Strain Relationship for Ideal and Real Soil (Courtesy Chen, 2013)

A typical stress versus strain plot for soils is shown in Figure 2.1. For perfectly plastic materials, the plot is simplified by ignoring the work softening and is assumed to have only two straight lines as shown. The transition of the soil from elastic behavior to plastic behavior is represented by the dashed line Figure2.1. The condition required to make this transition from elastic state to perfectly plastic state at yield is known as yield criterion (Chen, 2013). The yield criterion when expressed in terms of principal stresses in three dimensions is known as yield surface and is represented as

$$f(\sigma_{ij}, K_i) = 0 \tag{2.1}$$

This equation represents the stress state of a particle which exactly traces the yield surface in the stress space.

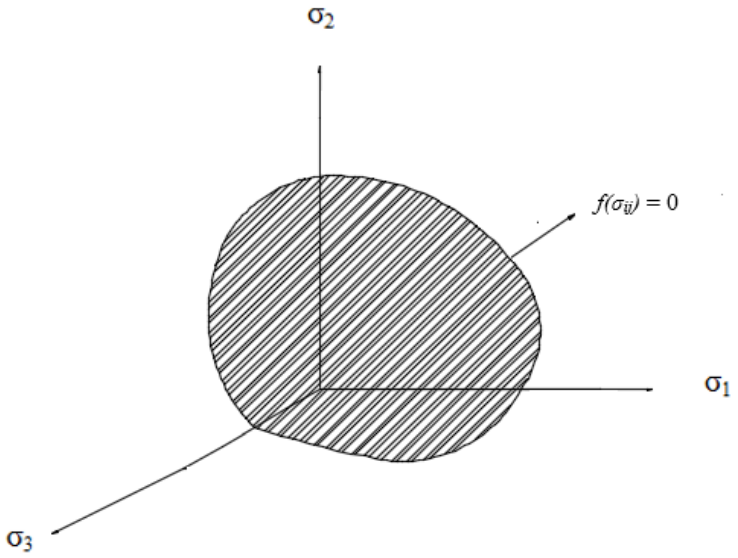

Figure 2.2 Yield Surface in the Principal Stress Plane

If the value of equation 1.1 is less than zero it means that the stress state of a particle is within the yield surface which is the elastic domain. It is not possible for a perfectly plastic material to lie outside the yield surface so the value of equation 1.1 can never be greater than zero. Figure 2.2 represents a typical yield surface with the three basic conditions of a yield surface.

2.1.1.1 Coulomb Yield Surface

The shear stress at any point in a soil is function of the cohesion stress and the compression stress at that point and is given by

$$\tau = c + \sigma \tan \varphi \qquad (2.2)$$

where

τ = shear stress

σ = compressive stress

c = cohesion

φ= angle of internal friction

When this equation is expressed in terms of the maximum, intermediate and minimum principal stresses σ_1, $\sigma 2$, σ_3 it is expressed as:

$$\sigma_1 - \sigma_3 = (\sigma_1 + \sigma_3)\sin\varphi + 2c\cos\varphi \qquad (2.3)$$

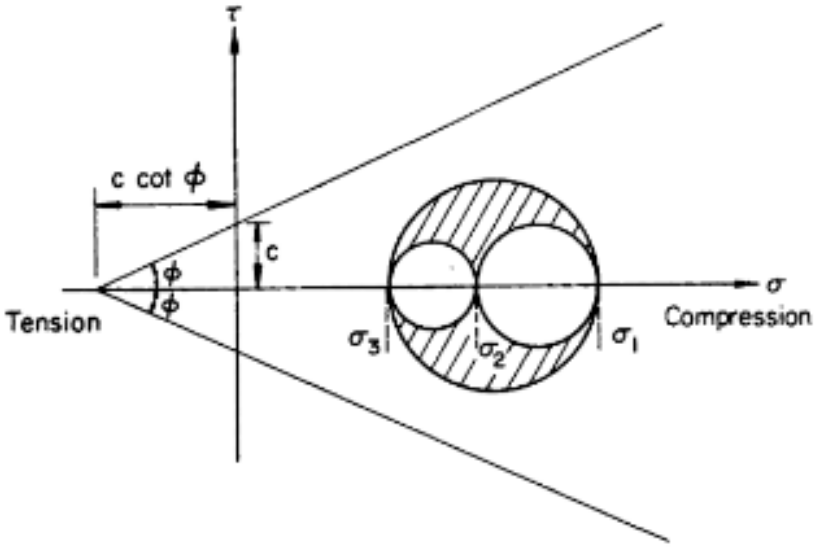

Figure 2.3 Coulomb's Yield Criterion Represented in σ-τ Plane (Courtesy Chen, 2013)

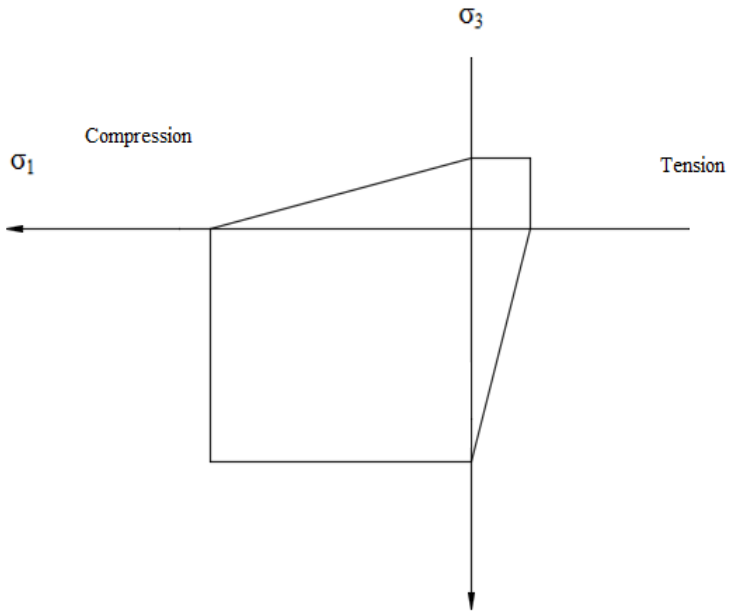

Figure 2.4 Coulomb Yield Surface in Major(σ1) and Minor (σ3) Principal Stress Plane

Figure 2.3 represents the Mohr's representation of yield surface in the σ-τ plane. If the same equation was represented in the principal stress plane with axes, $\sigma_1$and σ_3, it will be represented as shown in figure 2.4. Figure 2.5 shows the comparison of Coulomb Yield surface with respect to extended Tresca and Von Mises yield criterion in the π- plane (a plane which passes through the origin and is parallel to $\sigma_1 = \sigma_2 = \sigma_3$).

2.1.1.2 Tresca and Extended Tresca Yield Criterion

The Tresca model is a special case of the Coulomb model, where the soil is considered to be purely cohesive i.e. $\varphi = 0$ and $c = S_u$ in equation 1.1.This is generally used for undrained analysis and is represented as shown

$$\tau_{max} = \sigma_1 - \sigma_3 = 2S_u \quad (2.4)$$

where

τ_{max} = Maximum shear stress

S_u = Undrained shear strength

The Tresca yield surface is widely used for several geotechnical analysis like slope stability calculations and bearing capacity assessment (Chi, 2010). But this yield criterion does not provide tools for 3 dimensional analysis as it does not consider the effect of the intermidiate principal stressσ_2. In order to overcome this shortcoming, the extended Tresca yield criterion was developed where the effect of the intermediate stress was also considered by introducing a new factor β given by:

$$\beta = \frac{\sigma_1 - \sigma_3}{\sigma_1 + \sigma_2 + \sigma_3} \quad (2.5)$$

where

β is a constant term.

Tresca model forms a hexagonal yield surface when represented in the π-plane (deviatoric plane) as shown in figure 2.5.

2.1.1.3 Von Mises Yield Criterion

Von Mises Yield criterion is a modification of the Tresca yield criterion and it overcomes some of the problems faced with the Tresca yield criterion. This yield criterion has a circular cylinder shaped yield surface which overcomes several mathematical difficulties faced when analyzing a hexagonal surface. Von Mises criterion is written as shown below

$$J_2^{\frac{1}{2}} = \frac{1}{6}\{[(\sigma_1 - \sigma_2)^2 + \big((\sigma_2 - \sigma_3)\big)^2 + \big((\sigma_3 - \sigma_1)\big)^2]\}^{\frac{1}{2}} \quad (2.6)$$

where

J_2= Second invariant of the stress tensor.

Figure 2.5 shows a plot which compares the yield surface of Coulomb, Tresca and Von Mises yield surfaces in the π-plane.

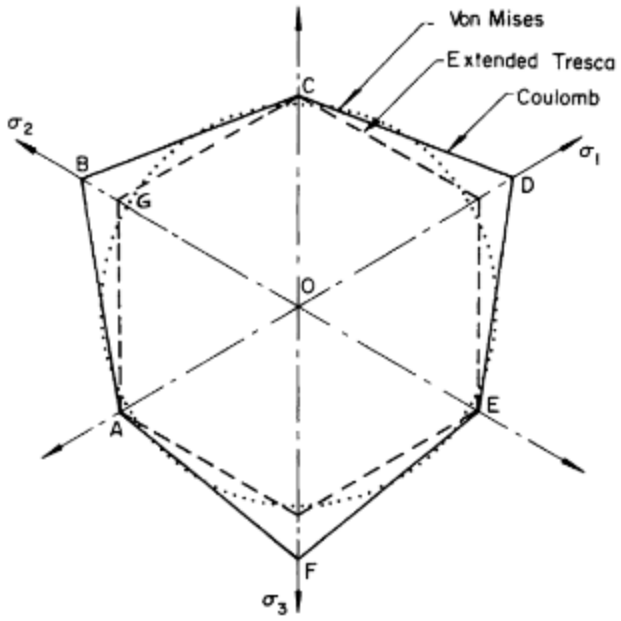

Figure 2.5 Representation of Coulomb, Extended Tresca and Von Mises Yield Surfaces on the π Plane (Courtesy Chen, 2013)

2.1.2 Flow Rule

The total strain of a material is composed of two components, the elastic strain and the plastic strain. A particle experiences elastic strain when it is inside the yield surface and it experiences plastic strain on the yield surface. The elastic strain of a body is represented by Hooke's Law. For an isotropic material the elastic strain is given by

$$\sigma_{ij} = \lambda\delta_{ij}\varepsilon_{kk} + 2\mu\varepsilon_{ij} \tag{2.7}$$

where

λ= K-2/3G and μ =Gare Lame's constants

K= Bulk modulus

G= Shear modulus

σ_{ij}= Elastic stress tensor

δ_{ij}= Kronecker Delta

ε_{kk}= Elastic strain tensor

ε_{ij}= Volume strain

A particle transitions from elastic behavior to plastic behavior when its stress state moves from inside the yield surface and reaches the surface. Since we assume a straight line for plastic behavior, the total magnitude of the plastic stain is infinite. So, generally plastic strain rates are calculated instead of plastic strains. The magnitude and the direction of a plastic flow are calculated using the plastic potential G as:

$$\varepsilon_{ij}^{p} = \lambda \frac{\partial G}{\partial \sigma_{ij}} \tag{2.8}$$

where

ε_{ij}^{p}= Plastic strain increment

λ = Constant

G = Plastic potential

If the gradient of the yield surface $\frac{\partial F}{\partial \sigma_{ij}}$ is equal to the gradient of the plastic potential $\frac{\partial G}{\partial \sigma_{ij}}$ then the particle is said to obey the associated flow law. If the particle obeys the associated flow law, then the strain increment can be calculated using the yield

function instead of the plastic potential. This implies that the direction of the plastic increment/flow is perpendicular to the yield surface as shown in the figure 2.6.

$$\varepsilon_{ij}^{p} = \lambda \frac{\partial G}{\partial \sigma_{ij}} = \lambda \frac{\partial F}{\partial \sigma_{ij}} \tag{2.9}$$

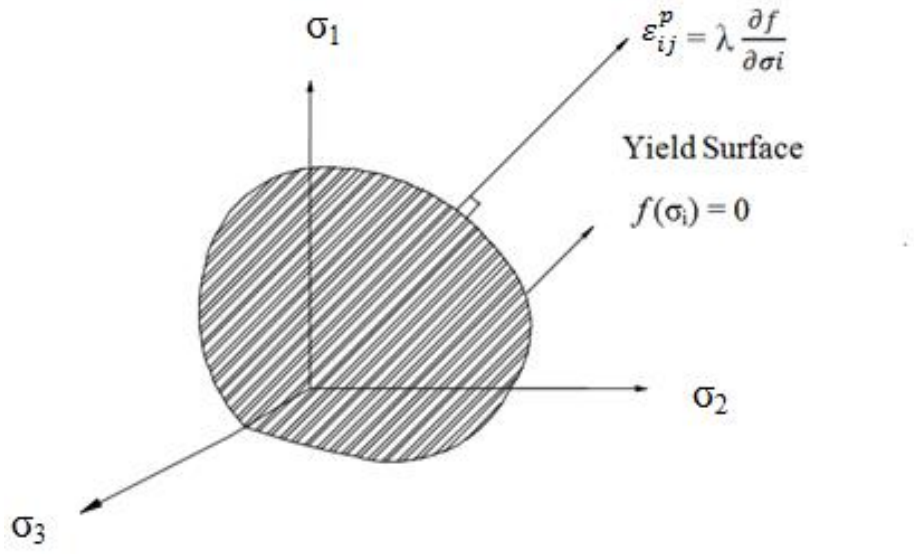

Figure 2.6 Plastic Strain of a Soil that Obeys Associated Plasticity Rule

2.1.3 Hardening

In perfectly plastic condition once the material reaches its yield stress, the particle will continue to have plastic deformation while the yield stress is maintained and if the stress reduces, the particle will revert back to elastic behavior. In case of hardening, it is assumed that yielding does not initiate the plastically deformation infinitely. Stress has to be increased continuously to increase the plastic deformation and if the stress is held

constant any particular level, it would have a corresponding plastic strain level. If the stress is decreased, it will not follow the initial elastic path and will result in permanent deformation. In a perfectly plastic case, the yield surface will always remain constant but in the case of hardening, the yield surface may change in shape, size and position and it is generally represented by

$$f(\sigma_{ij}, K_i) = 0 \tag{2.10}$$

where

K_i represents one or more hardening parameters.

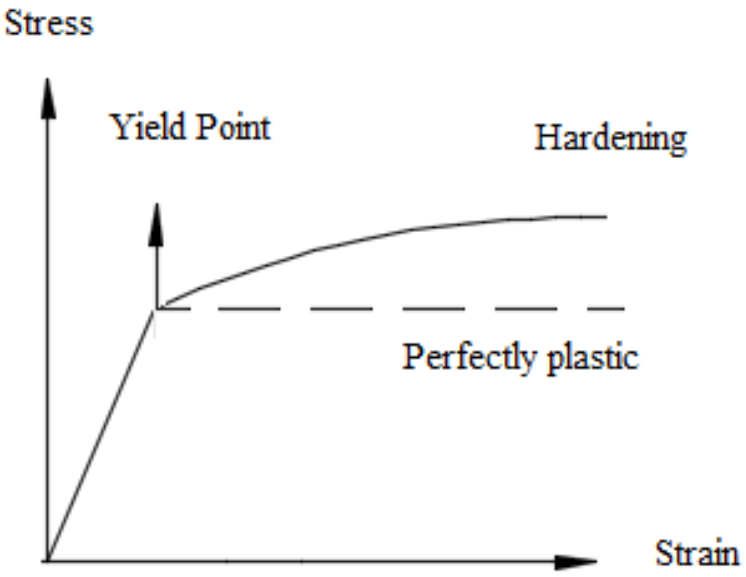

Figure 2.7 Strain Hardening

2.1.3.1 Strain Softening

In this case, the rate of plastic deformation decrease as the stress is increased after a particular stress level. In this case, the size of the yield surface decreases as the stress is increased.

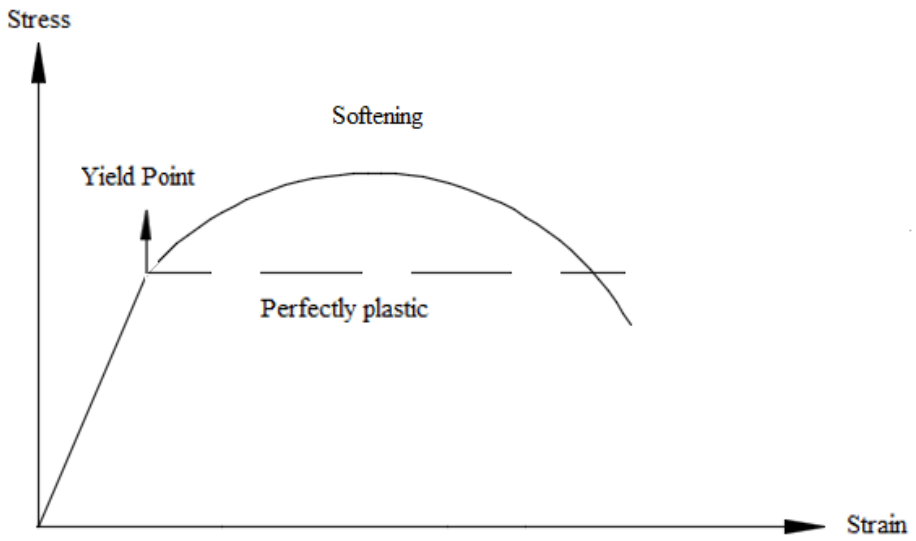

Figure 2.8 Strain Softening

2.1.3.2 Types of Hardening

Hardening can be broadly classified into three different categories which are Isotropic Hardening, Kinematic Hardening and Mixed Hardening.

2.1.3.2.1 Isotropic Hardening

In isotropic hardening, the shape of the yield surface remains the same but its size increases as the stress in increased. This can be generally represented as

$$f(\sigma_{ij}, K_i) = f(\sigma_{ij}) - K = 0 \quad (2.10)$$

In this equation $f(\sigma_{ij})$represents the shape of the surface and the size of the surface is governed by the hardening parameter K. Figure 2.9 represents the isotropic hardening.

2.1.3.2.2 Kinematic Hardening

In kinematic hardening, the size and the shape of the yield surface remains the same but the surface shifts from one point to another in the stress space. Kinematic hardening is generally represented as

$$f(\sigma_{ij}, K_i) = f(\sigma_{ij} - \alpha_{ij}) = 0 \quad (2.11)$$

where

α_{ij} is the hardening parameter known as back stress.

The total displacement of the yield surface is determined by the back stress. Figure 2.10 shows an example of kinematic hardening.

2.1.3.2.3 Mixed Hardening

This includes the variables from both the isotropic and the kinematic hardening which means that the yield surface will increase in size and also move from its original position as the applied stress is increased. So, mixed hardening can be represented as

$$f(\sigma_{ij}, K_i) = f(\sigma_{ij} - \alpha_{ij}) - K = 0 \quad (2.12)$$

where

K is the hardening factor that determines the size of the yield surface

α_{ij} is the hardening parameter that determines the location of the yield surface

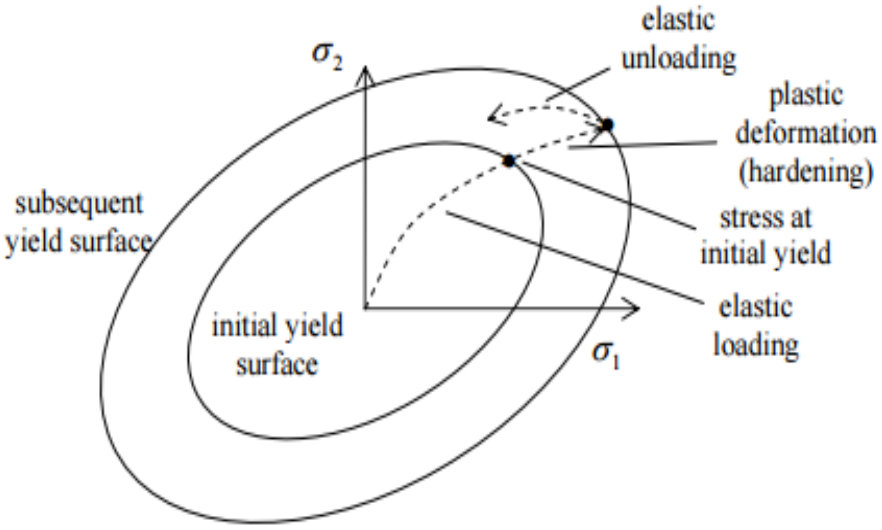

Figure 2.9 Isotropic Hardening (Courtesy Chen, 2013)

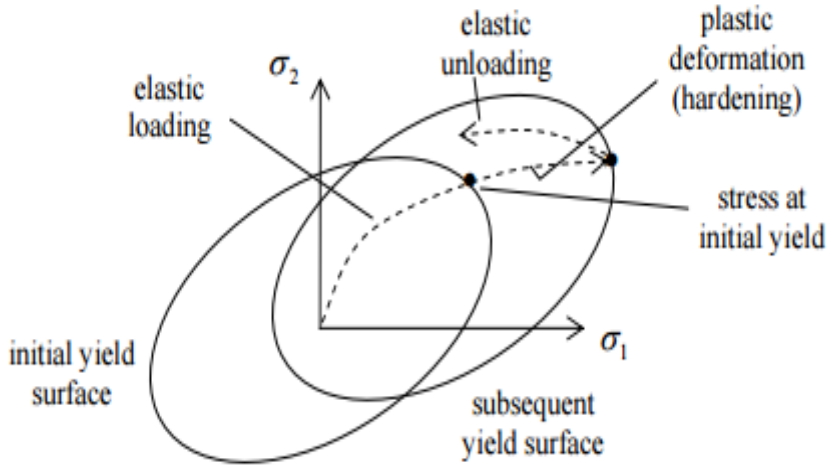

Figure 2.10 Kinematic Hardening (Courtesy Chen, 2013)

2.1.4 Lower Bound and Upper Bound Theorem

Lower bound and Upper theorems are essential plasticity tools to estimate the collapse load of a system. Both of these theorems have been developed for perfectly plastic materials. A general stress distribution which satisfies the equilibrium condition of a surface leads to estimate the collapse load in the lower bound theorem. In the upper bound theorem, generally a value higher than the actual collapse load is calculated by assuming a displacement or velocity field.

2.1.4.1 Lower Bound Theorem

If a stress distribution is present throughout a system in equilibrium internally and also balances certain external loads on the stress boundary while obeying the yield condition, then the system will not collapse under these loads and can carry them safely (Murff, 2006). Consider the example shown in figure 2.11, if a system is subjected to an external applied force of w_i it will result in a displacement of u_i. Figure 2.11 (b) shows the yield surface of the system. The work done by the actual stress field σ will always be greater than any other hypothetical stress field σ^*.

The total energy dissipated by this system can be given as

$$E = \Sigma w_i u_i = \int_v \sigma \grave{\varepsilon} dv \tag{2.134}$$

This energy dissipation will be the maximum energy dissipation for this system as any other assumed stress field σ^* will result in a lower energy dissipation and hence will also have a smaller w_i^* as given by equation 2.14

$$E^* = \Sigma w_i^* u_i = \int_v \sigma^* \dot{\varepsilon} dv \leq E \tag{2.14}$$

So from this we can say that the collapse load estimated from the lower bound theory is always lower than or equal to the actual collapse load.

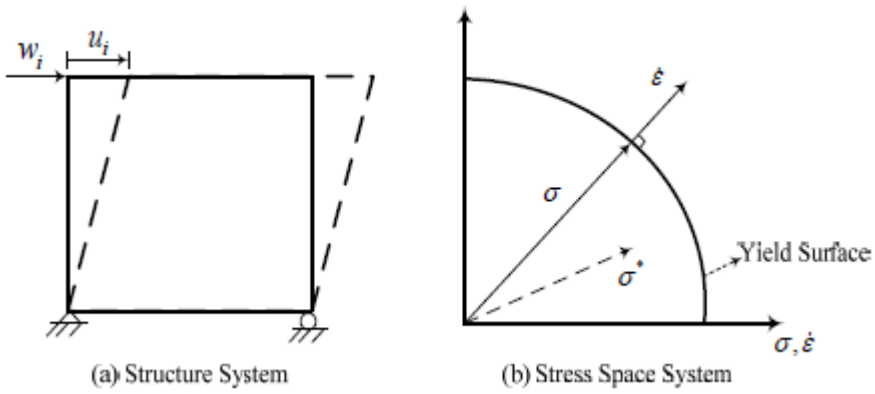

Figure 2.11 Estimated Collapse Load (Courtesy Chi, 2010)

2.1.4.2 Upper Bound Theorem

If the collapse load is estimated by comparing the rate of internal energy dissipation of a system to the rate at which the external forces work in a hypothetical mechanism of deformation (velocity or displacement) of this system, then it will always be equal to or higher than the actual collapse load (Murff, 2006). Figure 2.12 represents the general idea of Upper bound theorem. Here $D^*$is the internal energy dissipation due to the hypothetical velocity mechanism and the estimated collapse load is w_i^*. The total work done by this hypothetical situation is given by

$$\Sigma w_i^* u_i^* = \int_v D^* dv \int_v \sigma^* \dot{\varepsilon} dv \geq \int_v \sigma \dot{\varepsilon} dv = \Sigma w_i u_i \tag{2.15}$$

This implies that the plastic collapse load calculated using the Upper bound theorem will always be higher than or equal to the actual applied stress.

If the system follows the associated flow rule, the energy dissipated can be written as

$$D^* = \sigma^* \dot{\varepsilon} = \sigma_{ij} \varepsilon_{ij}^p = \sigma_{ij} [\lambda \frac{\partial F}{\partial \sigma_{ij}}] \tag{2.16}$$

From this we can also observe that the energy dissipation D^* changes along with yield function of the surface if the material follows the associated flow law.

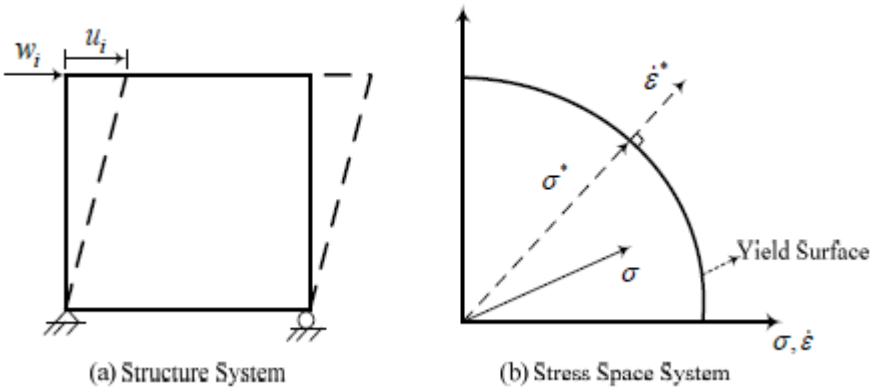

Figure 2.12 Plastic Strain of a Soil that Obeys Associated Plasticity Rule (courtesy Chi, 2010)

2.2 Previous Studies

2.2.1 SEPLA and Keying Trajectory

A SEPLA is installed at the required depth by driving a the plate anchor to the required position using a suction caisson. Since the caison is retrieved, this method of anchorage is relatively inexpensive. By using the suction caisson , the plate anchor can be placed at the required depth accurately. However, uncertainity exists in regard to the final position and hence the strength of the anchor after the suction caisson is retrived and the anchor is tensioned. When the anchor is loaded, it will start to rotate and will continue to do so until the face of the anchor on which the load is being applied is perpendicular to the applied tension. This process of movement of anchor from its initial vertical position to its final position is known as keying. During keying, the anchor loses capacity for two reasons. When the anchor keys, the soil surrounding it is remolded and thus the strength of the soil surrounding the plate anchor is reduced. But this is not a permanent loss as the soil will consolidate and retrieve its strength . The main source for the loss of capacity in an anchor during keying is the loss of embedment. When the plate anchor rotates during keying, it also translates horizontally and vertically. This depends on several factors like plate geometry, soil resistance and the angle of force application. The effects of all these parameters are explored in this thesis and the results are compared and verified with the limited number of available lab centrifuge tests and Finite Element Models. The process of keying is roughly depicted in figure 2.13

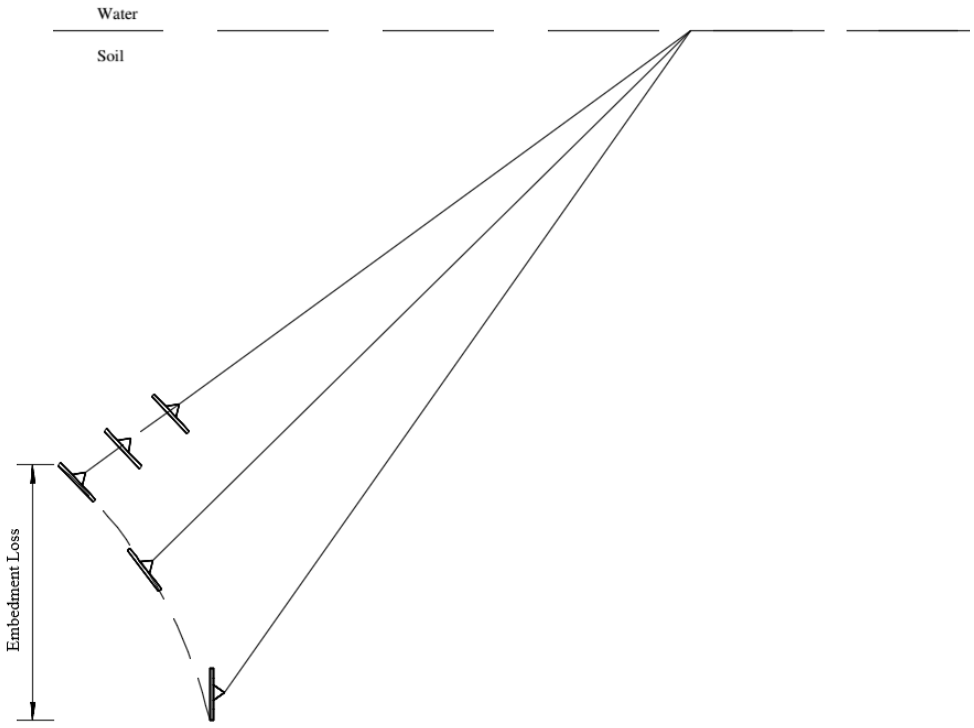

Figure 2.13 Trajectory of a SEPLA from its Initial Position to its Final Position

The concept of SEPLA was first introduced by Dove, et al, in 1998. Since this is a relatively new concept, only a few reduced scale laboratory tests have been performed and even fewer analytical models have been developed. Wilde, et al. (2001) has indicated a very wide range of embedment loss of 0.5-1.7 times the height of the anchor with the normalized eccentricity of the plate $e/B = 0.5$ when tetsed to failure at embedment ratios of 4-10.

Gaudin, et al. (2006) performed centrifuge tests to asses the influence of the installation process on the capacity of SEPLAs. The soil surrounding the vicinty of the anchor was found to lose its strength after retriving the caission and this strength was recovered over time.

Gaudin, et al. (2008) performed centrifuge tests to investigate the effect of keying on the performance SEPLAs. These tests were performed for anchors of different normalised loading eccentricity ratios (e/B) and different pullout angles. They reported reduction in embedment loss at lower pullout angles and higher eccentricity ratio.

Wang et al. (2011) performed Large Deformation Finite Element (LDFE) modelling to simulate the keying process for rectangular and strip paltes.A parametric study was performed considering the anchor geometry, soil properties, loading eccentricity and the inclinaton of loading. They reported lower embedment loss at lower pullout angle and loading eccentricities and the gradient of the soil was found to have minimal effect on the embedment loss.

Song et al,(2009) performed numerical analysis and centrfuge testing to calculate the embedment loss during keying. LDFE (large displacement finite element) modelling was been performed as a part of the numerical analysis to simulate the anchor trajectory which was observed during the centrifuge model tets. The embedment loss was found to stabilize at 0.25-0.5 times the anchor width at higherlength of shank (eccentricity of loading). The pullout angle was found to have a linear relationshp with the embedment loss. The effects of soil nonhomogenity, anchor roughness and soil shear strength were also investigated in their work.

CHAPTER III

ESTIMATION OF KEYING TRAJECTORY AND OF EMBEDMENT LOSS

3.1 Analysis of Anchors

In this study the anchor is idealized to be a rectangular plate with a rectangular shank connected at the centre of the plate. The main goals of the study are to calculate SEPLA capacity at any embedment depth and to and to predict the keying trajectory of the SEPLA when loaded at any mooring angle.

Two main theories have been employed to predict the behavior of a SEPLA during keying when loaded. The plastic limit method is developed by O'Neill, et al, (2003) is used to calculate the capacity of the SEPLA and the displacement of the anchor. The upper bound collapse load analysis developed by Aubeny et al. (2005, 2008) is used to study the effect of anchor-chain interaction. The chain-anchor and the chain-soil interactions have been studied which helps to determine the tension and the angle of the chain on the surface of the water and at the padeye of the anchor at inside the sea floor.

3.2 Plate Capacity

3.2.1 Plastic Limit Method

The theory of plastic yield function and the associated flow rule were utilized to develop a plastic model to predict the trajectory and evaluate the shackle tension for rectangular and wedge shaped anchors by O'Neill, et al, (2003), utilizing the chain solutions developed by Neubecker and Randolph (1995). The load applied to the anchor through the mooring line was expressed in terms of its components. The normal

component (V), the tangential component (H) and the moment (M) resulted in a tangential force T_a. A schematic of this is shown in figure 3.1. An offset form of Murff's (1994) equation was developed to characterize the yield behavior of an anchor subjected to a force T_a given by:

$$f = \left(\frac{V - V_1}{V_{max} - V_1}\right)^q + \left[\left(\frac{|M - M_1|}{M_{max} - M_1}\right)^m + \left(\frac{|H - H_1|}{H_{max} - H_1}\right)^n\right]^{\frac{1}{p}} - 1 \qquad (3.1)$$

where

f = Plastic yield function

V_{max} = Maximum normal load

H_{max}= Maximum tangential load

M_{max}= Maximum moment load

V_1, H_1 and M_1= Offset Loads

m, n, p, q = are the interaction coefficients

Bransby and O'Neill (1999) have provided the solutions for the interaction coefficients m, n, p, and q and the normalized peak load factors V_{max}/L_fS_u, H_{max}/L_fS_u and M_{max}/L_fS_u from finite element modeling for a fluke length to thickness ratio of 7. Since then Elkhatib and Randolph (2005), Elkhatib (2006), Cassidy et al, (2012) and Wei et al, (2014) have worked on these parameters and a complete list of these parameters is tabulated in Table 3.1.

The maximum values of loads in normal & tangential directions and due to moment were calculated using upper bound methods developed by O'Neill and Bransby 1999. These terms were expressed as:

$$\frac{V_{max}}{L_f S_u} = 4\left(\pi - \alpha + \frac{tan\alpha}{2}\right) + 4\frac{t}{L_f}\left(\frac{1}{2} + cos\alpha\right) \quad (3.2)$$

$$\frac{H_{max}}{L_f S_u} = 4\frac{t}{L_f}\left(\pi - \alpha + \frac{tan\alpha}{2}\right) + 4\left(\frac{1}{2} + cos\alpha\right) \quad (3.3)$$

$$\frac{M_{max}}{{L_f}^2 S_u} = \frac{\pi}{2}\left(1 + \left(\frac{t}{L_f}\right)^2\right) \quad (3.4)$$

where

L_f = Length of the fluke

t = thickness of the fluke

α = angle of the wedge (3.2 and 3.3)

The derivatives of the yield equation 3.1 with respect to one of the force components will result in the strain increment in the corresponding direction (Yang, et al, 2012). Equation 3.5 shows the incremental displacement in the normal direction when a normal load N is applied.

$$\delta n = \lambda \frac{\partial f}{\partial H} \tag{3.5}$$

where

λ is a constant positive factor.

The values of each strain cannot be uniquely determined by this method because the value of term λ is not known but it is the same for all the strain components. So the relative values of strains with respect to each other (δt/δn, δβ/(δn⁄Lf)) can be determined as shown

$$\frac{\delta t}{\delta n} = \frac{\partial f}{\partial V} \Big/ \frac{\partial f}{\partial H} \tag{3.6}$$

$$\frac{\delta \beta}{\delta n / L_f} = \frac{\partial f}{\partial \left(M / L_f\right)} \Big/ \frac{\partial f}{\partial H} \tag{3.7}$$

If a suitable normal incremental displacement (δn) is chosen, then the corresponding displacements in tangential direction (δt) and the rotation $\delta\beta$ can be calculated using equations 3.6 and 3.7.

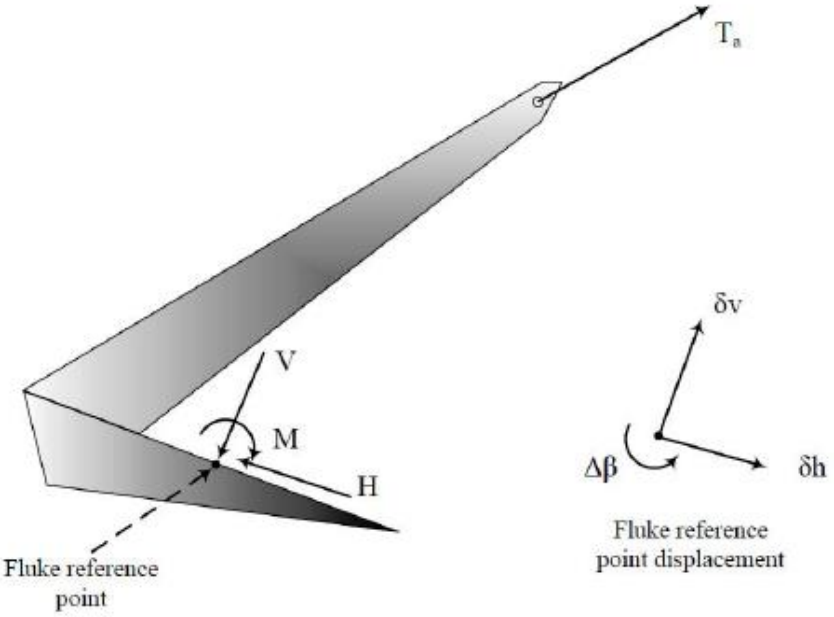

Figure 3.1 The Schematic of Vector Component System Used by O'Neill et al, (2003)

Figures 3.2, 3.3 and 3.4 show the isolated effects of the normal, tangential and moment loads applied to an anchor analyzed by upper bound theorem.

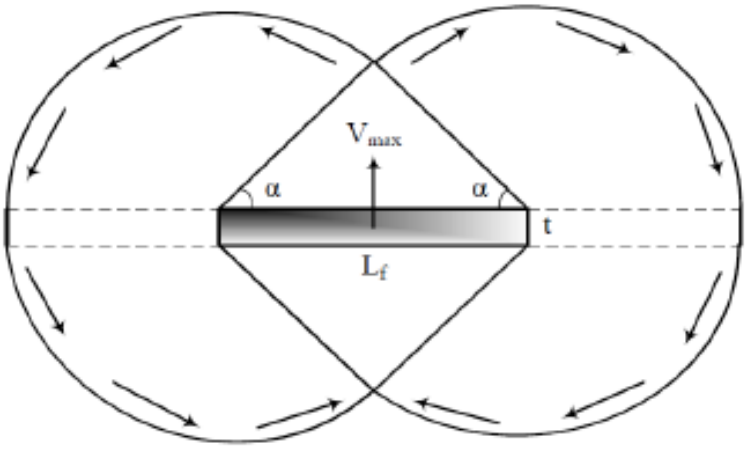

Figure 3.2 Upper Bound Mechanism of an Anchor Subjected to Pure Normal Load (Courtesy Chi, 2010)

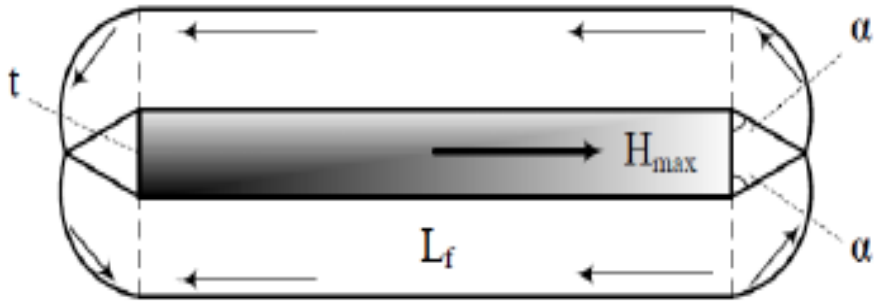

Figure 3.3 Upper Bound Mechanism of an Anchor Subjected to Pure Tangential Load (Courtesy Chi, 2010)

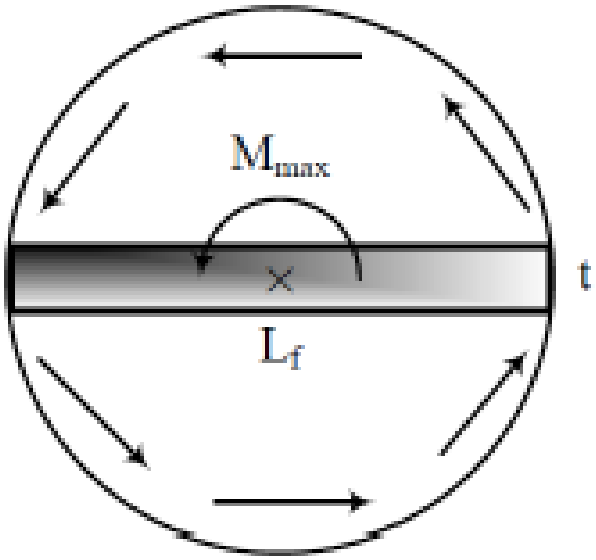

Figure 3.4 Upper Bound Mechanism of an Anchor Subjected to Pure Moment (Courtesy Chi, 2010)

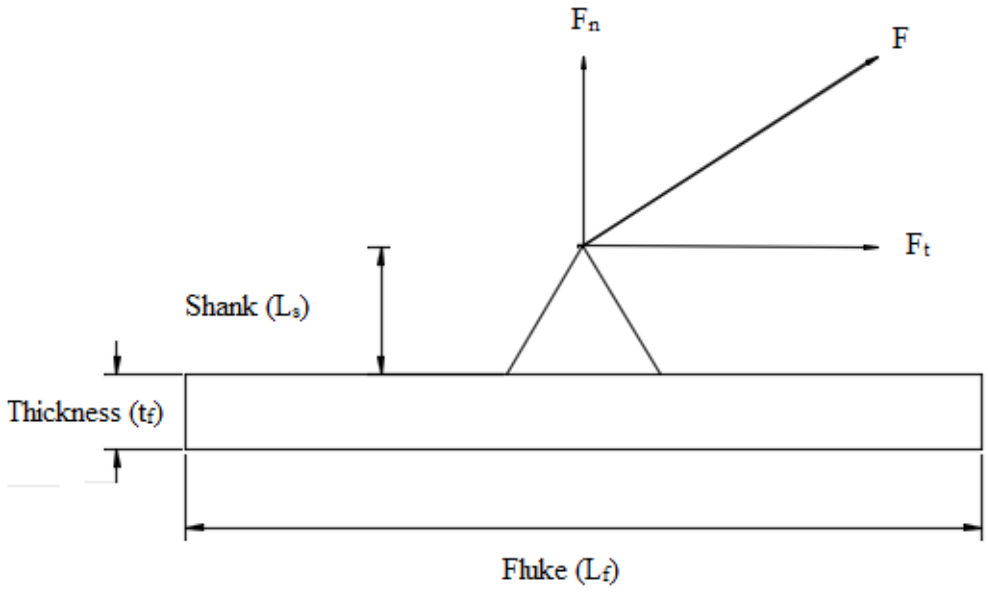

Figure 3.5 A Typical Plate Anchor

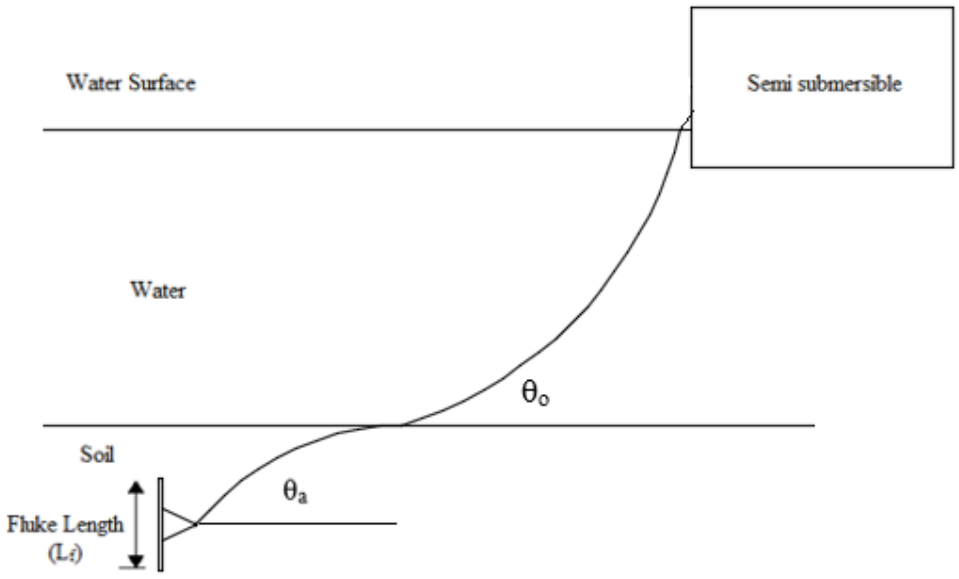

Figure 3.6 Typical Setup of a SEPLA before Loading

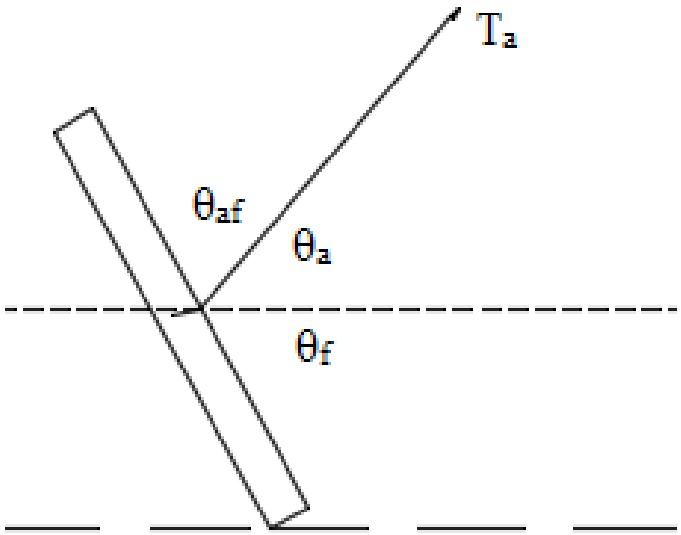

Figure 3.7 SEPLA Subjected to Tension Ta

3.2.2 Current Analysis Method for Plate Capacity

The current analysis is based on a SEPLA as shown in figure 3.5. The fluke length is denoted by L_f and the length of the shank is denoted by L_s. The length of the shank also serves as the horizontal eccentricity at which the load is applied (e_h). The angle of the mooring like at the padeye is denoted by θ_a and the angle that the mooring line makes at the surface of the water is denoted by θ_o. The inclination of the fluke is given by θ_f. SEPLAs are installed vertically before the application of force, so θ_f before the process of keying is therefore 90˚ ($\pi/2$). The force at the padeye T_a, is split into its normal, tangential and rotational components F_n, F_t and M.

$$F_n = F\ cos\theta_a = F\ c_1 \tag{3.8}$$

$$F_n = F\ sin\theta_a = F\ c_2 \tag{3.9}$$

$$M = FL_f\left[\frac{L_s}{L_f}cos\theta a + \frac{e_s}{L_f}sin\theta a\right] = Fc_3 \tag{3.10}$$

These terms are normalized by dividing them by the soil strength (S_u) and the area of the fluke (A_f) to obtain dimensionless parameter N_e. The normal tangential and moment components can therefore be expressed as N_n, N_t and N_m as shown

$$N_e = F / S_u A_f \tag{3.11}$$

$$N_n = F / S_u A_f = N_e\ c_1 \tag{3.12}$$

$$N_t = F / S_u A_f = N_e\ c_2 \tag{3.13}$$

$$M = F / S_u A_f = N_e\ c_3 \tag{3.14}$$

The ultimate capacities in the normal direction and for the moment can be calculated by substituting these terms in equations 3.2 and 3.4 and assuming the wedge angle α to be equal to 45˚ (π/4) and considering plane strain condition. The maximum capacity in the tangential direction is calculated using the relationship provided by Anderson, et al, (2003). These solutions for the ultimate capacities are strictly valid for plane strain condition

$$N_{n\,max} = \frac{F_{n\,max}}{L_f S_u} = 3\pi + 2 + 2\frac{t}{L_f}\left(\alpha_d + \frac{1+\alpha_d}{\sqrt{2}}\right) \tag{3.15}$$

$$N_{t\,max} = \frac{F_{t\,max}}{L_f S_u} = 2\left(\alpha_d + N_{tip}\frac{t}{L_f}\right) \approx 2\alpha_d + 15\frac{t}{L_f} \tag{3.16}$$

$$N_{m\,max} = \frac{M_{max}}{{L_f}^2 S_u} = \frac{\pi}{2}\left(1 + \left(\frac{t}{L_f}\right)^2\right) \tag{3.17}$$

Where

$F_{n\,max}$ = maximum normal load

$F_{t\,max}$ = maximum tangential load

M_{max} = maximum moment

α_d = coefficient of anchor surface roughness

N_{tip} = 7.5 (N_c=7.5 for plane strain)

The solutions provided in equations 3.15-3.17 were compared to finite element solutions for a plate with adhesion values varying from 0 to 1 and with $L_f / t_f = 7$ by Murff, et al, (2005) and it was found that these equations were in very good agreement with the FE solutions.

Equation 3.1 written in terms of F_n, F_t and M will take the form of equation 3.18 as shown. This will account for the interactive effects of force components and helps to assess the behavior of a SEPLA.

$$f = \left(\frac{|F_n|}{F_{n\,max}}\right)^q + \left[\left(\frac{|M|}{M_{max}}\right)^m + \left(\frac{|F_t|}{F_{t\,max}}\right)^n\right]^{\frac{1}{p}} - 1 = 0 \qquad (3.18)$$

where

F_n = normal component of the applied force

F_t = tangential component of the applied force

M = moment component of the applied force.

The interaction coefficients describe the shape of the yield surface in the force plane. The interaction coefficients suggested by carrying out finite element analysis by various works is listed in Table 3.1. In this study, the effect various interaction coefficients on the trajectory of the anchors has been studied and their results have been presented in the next chapter. Table 3.2shows the parameters of the model anchor used in this study.

Equation 3.19 can written in terms of normalized bearing factors in equations 3.11, 3.12 and 3.13 as

$$f = \left(\frac{N_e|c_1|}{N_{n\,max}}\right)^q + \left[\left(\frac{N_e|c_3|}{N_{m\,max}}\right)^m + \left(\frac{N_e|c_2|}{N_{t\,max}}\right)^n\right]^{\frac{1}{p}} - 1 = 0 \qquad (3.19)$$

Table 3.1 Yield Function Parameters (courtesy Wei, et al, 2014)

Reference	L_f/t_f	α_d	Type	V_{max}/L_fS_u,	H_{max}/L_fS_u	H_{max}/L_fS_u	m	n	p	q
Bransby& O'Neill (1999)	7	1	2D	11.87	4.29	1.49	1.261	3.72	1.09	3.16
Elkhatib and Randolph (2005)	20	0.4	2D	11.58	1.97	1.53	1.52	5.31	1.01	2.75
	20	1	2D	11.62	3.19	1.59	1.14	4.92	1	3.39
	7	0.4	2D	11.78	3.38	1.55	2.58	3.74	1.09	1.74
	7	1	2D	11.93	4.65	1.63	1.27	3.46	1.03	3.23
Elkhatib (2006)	20	1	3D	13.21	3.22	2.05	1.07	4.19	1.1	4.02
Cassidy et al. (2012)	29	1	2D	14	3	2	1.1	4.2	1.1	4
Wei et al. (2014)	29	1	2D	11.68	2.83	1.63	1.27	5.23	1.08	3.39
	29	1	2D	11.70	6.28	1.63	1.24	1.80	1.06	3.33

Table 3.2 **Parameters of Anchor, Chain and Soil**

Anchor Geometry	
Fluke Length (L_f)	4 m
Fluke width (w_f)	4 m
Fluke thickness (t_f)	0.2 m
Shank Length (L_s)	2 m
Anchor Line Properties	
Line Diameter (b)	0.073 m
Bearing Factor (N_c)	12
Multiplier (E_n)	1(for line) 2.5 (for chain)
Frictional Resistance (μ)	0.1
Pull out angle (Force angle)	45˚
Soil Properties	
Undrained shear strength (S_u)	2 kPa
Strength Gradient	1.6 /m
Sensitivity	1
Depth of Embedment	12 m

To predict the trajectory of a SEPLA during keying, the relative values of motions is essential. If a system is subjected to combined load at yield and assumed to obey the associated flow rule, then Prager (1959) showed that these forces can be assumed to be

generalized stresses. The plastic displacement as a result of these stresses can be assumed to be plastic strains. The normal and tangential velocity along with the angular velocity can be calculated by taking the partial derivative of the yield equation 3.19

$$v_n = \lambda \frac{\partial f}{\partial F_n} \tag{3.20}$$

$$v_n = \lambda \frac{q}{F_{n\,max}} \left(\frac{F_n}{F_{n\,max}} \right)^{q-1} \tag{3.21}$$

$$v_t = \lambda \frac{\partial f}{\partial F_t} \tag{3.22}$$

$$v_t = \lambda \frac{n}{p F_{t\,max}} \left(\frac{F_t}{F_{t\,max}} \right)^{n-1} \left[\left(\frac{M}{M_{\,max}} \right)^{m} + \left(\frac{F_t}{F_{t\,max}} \right)^{n} \right]^{\frac{1}{p}-1} \tag{3.23}$$

$$\beta = \lambda \frac{\partial f}{\partial M} \tag{3.24}$$

$$\beta = \lambda \frac{m}{pM_{max}} \left(\frac{M}{M_{max}}\right)^{m-1} \left[\left(\frac{M}{M_{max}}\right)^{m} + \left(\frac{F_t}{F_{t\,max}}\right)^{n}\right]^{\frac{1}{p}-1} \quad (3.25)$$

3.3 Anchor Chain Tension

The load applied on the floating unit is transferred to the anchor through the anchor chain which runs through the water body and inside the ocean floor to the embedment depth of the padeye. The chain can be several thousand feet in length. The geometry of the chain will change inside the water and the hence the angle of force application on the surface of water will not be the same as that on the padeye of the SEPLA. The difference in these angles of force application will also result in different chain tension on the surface of the water and at the padeye. A solution to this problem was provided by Neubecker and Randolph (1995) by linearizing the equations proposed by Vivaret et al, (1982) helped to calculate the anchor line tension and geometry in uniform strength soils and soils with uniform strength gradient which were validated by laboratory tests. Aubeny et al. (2005, 2008) combined the chain solutions to predict the capacity and trajectory of anchors (Chi 2010). The chain solutions were used to calculate the angle at the padeye and the bearing factors obtained using the upper bound solutions as shown in equations 3.11-3.14 were used in the prediction.

An anchor chain segment with length ds and tension T acting at the centroid of section is shown in figure 3.8. The normal and tangential resistances offered by the soil are Q and F respectively in the normal and tangential directions and the self-weight of the chain is given by W (Chi 2010)

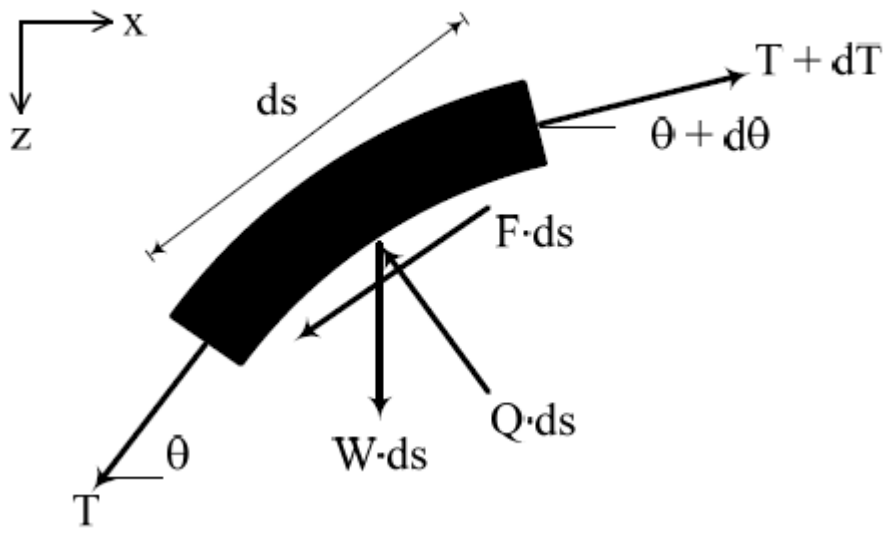

Figure 3.8 Cross Section of a Chain Element at Equilibrium (Courtesy, Chi 2010)

Since the element is in the state of equilibrium, the forces acting on the elements can be resolved in normal and tangential directions to obtain the equilibrium equations as shown (Chi 2010):

$$\Sigma F_n = 0 \rightarrow T\frac{d\theta}{ds} + Q - w\cos\theta = 0 \tag{3.26}$$

$$\Sigma F_t = 0 \rightarrow \frac{dT}{ds} - F + w\cos\theta = 0 \tag{3.27}$$

For any element with a frictional coefficient of friction μ, the normal and the tangential forces can be written as

$$F = \mu Q \tag{3.28}$$

where

μ is the frictional coefficient (0.1-1.5)

Chi (2010) showed that by substituting the equations 3.26 and 3.27 in 3.28 will result in the following equation

$$\frac{d}{ds}\left(Te^{\mu\theta}\right) = we^{\mu\theta}(sin\theta + cos\theta) \tag{3.29}$$

The self-weight of the section is negligible compared to the soil resistance on the section. So the right hand side of equation 3.29 will not exist.

$$\frac{d}{ds}\left(Te^{\mu\theta}\right) = 0 \tag{3.30}$$

Integrating 3.30 we get

$$\left(Te^{\mu\theta}\right) = C \tag{3.31}$$

where

C is a constant.

The tension and the angle of force application on the surface of the water are T_o and θ_o. The tension and the angle of force application will not be the same at the padeye of the SEPLA and are represented by T_a and θ_a. Substituting the value of tensions and angles in equation 3.31 will result in a tension relationship between the padeye and the surface (Chi 2010)

$$T_o e^{\mu\theta_o} = C = T_a e^{\mu\theta_a} \tag{3.32}$$

$$T_o = T_a e^{\mu(\theta_a - \theta_o)} \tag{3.33}$$

Equation 3.33 can be generalized for any T and θ as shown in equation 3.34

$$T = T_a e^{\mu(\theta_a - \theta)} \tag{3.34}$$

Substituting equation 3.34 in equation 3.26 and assuming the chain is weightless

$$(-T_a \sin\theta) e^{\mu(\theta_a - \theta)} \frac{d\theta}{dz} + Q = 0 \tag{3.35}$$

Integrating this we get

$$\int_{\theta}^{\theta_a} T_a \sin\theta \, e^{\mu(\theta_a - \theta)} d\theta = \int_{z}^{D} Q dz \tag{3.36}$$

$$\frac{T_a}{1+\mu^2}\left[e^{\mu(\theta_a - \theta)}(\cos\theta) + (\mu \sin\theta)\right]\Big|_{\theta}^{\theta_a} = \overline{Q}\,(z)\Big|_{z}^{D} \tag{3.37}$$

$$\overline{Q}\,(D - z) = \frac{T_a}{1+\mu^2}\left[e^{\mu(\theta_a - \theta)}(\cos\theta + \mu\sin\theta) - (\cos\theta_a + \mu\sin\theta_a)\right] \tag{3.38}$$

where

D = depth of the padeye

z = incremental rise

$\bar{Q}$ = Average normal resistance of soil

The average normal resistance of the soil at a depth (D-z) is given by

$$\bar{Q}\,(D-z) = E_n b N_c \left(S_u + \frac{k(D-z)}{2}\right)(D-z) \tag{3.39}$$

where

E_n = chain bar diameter multiplier

N_c = bearing factor for anchor lines

b = chain diameter

S_u = undrained shear strength of the soil on the ocean floor

k = strength gradient of the soil

Equation 3.38 is used to estimate the padeye angle θ_a for a particular force angle θ_o on the surface of the water.

3.4 Trajectory Prediction

The load capacity of a SEPLA at any particular embedment depth can be calculated by using the equations 3.8-3.19. The prediction of the SEPLA trajectory requires advancing the anchor in a particular direction and evaluating its impact in other directions which is achieved by using equations 3.20-3.25. As discussed in the previous section, the interaction of chain is also critical in calculating the trajectory of the SEPLA. The actual

angle of force at the padeye is calculated and different tensions at the padeye and on the surface of the water are employed to predict the trajectory of the SEPLA.

3.4.1 Algorithm

The value of λ is constant in equations 3.20-3.25, so these equations can be compared for a particular angle of force application. The values of v_n, v_t and β are calculated by using equations3.21, 3.23 and 3.25. For a particular angle of force, v_n, v_t and β are compared and the term with the maximum value noted. The direction of motion of the anchor at this particular angle is governed by the maximum value.The anchor is advanced by a suitable value so that the approximation presented in equation 3.26 can be made.

$$\frac{d\beta}{dn} \approx \frac{\Delta\beta}{\Delta n} \tag{3.40}$$

The relative motions in the remaining directions can be calculated by using equations 3.41 and 3.42. If for example, the value of v_n is greater than v_t and β at a particular angle, then the SEPLA is assumed to be displaced (Δn) in the normal direction and the corresponding displacement in tangential direction (Δt) and the rotation (Δβ) caused due to this normal displacement is calculated.

$$\Delta t = \Delta n \frac{v_t}{v_n} \tag{3.41}$$

$$\Delta\beta = L_f \, \Delta n \frac{\beta}{v_n} \tag{3.42}$$

The increment in rotation Δβ provides the actual rotation that the SEPLA undergoes at this particular angle of force. This incremental rotation is the reflected in the fluke angle θ_f. If the SEPLA rotates by Δβ radians in the anticlock wise direction, then the fluke angle will be

$$\theta_{f\ new} = \theta_f - \Delta\beta \tag{3.43}$$

where

$\theta_{f\ new}$ = the new fluke angle after rotation.

The translation of the SEPLA is calculated in terms of incremental normal and tangential displacements as shown in equation 3.26. The normal and tangential displacements are converted to the horizontal and vertical displacements shown in equations 3.44 and 3.45.The total cumulative distance translated by the anchor from its initial position is denoted by s and is calculated as shown in equation 3.46.

$$\Delta x = \Delta n \, sin\theta_f - \Delta t \, cos\theta_f \tag{3.44}$$

$$\Delta z = \Delta n \, cos\theta_f + \Delta t \, sin\theta_f \tag{3.45}$$

$$\Delta s = \sqrt{\Delta x^2 + \Delta z^2} \tag{3.46}$$

This new orientation of the fluke will change the angle of force at the centroid of the SEPLA (θ_{af}) which leads to changes the in the value of the N_e. The changes in N_e will again trigger the cycle of changes as shown by equations 3.20-3.28.

The tension T_a at the padeye can be calculated using equation 3.38. An anchor capacity curve is obtained as a function of angle of force at the padeye as shown in figure 3.9. Equation 3.11 is used to calculate the anchor capacity curve in terms of total anchor capacity F as a function of the angle of force application θ_a. The intersection of the two curves Ta vs. θ_a and F vs. θ_a produces a unique locus (T_a, θ_a) which represents the anchor chain tension and the angle of force at padeye for a given θ_o.

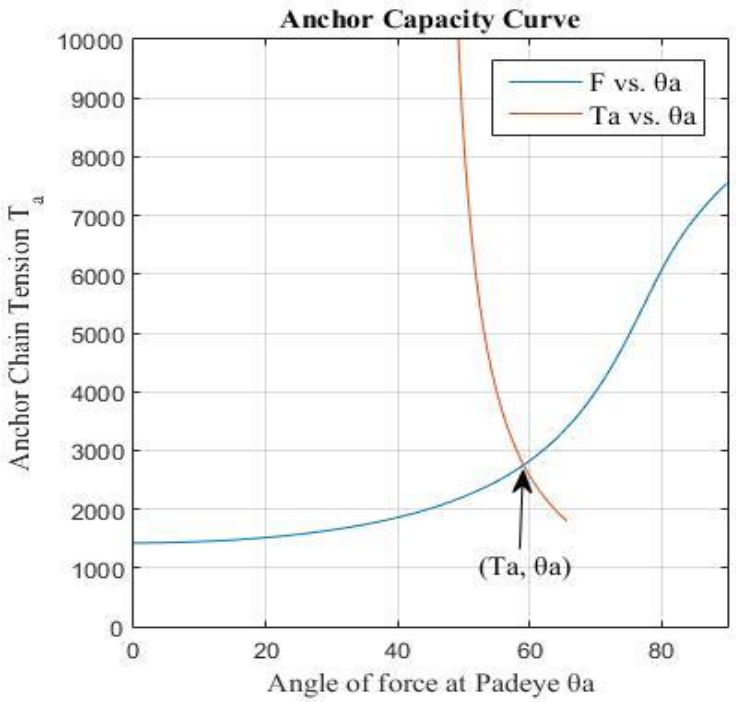

Figure 3.9 Anchor Capacity Curve to Calculate Ta and θa

A recursive algorithm which calculates the above mentioned parameters until the angle of force application is normal to the cross sectional area of the fluke is employed to evaluate the trajectory of the anchor. The cumulative value of the incremental displacements and rotations will provide the keying trajectory of a SEPLA. The algorithm used is shown below

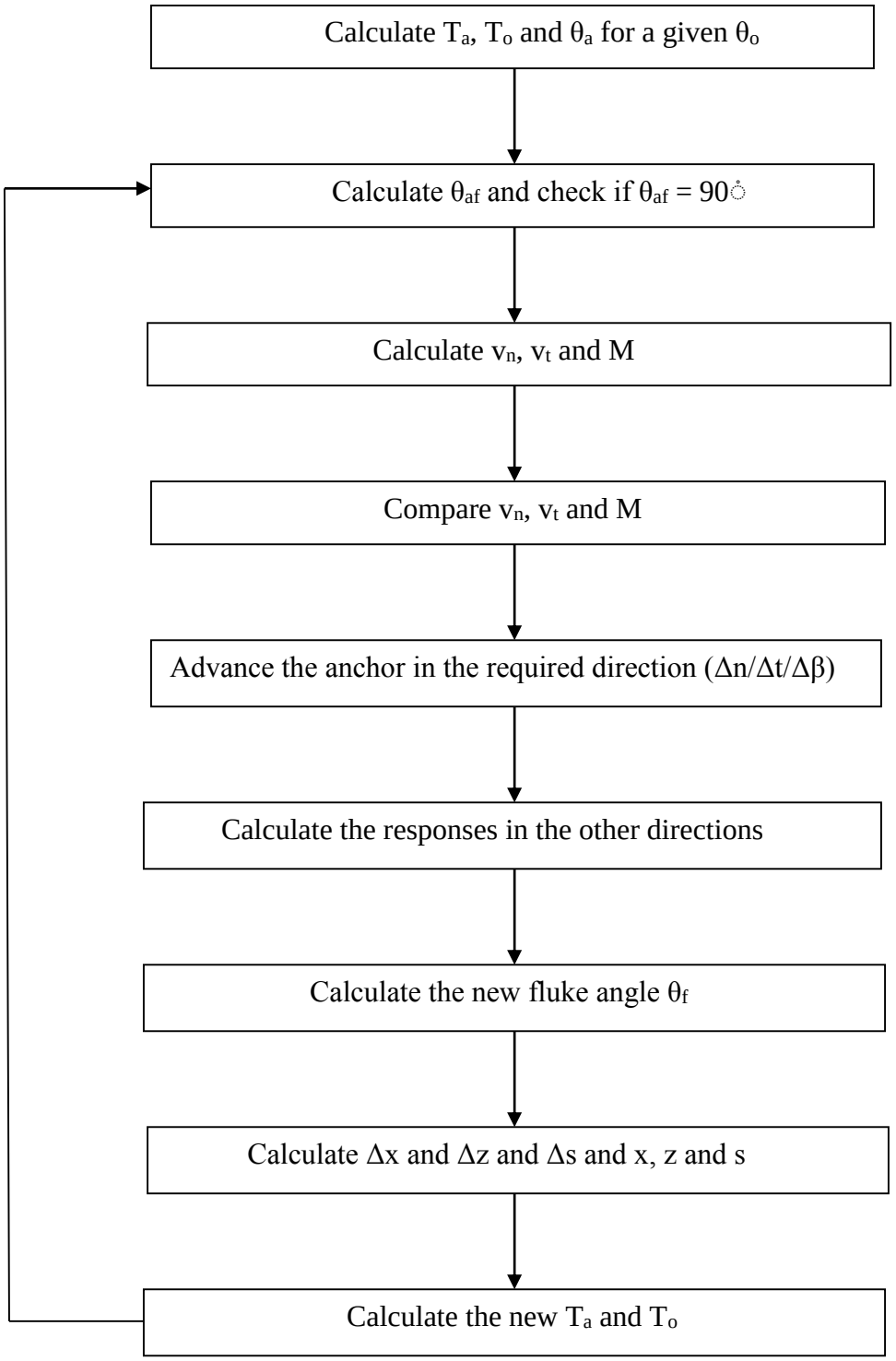

Figure 3.10 Algorithm of the program

3.4.2 Anchor Keying Trajectory Prediction

The algorithm explained in the previous section was used to predict the keying trajectory of a SEPLA whose parameters are listed in Table 3.2. The plots of keying trajectory, Bearing Factor, Tension at the padeye, the embedment loss and the locus of T_a, θ_a have been shown in figures 3.10-3.14.

The keying trajectory can be broadly classified into two stages. Initially the SEPLA rotates in the counter clockwise direction and moves tangentially (parallel) to the fluke of the anchor. The anchor moves backward and upward during this stage of motion (Yang et al 2012). As the fluke continues to rotate and becomes closer to being perpendicular to the applied force, the rotation and the tangential motion will start to diminish and after a particular point, the fluke starts move in the normal direction. In the second stage of the motion, the tangential movement and the rotation are insignificant compared to the motion in normal direction. During this stage, the anchor will move upward in the direction of force application. Figure 3.10 shows that the anchor will finally orient itself perpendicular to the angle of applied force indicating the mobilization of ultimate capacity.

Figure 3.13 sheds light on the rate of embedment loss during keying. It can be seen that the fluke starts to rotate from its initial orientation of 90˚ to the horizontal to about 39˚ to the horizontal. This indicates that θ_a is about 51˚ as the fluke is perpendicular to pullout angle. The linear part of the curve corresponds to the first stage of keying and the constant part of the curve corresponds to the second stage of the keying. During the first stage of keying, as the anchor rotates, the rate of embedment loss is constant. The loss of

embedment is proportional to the rate of rotation of the anchor. During the second stage of the motion the anchor does not rotate as it is nearly perpendicular to the pullout force. The anchor moves in the direction of the pullout angle until its perpendicular to the pullout angle and mobilizing the ultimate capacity.

Figures 3.11 and 3.12 shows the bearing factor and tension at the padeye of the anchor with respect to the cumulative distance of the keying trajectory.

A detailed parametric study of several parameters has been carried out in Chapter IV and the validation of the results obtained by comparing them to the available centrifuge tests and F.E models has been performed in Chapter V.

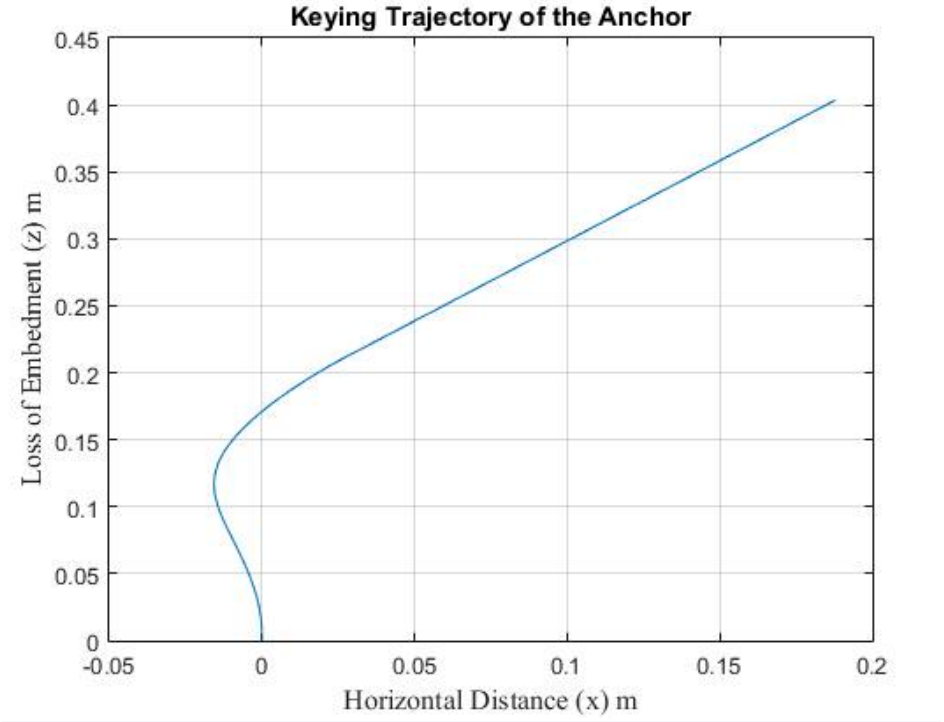

Figure 3.11 Keying Trajectory of the Anchor

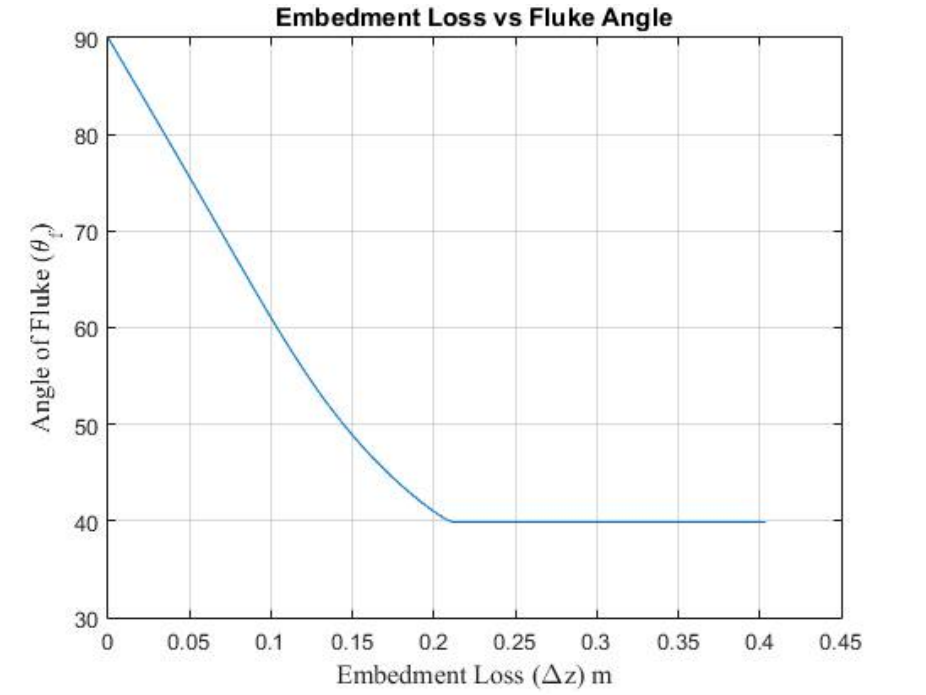

Figure 3.12 Bearing Factor vs. Cumulative Distance

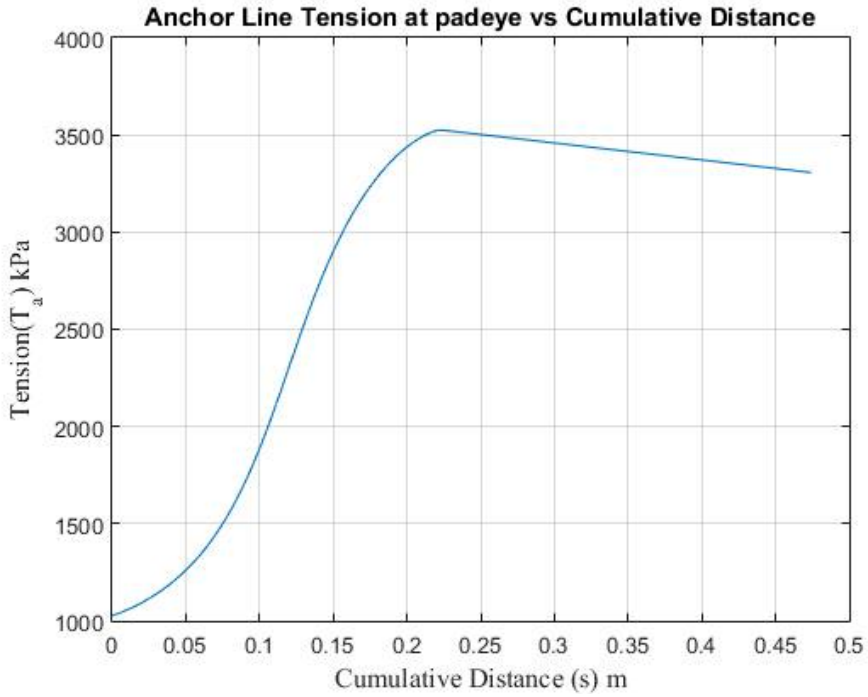

Figure 3.13 Anchor Line Tension vs. Cumulative Distance

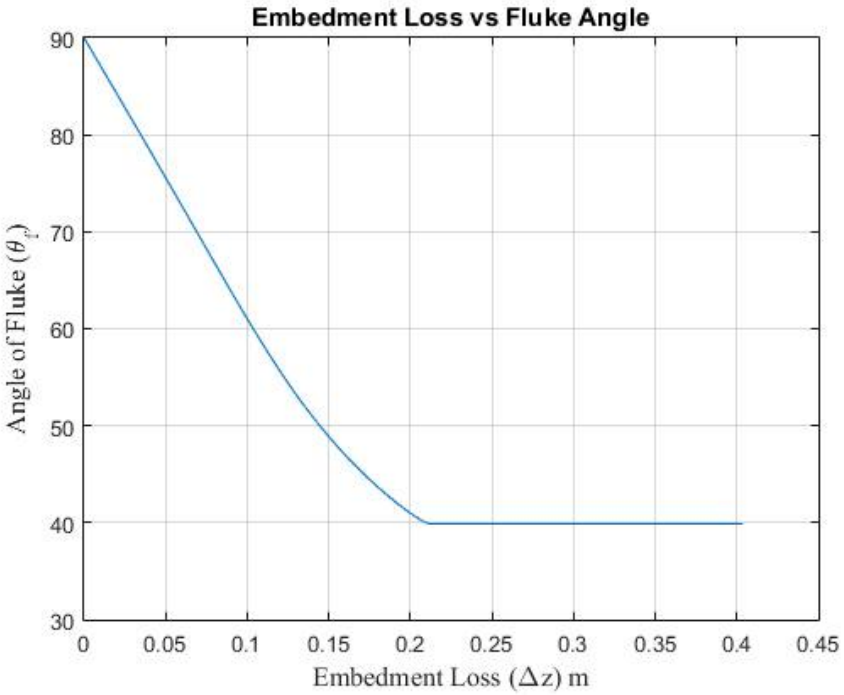

Figure 3.14 Embedment Loss of the Anchor vs. Fluke Angle

CHAPTER IV

PARAMETRIC STUDY OF THE KEYING TRAJECTORY

4.1 Parametric Study

The effects of various parameters on the keying trajectory are explored in this chapter. The main parameters that affect the keying trajectory can be broadly classified into 3 main groups: (1) Anchor geometry (2) Soil properties and (3) Anchor line properties. A detailed study of these properties will help in designing anchor and anchor chain that will result in the lowest possible embedment loss during keying for a given soil condition. An important parameter that dictates the keying trajectory of the anchor is the interaction coefficients used in the study. Table 3.1 contains coefficients derived by various researches. These coefficients have been derived for a particular combination of roughness (α_d) and thickness of the fluke (t_f), so these individually cannot be used for a parametric study. Equations 3.15, 3.16 and 3.17 a modified version of the equation suggested by O'Neill et al, (1999). The equations are functions of roughness (α_d) and thickness of the flange (t_f). The interaction coefficients suggested by Bransby and O'Neill (1999) suggested for thickness ratio (L_f/t_f) =7 and fully bonded condition (α_d=1) has been used along with equations 3.15-3.17. The results obtained from this assumption are not very accurate (over predicts the embedment loss by about 5%- 35%) but they provide a means to study the effect of each parameter on the keying trajectory. All the possible parameters relevant to the current geometry and the soil conditions have been explored

and the results obtained by the using the parameters derived by Wei et al, (2014) was found to be the most accurate.

The parametric study is carried out for the anchor, anchor line and soil properties mentioned in Table3.2 and the parameter under consideration is varied while the other parameters remain unchanged.

4.1.1 Anchor Geometry

The effects of normalized length, width and thickness of the fluke along with the length of the shank (eccentricity ratio of the load) have been performed.

4.1.1.1 Length of the Fluke (L_f)

The effect of length of fluke on keying trajectory, the embedment loss, tension at the padeye and bearing factor are shown in figures 4.1-4.4. The length of the fluke is varied while all the other parameters are held constant and a load eccentricity (L_s/L_f) of 0.5. If the length of the anchor changes, the length of the shank (L_s) and hence the eccentricity of the force also changes. From figures 4.1 and 4.2 it can be seen that as the length of the anchor increases, the embedment loss also increases. The changes in embedment depth however are not very significant. The increase in the length of the plate will result in a higher moment on the plate thus resulting in a higher rotation. The amount of backward movement also increase with the increase in length because of the higher moment on the anchor. The maximum capacity of the anchor increases with the length of the fluke. A higher fluke length will result in a higher area of the fluke which will help mobilizing more force leading to a higher ultimate- capacity.

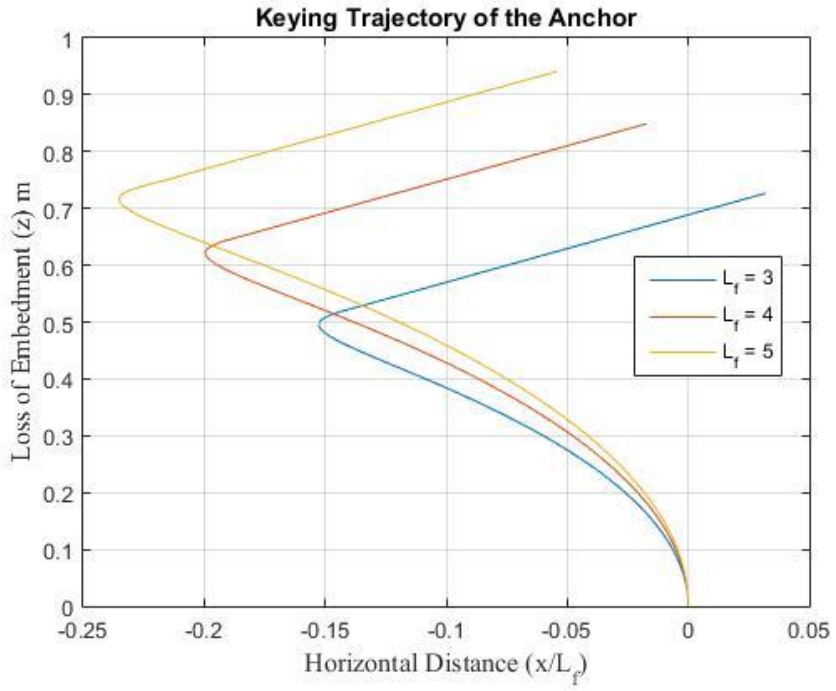

Figure 4.1 Effect of Fluke Length on Keying Trajectory

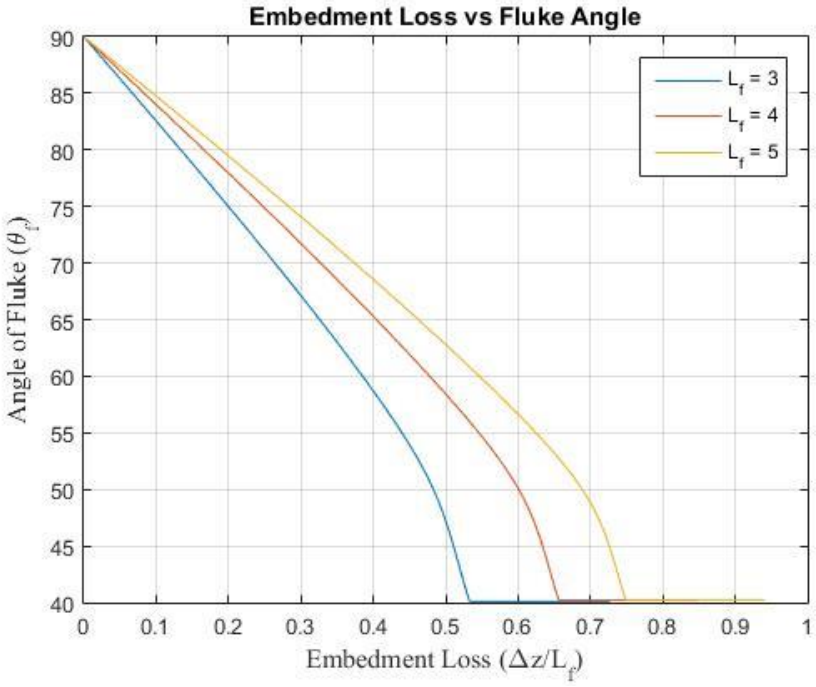

Figure 4.2 Effect of Fluke Length on the Embedment Loss

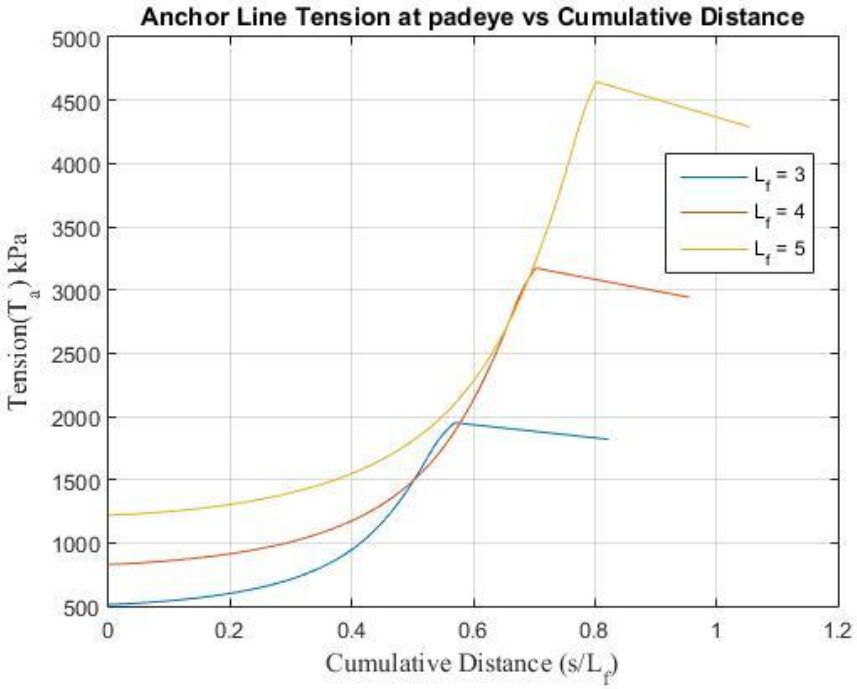

Figure 4.3 Effect of Fluke Length on the Tension Capacity

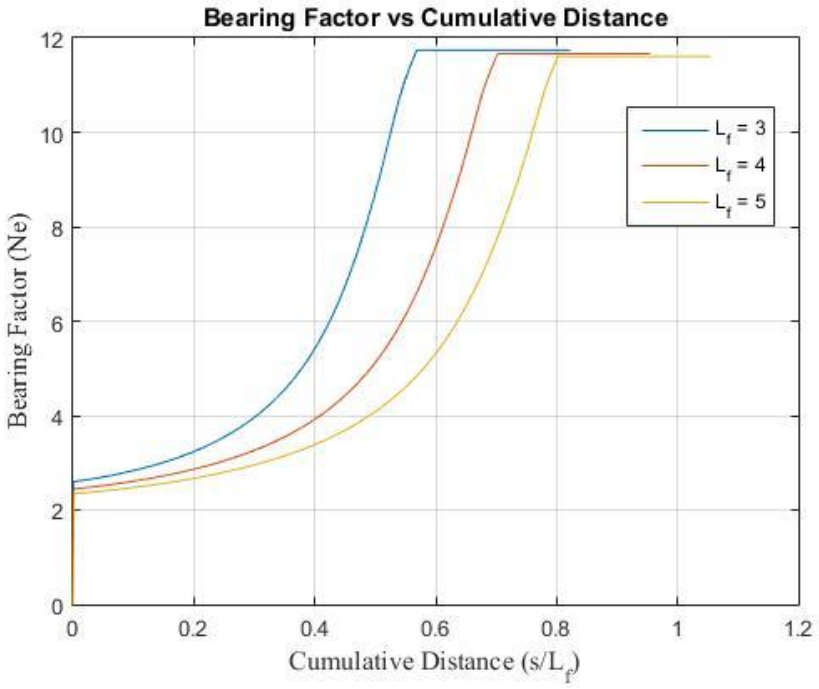

Figure 4.4 Effect of Fluke Length on the Bearing Factor

4.1.1.2 Width of the Fluke

The effect of width of fluke on keying trajectory, the embedment loss, tension at the padeye and bearing factor are shown in figures 4.5-4.8. The variation of width does not have a marked change in the embedment loss relative to the fluke length as seen in figures 4.5 and 4.6. However the width of the fluke has an inverse relationship with the embedment loss. As the width of the fluke increases, the embedment loss decreases slightly. The maximum capacity increases with the increase in the width as the area of fluke increases. The effect of a strip anchor is created by changing the width of the fluke to infinity. The embedment loss of a strip anchor is slightly lower than a rectangular anchor.

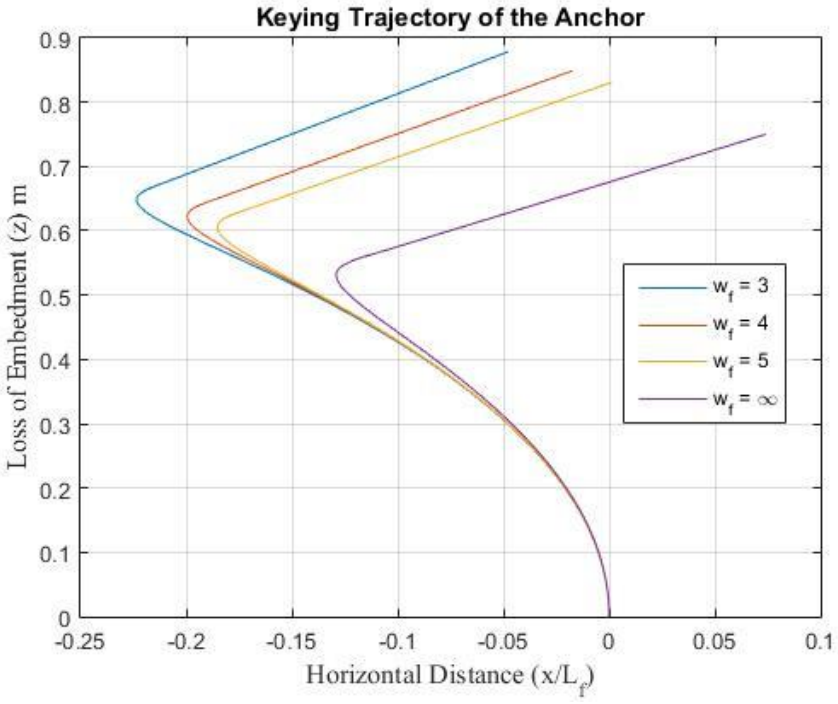

Figure 4.5 Effect of Fluke Width on the Keying Trajectory

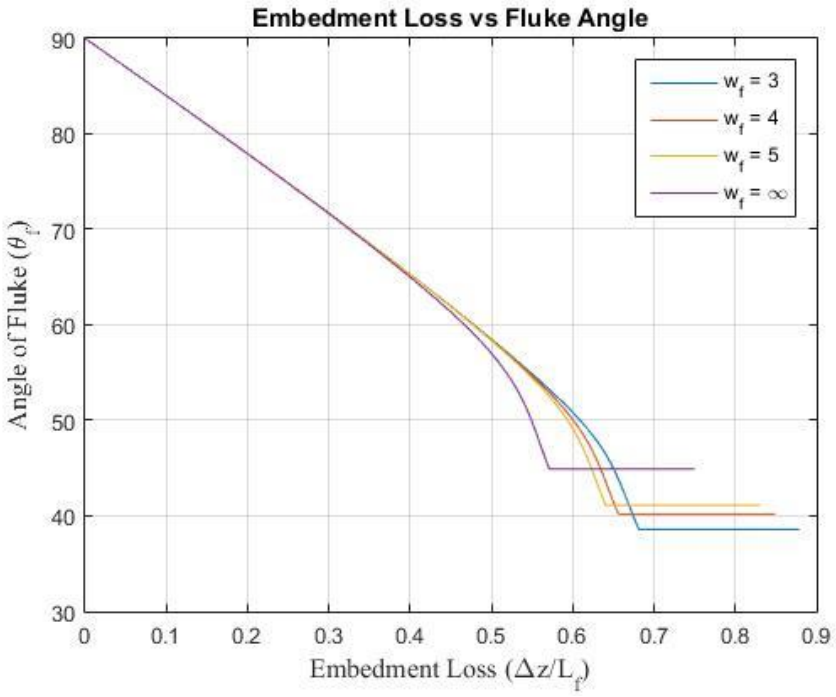

Figure 4.6 Effect of Fluke Width on the Embedment Loss

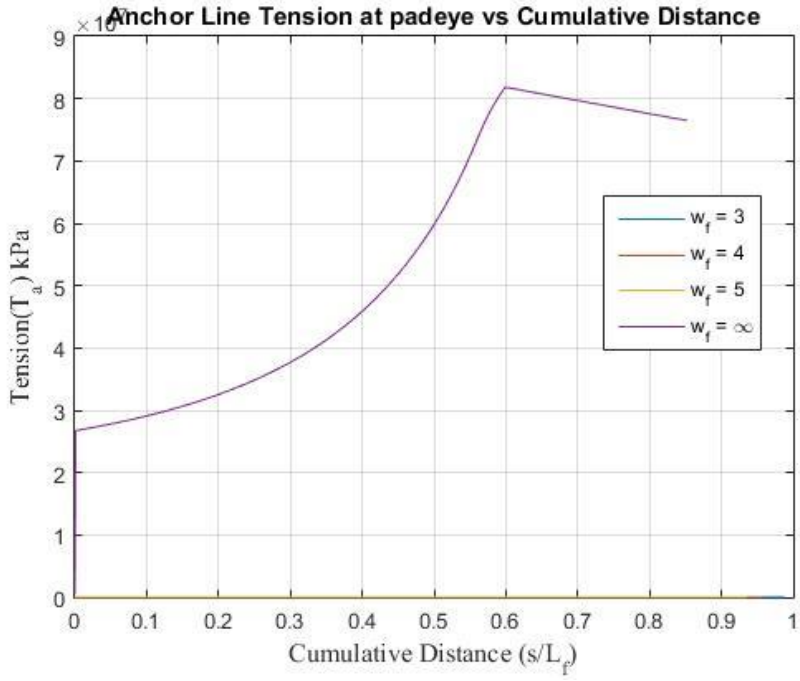

Figure 4.7 Effect of Fluke Width on the Tension Capacity

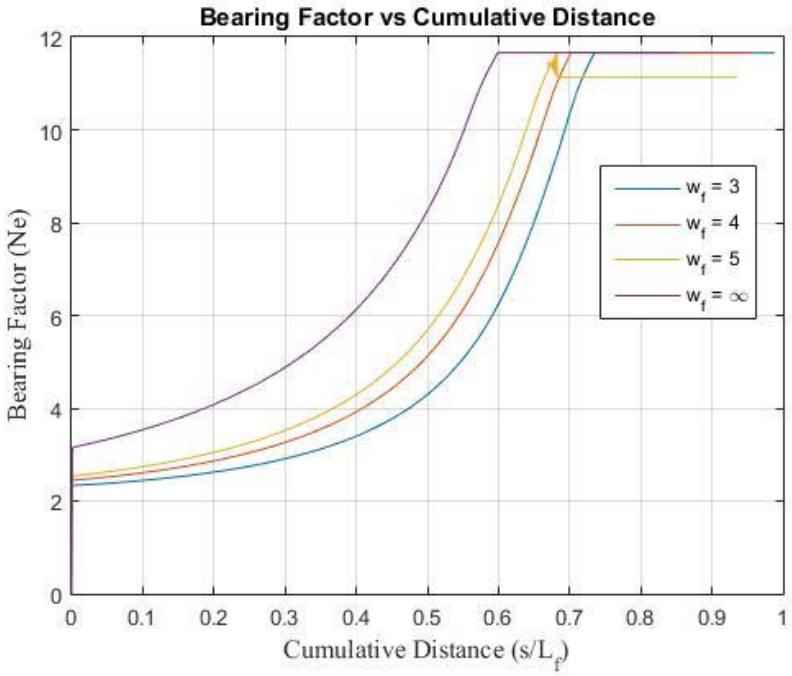

Figure 4.8 Effect of Fluke Width on the Bearing Factor

4.1.1.3 Fluke Area ($L_f \times w_f$)

The effect of fluke area on keying trajectory, the embedment loss, tension at the padeye and bearing factor are shown in figures 4.9-4.12. This is a combined effect of fluke length and fluke width. It is evident from figure 4.9 and 4.10 that an anchor length will result in a higher embedment loss than an anchor with a higher width. This also confirms the observation made in the previous section that the effect of width on the embedment loss is small compared to the effect of length. From figure 4.9 we can see that for a given fluke area, the anchor with the higher fluke length has a considerably higher embedment loss compared to the one with the higher width. The embedment loss for a square anchor for the two fluke lengths lies between the two extremities.

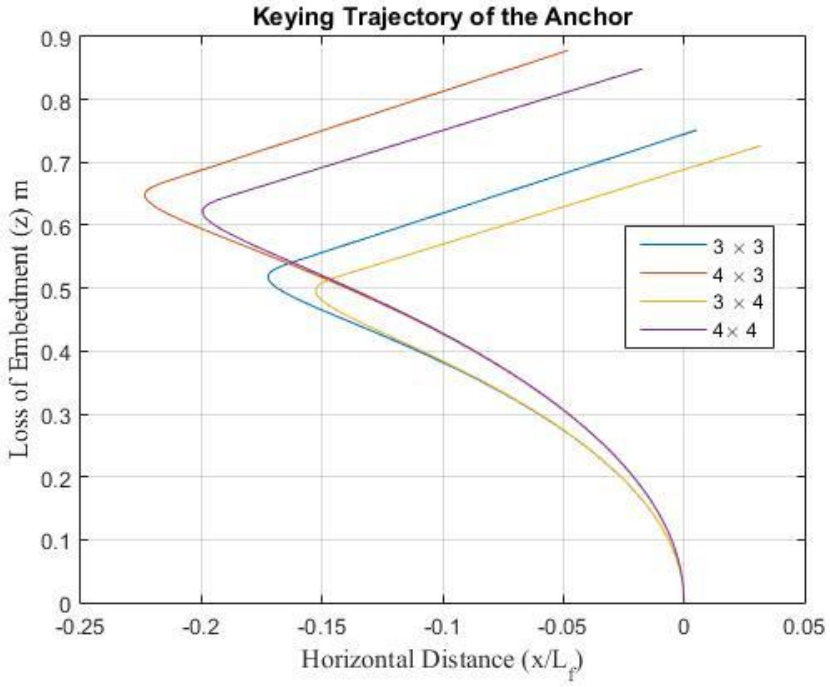

Figure 4.9 Effect of Fluke Area on the Keying Trajectory

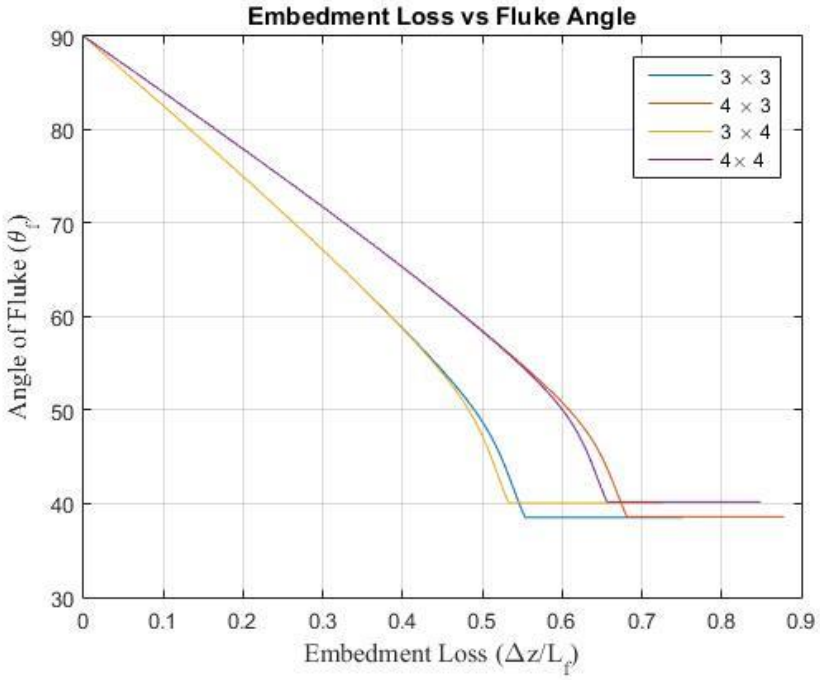

Figure 4.10 Effect of Fluke Area on the Embedment Loss

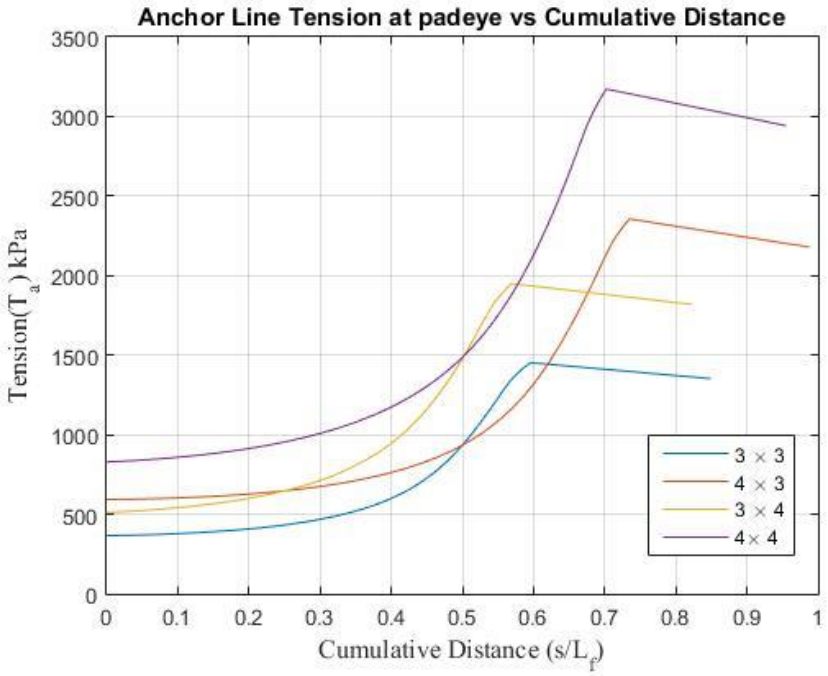

Figure 4.11 Effect of Fluke Area on the Tension Capacity

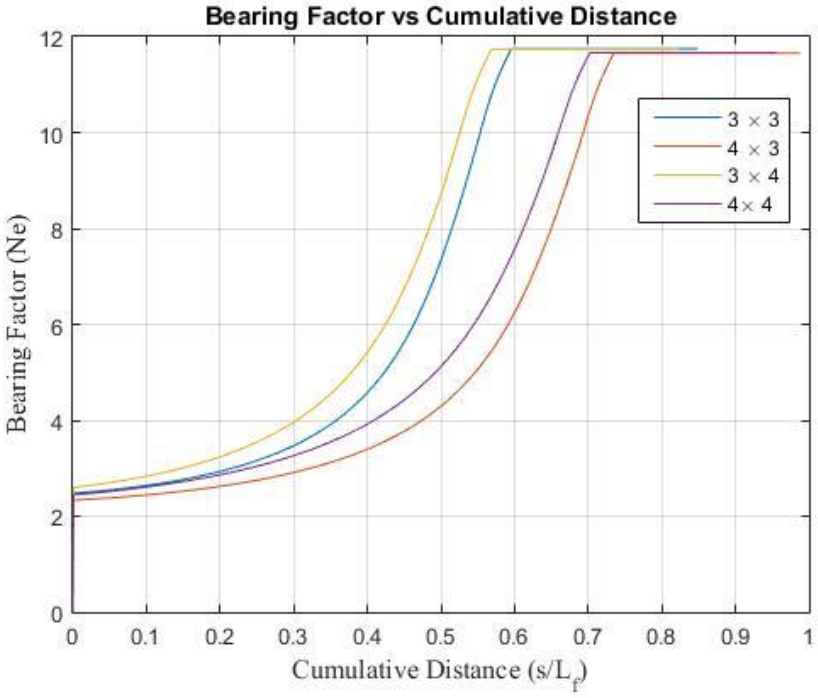

Figure 4.12 Effect of Fluke Area on the Bearing Factor

Figure 4.12 provides insight about the tension capacity of the anchors with different geometries of the fluke. It is interesting to see that for a given area, the anchor with the higher fluke length has the higher capacity. The length of the shank is a function of the fluke length ($0.5 \times L_f$). The increasing fluke length results in increasing shank length and hence increases the effective area of the anchor in contact with the soil which justifies the higher tension capacity for higher fluke length.

4.1.1.4 Aspect Ratio (L_f/w_f)

The effect of aspect ratio on the embedment loss, tension at the padeye and bearing factor are shown in figures 4.13-4.16. The study of different geometric aspect ratios help to compare the embedment loss of various plate anchors. The general anchor aspect ratio of SEPLA is L_f/w_f =1:2, the general configuration of PDPA is Lf/wf =2:1 and the general configuration of DEPLA is L_f/w_f =1:2. In this study the length of the fluke L_f was held constant (L_f = 4) and the width of the fluke was varied to study the embedment loss of different types of plate anchors. The effect of aspect ratio is a combined effect of the effect of length and the width of the flange. As the aspect ratio increases, the embedment loss also increases. Figure 4.13 shows the embedment loss of different types of plate anchors. It is observed that SEPLA has the lowest aspect ratio and hence the lowest embedment loss and the PDPAs have the highest embedment loss because of higher aspect ratio. The tension capacity of the PDPAs are higher than the tension capacities of SEPLAs and DEPLAs.

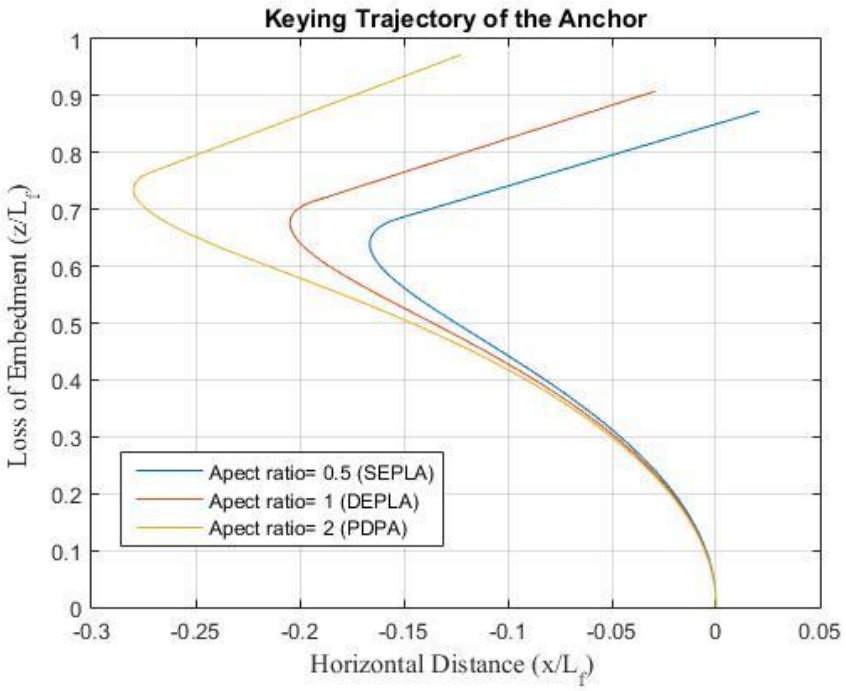

Figure 4.13 Effect of Aspect Ratio on the Keying Trajectory

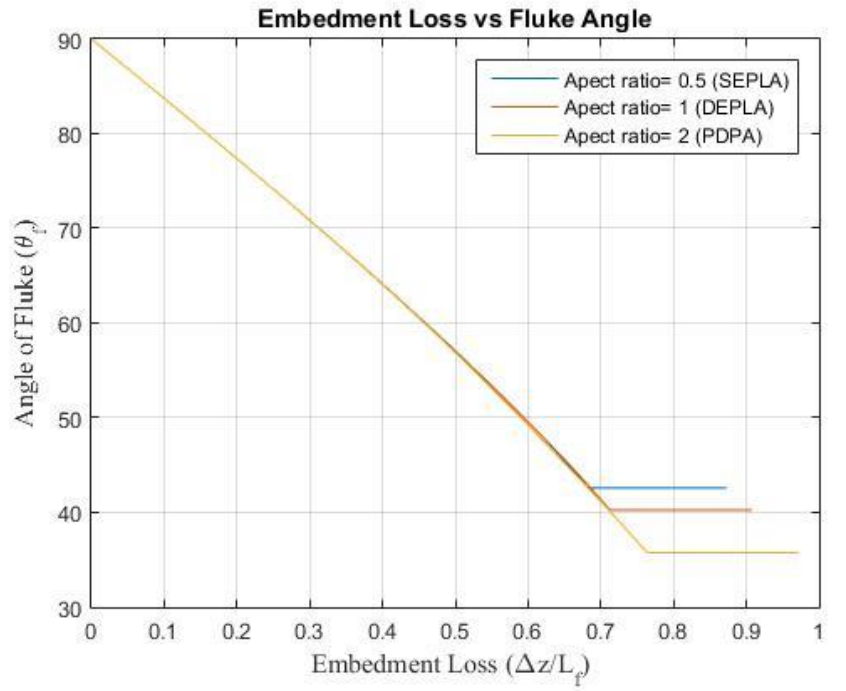

Figure 4.14 Effect of Aspect Ratio on the Embedment Loss

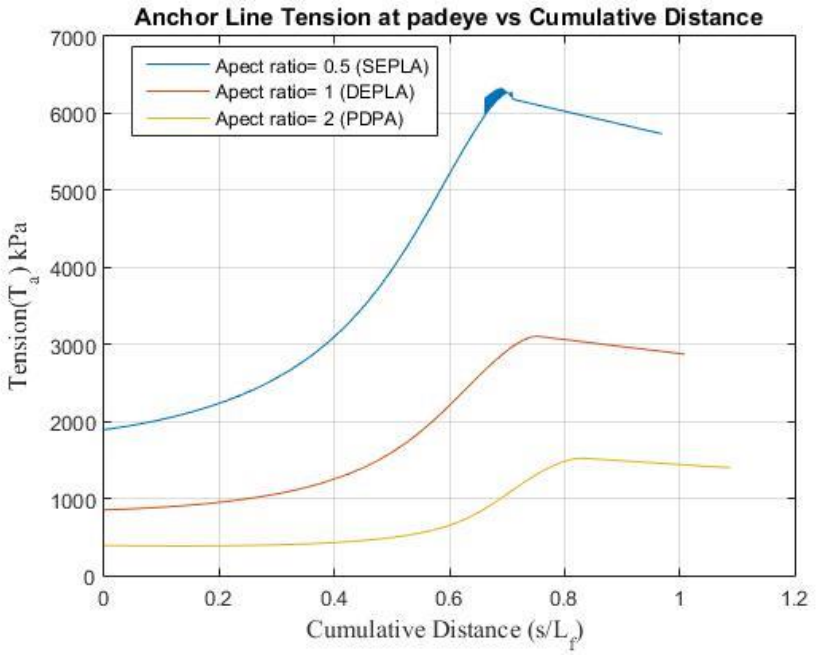

Figure 4.15 Effect of Aspect Ratio on the Tension Capacity

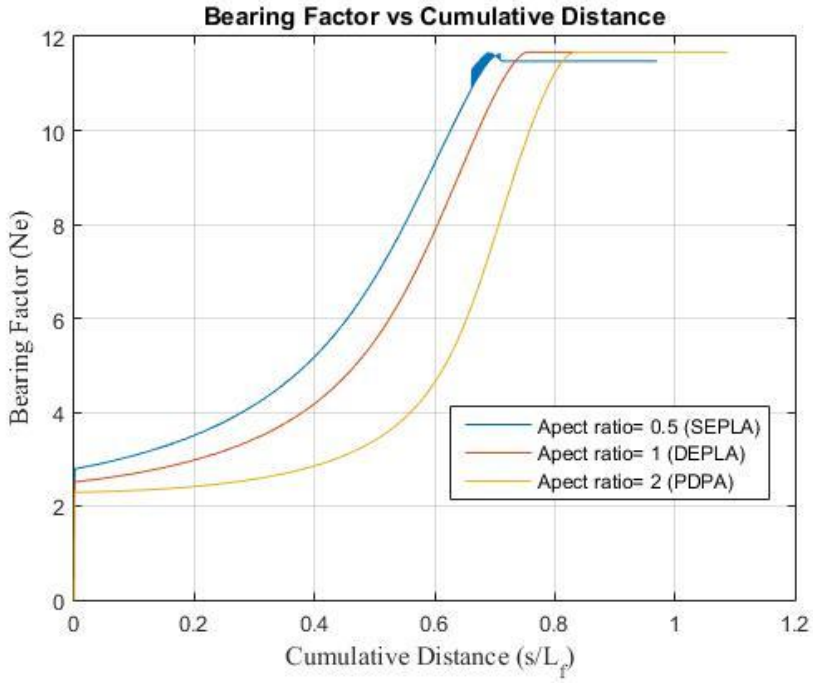

Figure 4.16 Effect of Aspect Ratio on the Bearing Factor

4.1.1.5 Thickness of the Fluke (t_f)

The effect of fluke thickness on keying trajectory, the embedment loss, tension at the padeye and bearing factor are shown in figures 4.13-4.16. The interaction parameters used in the analysis was derived for a thickness ratio of 7(L_f/t_f =7) by O'Neill and Bransby (1999). The same values have also been for other thickness ratios in this study. The values obtained in the plots for different embedment ratios will not be accurate but it will give an indication of the effect of thickness on various parameters. The thickness of the fluke is inversely proportional to the embedment loss. As the thickness of the fluke increases, the resistance to tangential movement also increases. Higher resistance to the tangential movement will lead to lower movement in the tangential direction resulting in lower loss of embedment. From Figure 4.13 it is evident that increasing the thickness of the fluke drastically decreases the embedment loss. The capacity of the anchor has a liner relationship with the anchor thickness. As the thickness decreases, the total contact surface of the anchor with the soil reduces thus resulting in a lower tension capacity.

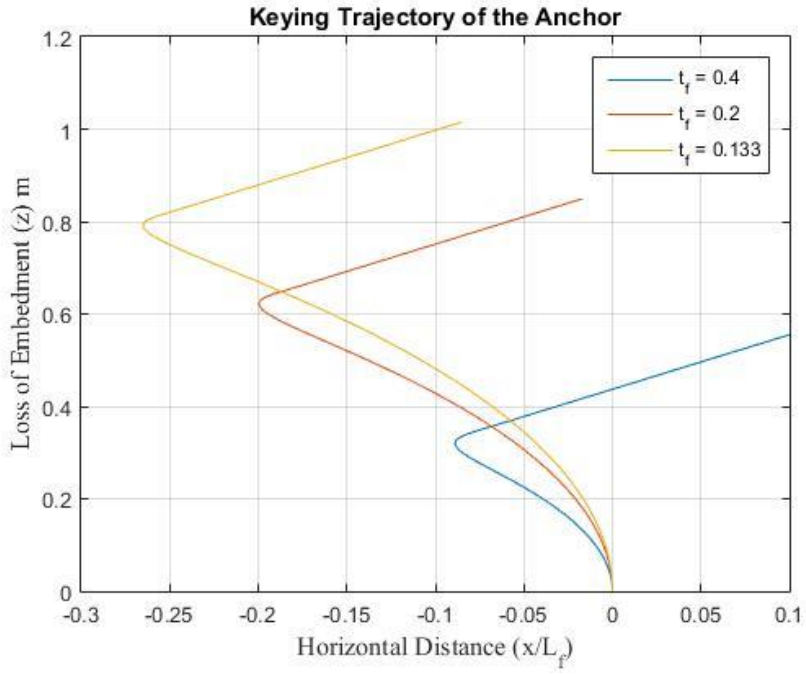

Figure 4.17 Effect of Thickness on the Keying Trajectory

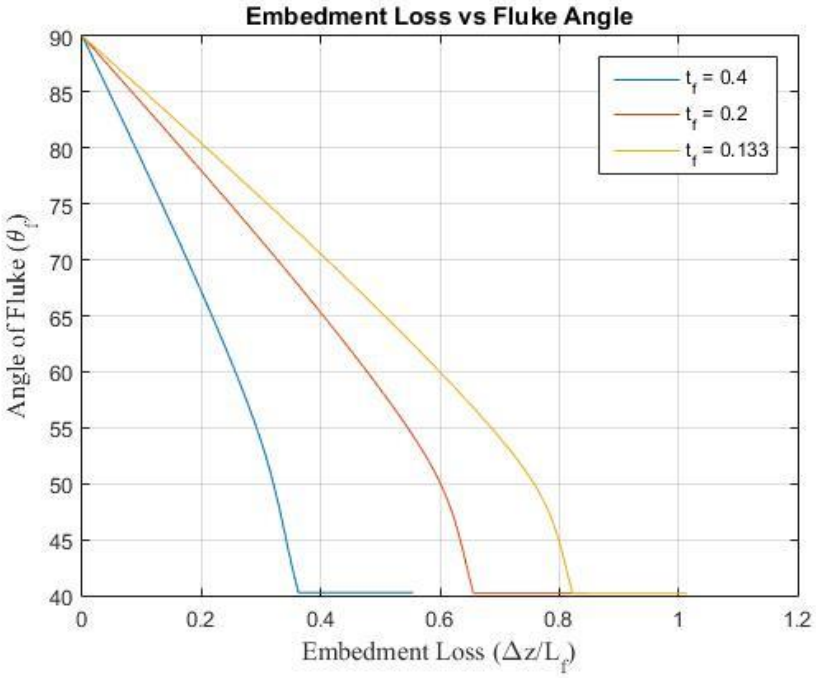

Figure 4.18 Effect of Thickness on the Embedment Loss

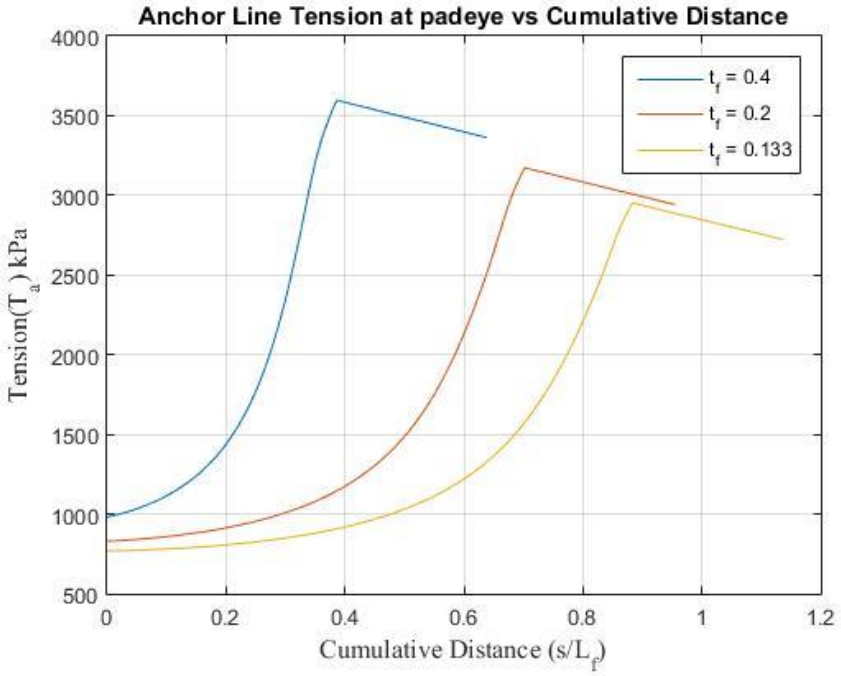

Figure 4.19 Effect of Thickness on the Tension Capacity

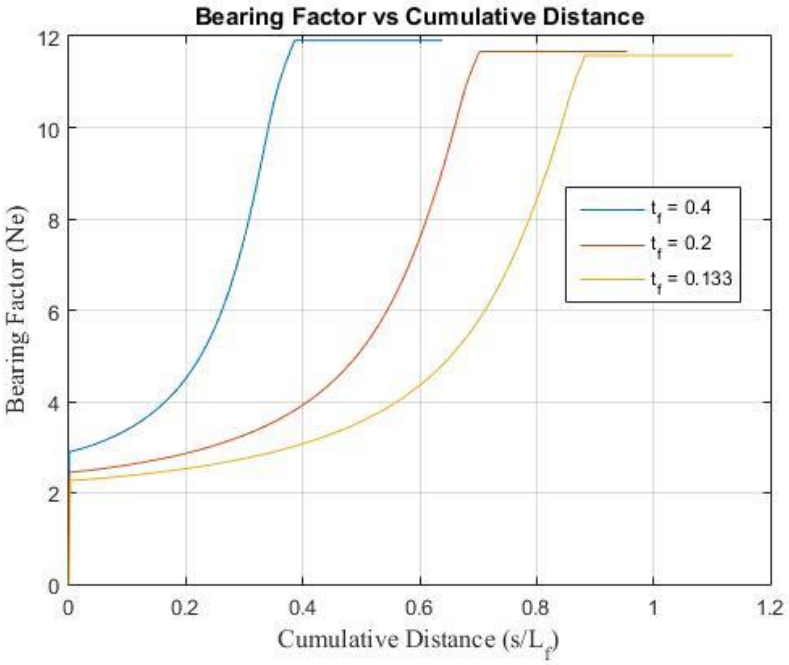

Figure 4.20 Effect of Thickness on the Bearing Factor

4.1.1.6 Shank Length/Load Eccentricity (e_s/L_f)

The effect of load eccentricity on keying trajectory, the embedment loss, tension at the padeye and bearing factor are shown in figures 4.17-4.20. The eccentricity of the load at the padeye has a very considerable effect on the keying trajectory. The keying trajectory of the anchor for e_s/L_f = 0.17, 0.5, 1, 1.5 have been predicted. The embedment loss is very high at low eccentricity and reduces dramatically with increasing length of the shank. At lower eccentricity the anchor does not undergo any rotation which results in no backward motion as seen in figure 4.17. As the eccentricity increases, the amount of backward motion also increases. The effect of eccentricity on the loss of embedment becomes less significant over eccentricities of $e_s/L_f > 0.5$ and becomes almost negligible over $e_s/L_f>1$.

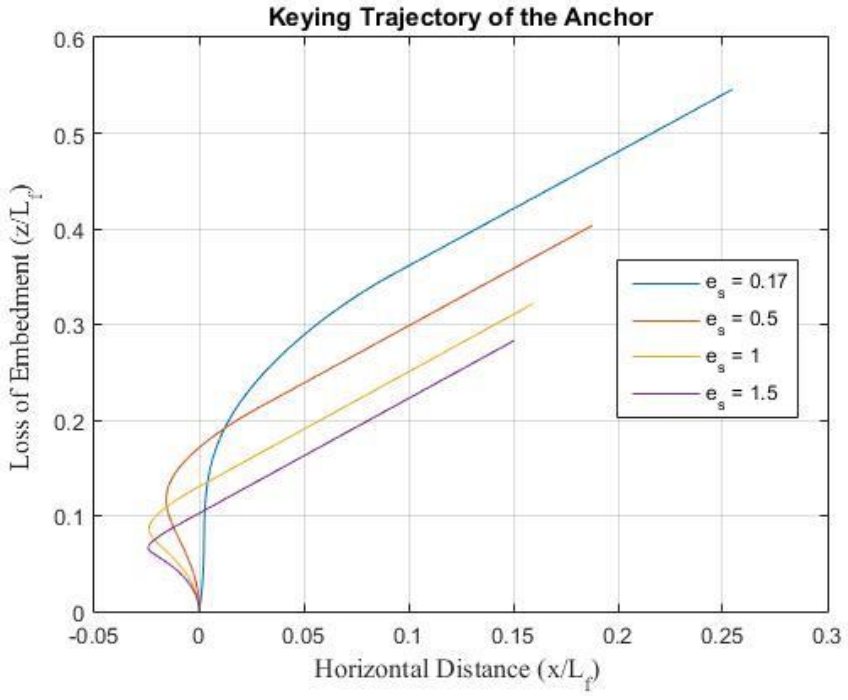

Figure 4.21 Effect of Eccentricity on the Keying Trajectory

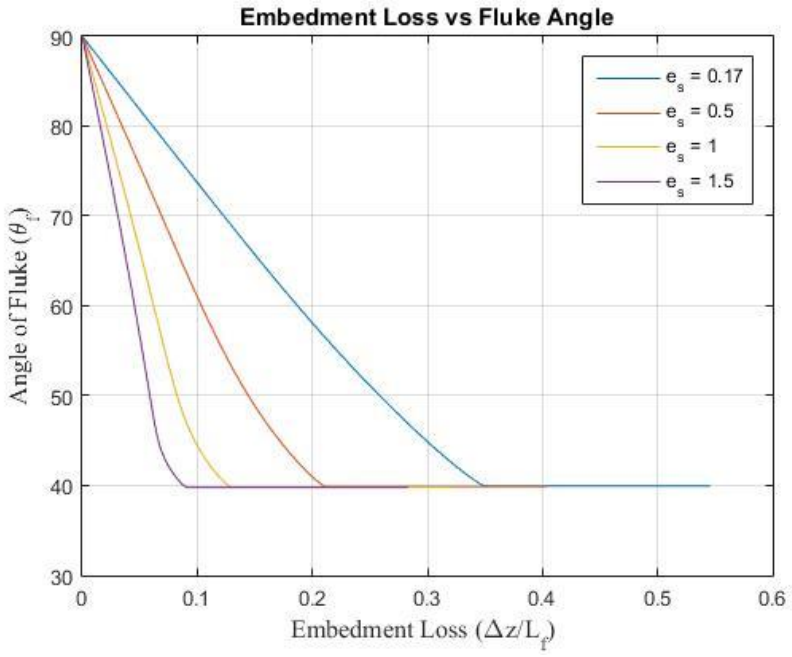

Figure 4.22 Effect of Eccentricity on the Embedment Loss

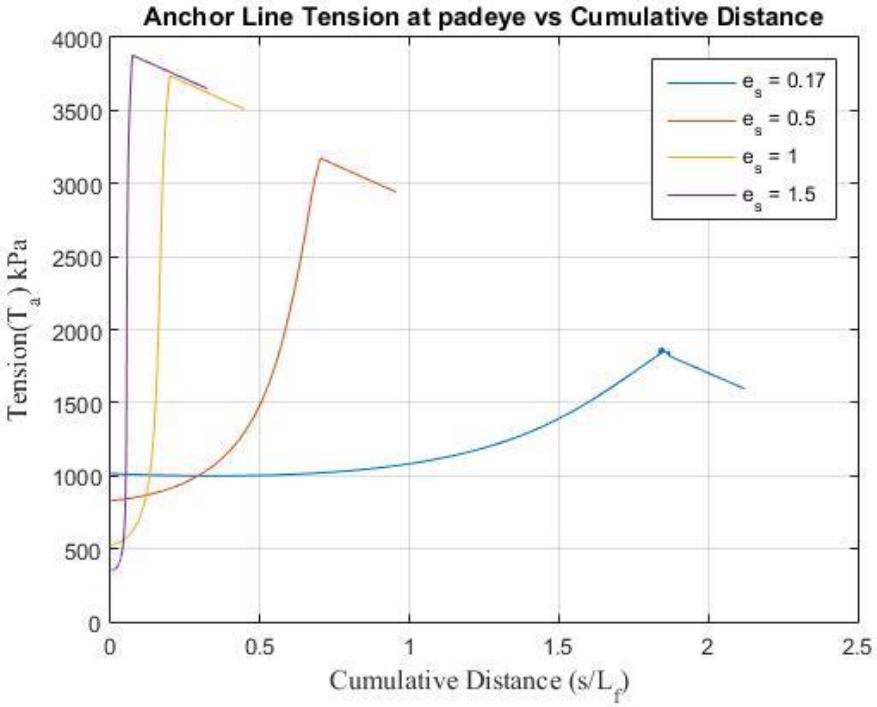

Figure 4.23 Effect of Eccentricity on the Tension Capacity

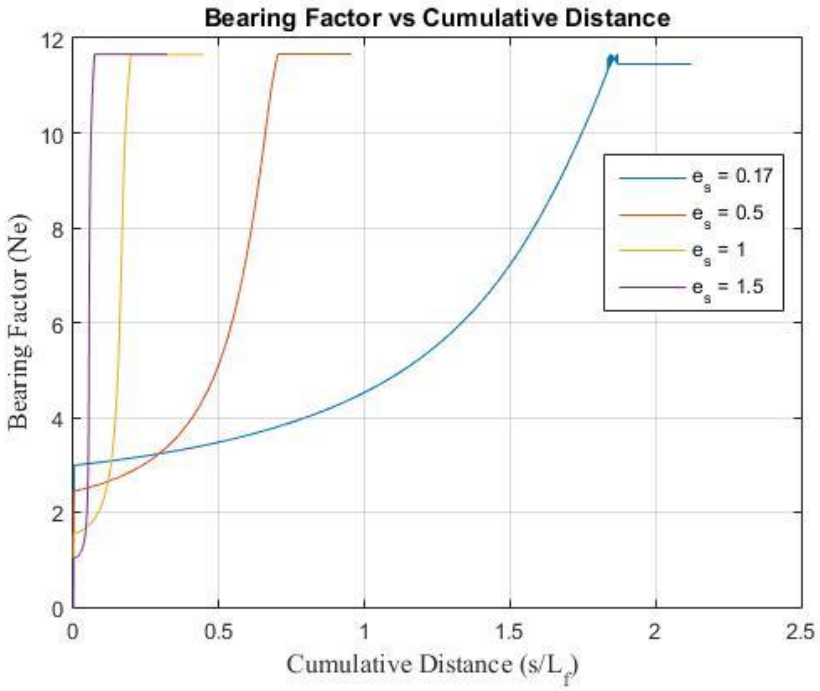

Figure 4.24 Effect of Eccentricity on the Bearing Factor

4.1.2 Anchor Line

The main features that are explored in this section are the angle of force application and the type of anchor line used for loading the anchor. The geometry of the model anchor is mentioned in Table 3.2.

4.1.2.1 Angle of Force Application / Pullout Angle (θo)

The pull out angle has the biggest impact on the keying trajectory. It is assumed that the pullout angle at the surface remains constant and the pullout angle at the padeye can be calculated using equation 3.38. The keying trajectory presented in this section is calculated for the pullout angle at the padeye. The effect of pullout angle on keying trajectory, the embedment loss, tension at the padeye and bearing factor are shown in figures 4.21-4.24. The keying trajectory for a wide range of pull out angles has been

calculated as shown in figure 4.21. The embedment loss also varies considerably with the pull out angle. The embedment loss decreases considerably for lower pullout angles because the anchor will have to rotate less to complete keying at lower pullout angles. The amount of backward movement also decreases considerably with lower pull out angles. The backward movement almost completely vanishes for very low pullout angles as shown in figure 4.21. The pullout angle at padeye (θa)is always found to be higher than the pullout angle at the surface (θo). The padeye pullout angle has an unusual behavior when loaded at 0˚ and 90˚. At 0˚ the padeye angle is about 21˚ and at 90˚ the padeye angle is also 90˚. All the angles that lie in-between the two limits show similar behavior. The padeye angles for 15˚, 30˚, 45˚, 60˚, and 75˚ are 26˚, 37˚, 50˚, 64˚ and 79˚. The tension capacity of the anchor also varies considerably with the pullout angle. Figure4.23 shows the variation of tension with different pullout angles. A major factor in calculating the tension capacity is the embedment loss during the keying process. Since the embedment loss is lower for lower pullout angles, the capacity is expected to be high. As expected the tension capacity for the anchors is higher at lower angles and decreases considerably for higher pullout angles.

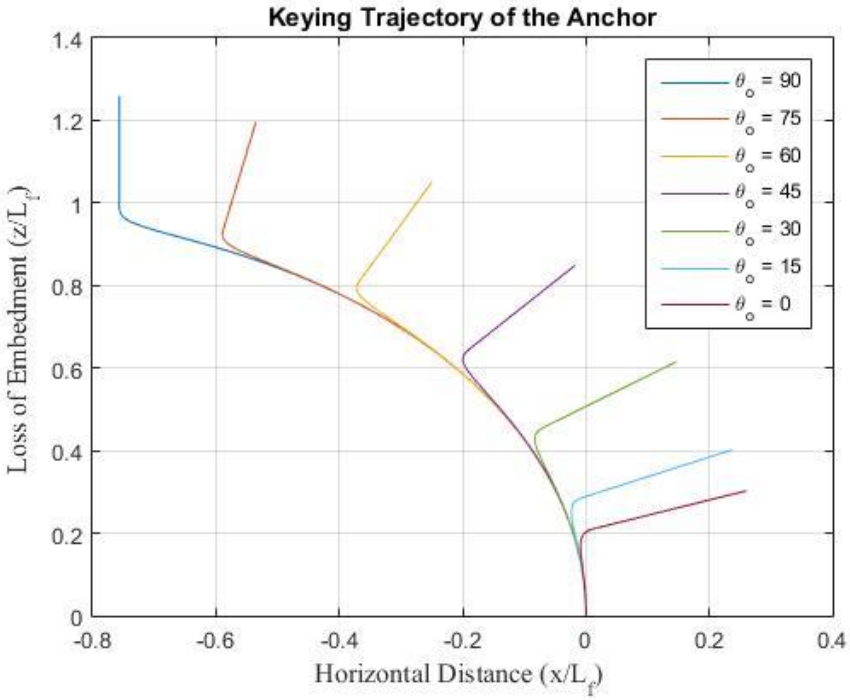

Figure 4.25 Effect of Pullout Angle on the Keying Trajectory

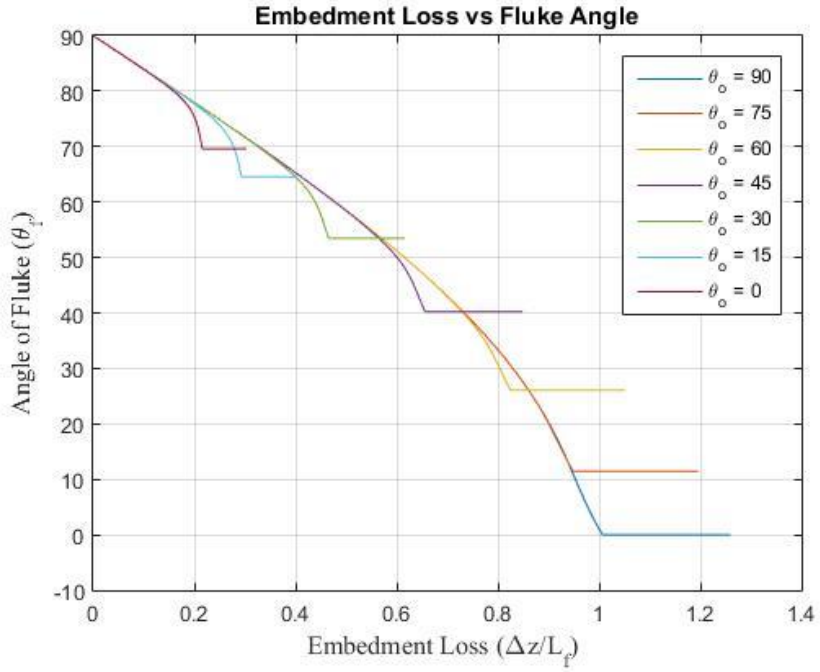

Figure 4.26 Effect of Pullout Angle on the Embedment Loss

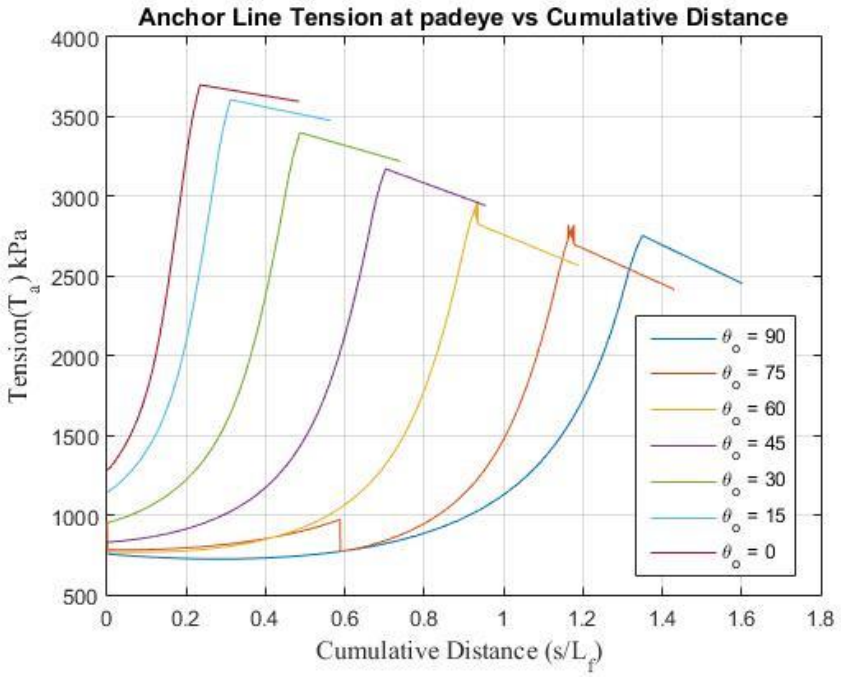

Figure 4.27 Effect of Pullout Angle on the Tension Capacity

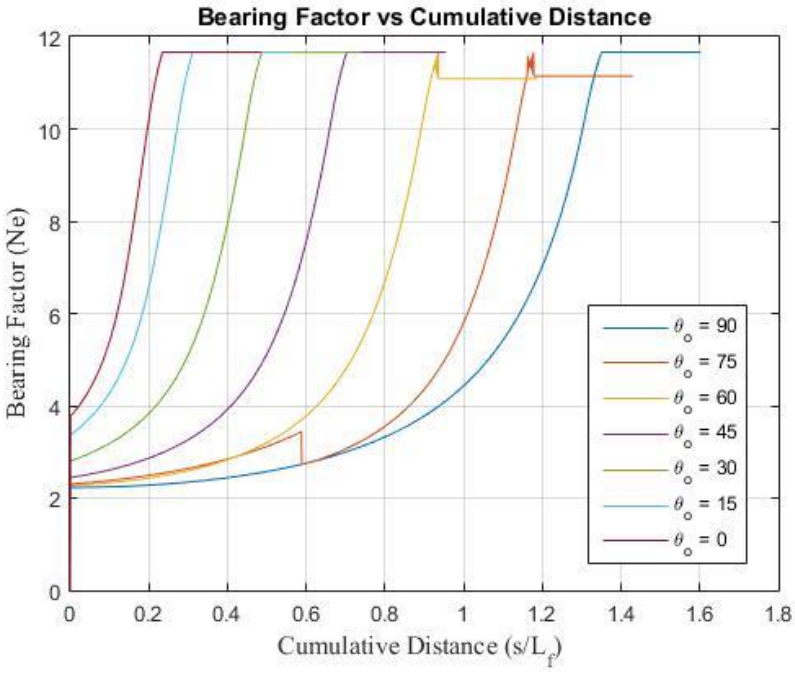

Figure 4.28 Effect of Pullout Angle on the Bearing Factor

4.1.2.2 Type of Anchor Line

The effect of type of anchor line is also found to have an impact on the trajectory of the anchor. The effect of chain and wire are explored in this section. The effect of anchor line on keying trajectory, the embedment loss, tension at the padeye and bearing factor are shown in figures 4.25-4.28. The embedment loss due to a wire is found to be less than the embedment loss due to a chain. This can be attributed to the fact that the pullout angle at the padeye for a chain is higher than that of a chain. The higher padeye angle will result in higher embedment loss as the anchor will have to undergo higher rotation to complete the keying process. The tension capacity for the case of chain is slightly higher as expected because of the lower pullout angle at the padeye.

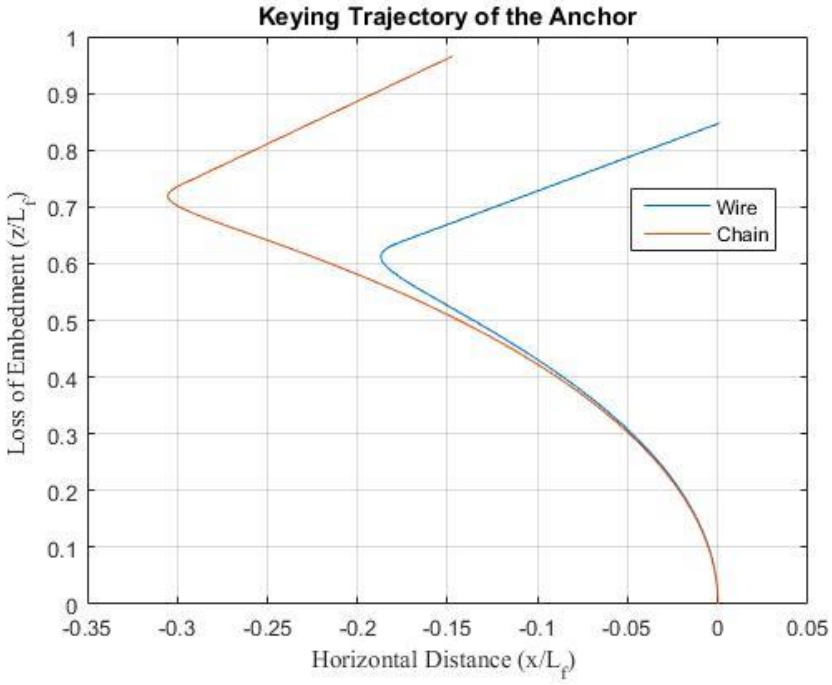

Figure 4.29 Effect of Anchor Line on the Keying Trajectory

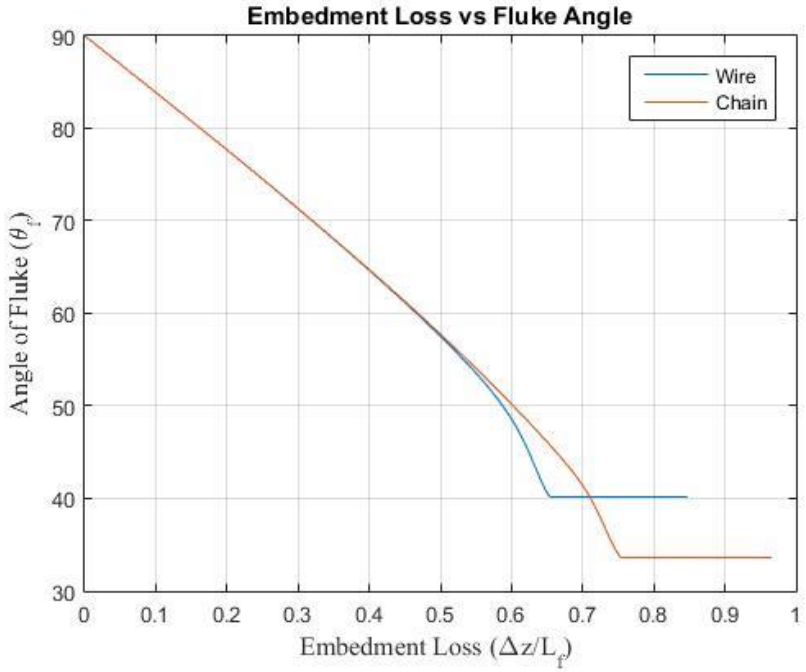

Figure 4.30 Effect of Anchor Line on the Embedment Loss

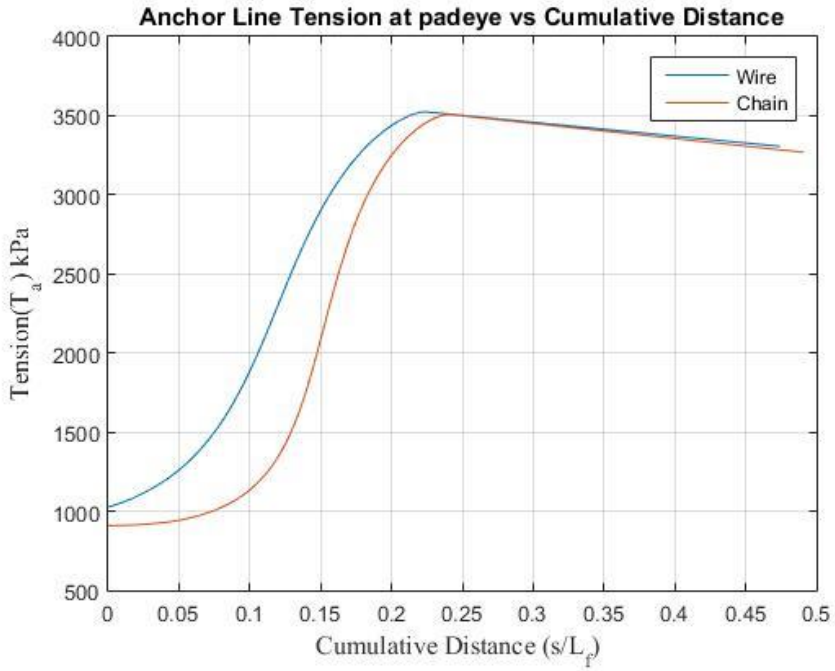

Figure 4.31 Effect of Anchor Line on the Tension Capacity

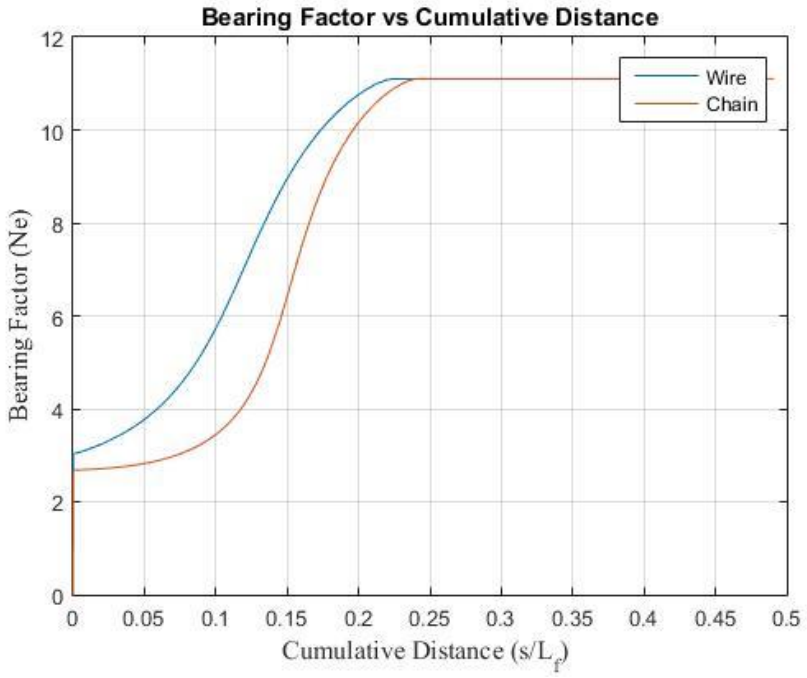

Figure 4.32 Effect of Anchor Line on the Bearing Factor

4.1.3 Soil Properties

The effect of sensitivity (S_t) of the soil and the strength of the soil are observed in this section. The effect of soil strength is studied by (1) varying the maximum shear strength (2) varying the strength gradient (k).

4.1.3.1 Sensitivity (S_t)

The study of sensitivity is important because it is directly related to the contact roughness coefficient (α_d) as shown in equation 4.1.

$$S_t = \frac{1}{\alpha_d} \tag{4.1}$$

So studying sensitivity is a valuable tool to understand the effect of roughness coefficients on the keying process. The values obtained are not accurate because the

interaction coefficients used are derived for a specific roughness coefficient. So this parametric study will provide a generic behavior of keying process to changing roughness coefficient. The effect of sensitivity on keying trajectory, the embedment loss, tension at the padeye and bearing factor are shown in figures 4.29-4.32. It can be seen that sensitivity affects the keying trajectory considerably. An increase in the sensitivity will lead to drastic increase in the embedment depth. The amount of backward motion also considerably increases for higher sensitivities. As the sensitivity increases, the contact roughness starts to decrease which results in lower holding capacity of the anchor. The contact between the anchor and the soil transitions from rough to smooth as the sensitivity increases. As a result of this, the plate will move freely through the soil when loaded and hence the backward motion and the embedment loss also increase substantially for higher sensitivity. Since the contact between soil and anchor decreases with higher sensitivity, the tension capacity of the anchor also decreases remarkably as with higher sensitivity seen in figure 4.31. The figures 4.29-4.32 suggest that sensitivity has the highest impact on the keying trajectory of the anchor. In order to confirm this behavior, more interaction coefficients for a variety of sensitivities should be developed as it will result in more accurate prediction of the keying process.

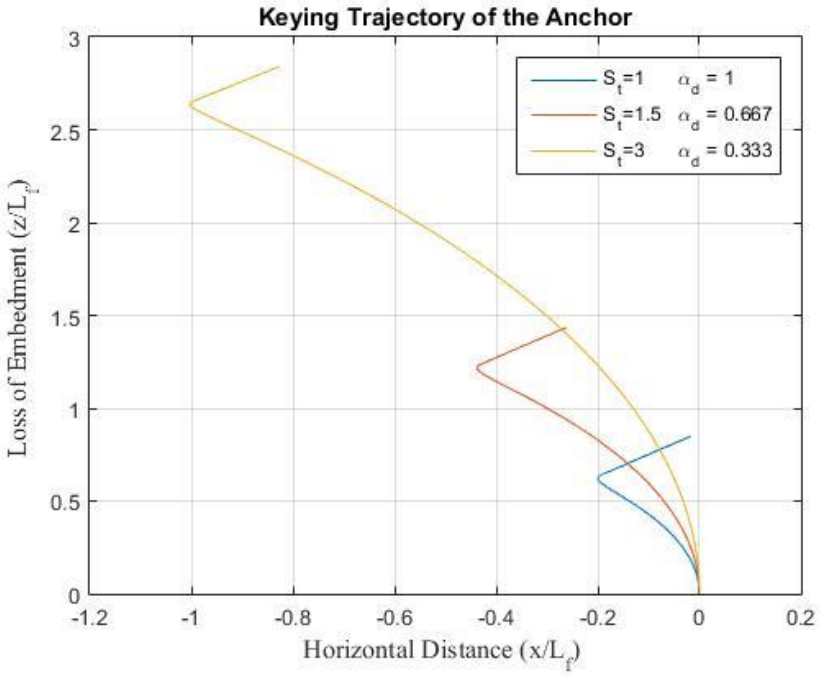

Figure 4.33 Effect of Sensitivity on the Keying Trajectory

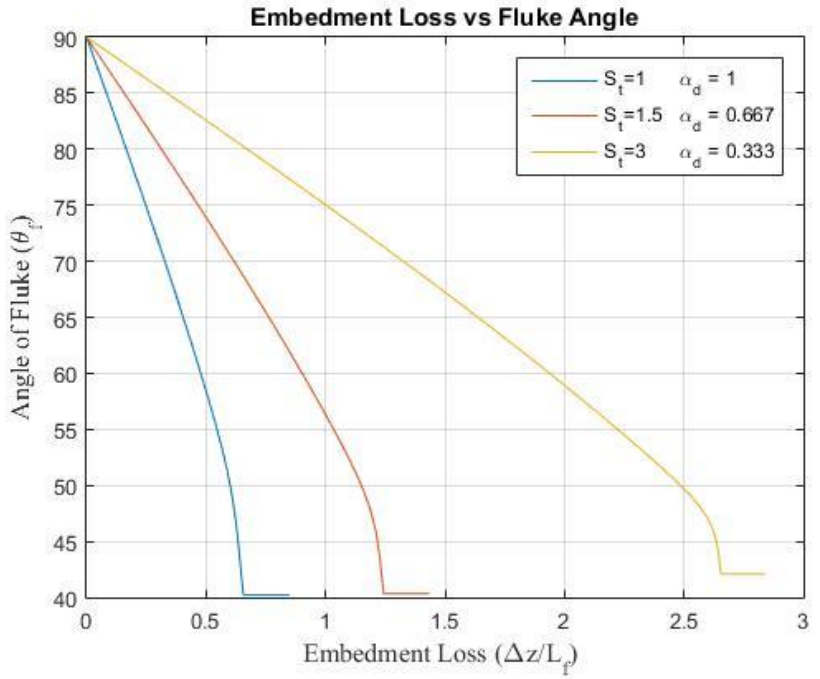

Figure 4.34 Effect of Sensitivity/Roughness on the Embedment Loss

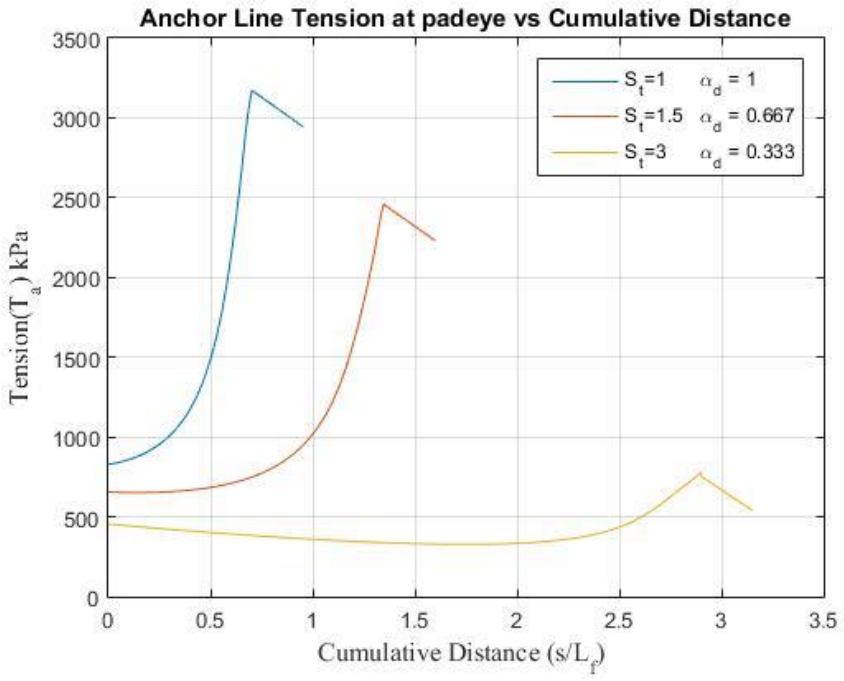

Figure 4.35 Effect of Sensitivity/Roughness on the Tension Capacity

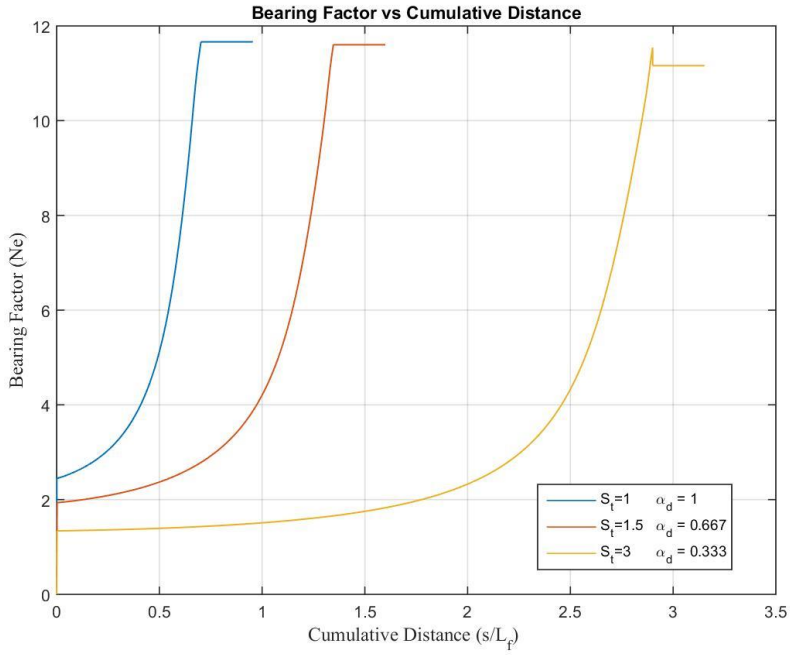

Figure 4.36 Effect of Sensitivity/Roughness on the Bearing Factor

4.1.3.2 Strength of Soil

The effect of strength of the soil on the keying trajectory is studied by (1) varying the maximum shear strength with constant strength gradient (2) varying the strength gradient with a constant shear strength. The effect of both the cases are provided below

4.1.3.2.1 Shear Strength (S_u)

The effect of shear strength on keying trajectory, the embedment loss, tension at the padeye and bearing factor are shown in figures 4.33-4.36. It can be seen that the shear strength has very negligible effect on the keying process. The keying trajectory and the embedment loss are have negligible changes with varying shear strength of the soil. As expected, the tension capacity of the anchor increases with higher shear strength as seen in figure 4.35.

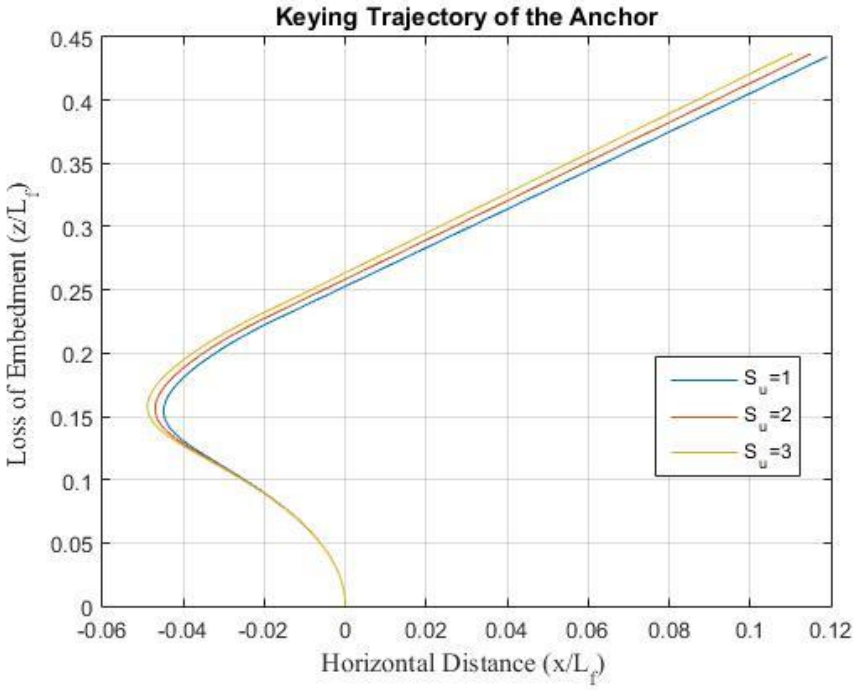

Figure 4.37 Effect of Shear Strength of Soil on the Keying Trajectory

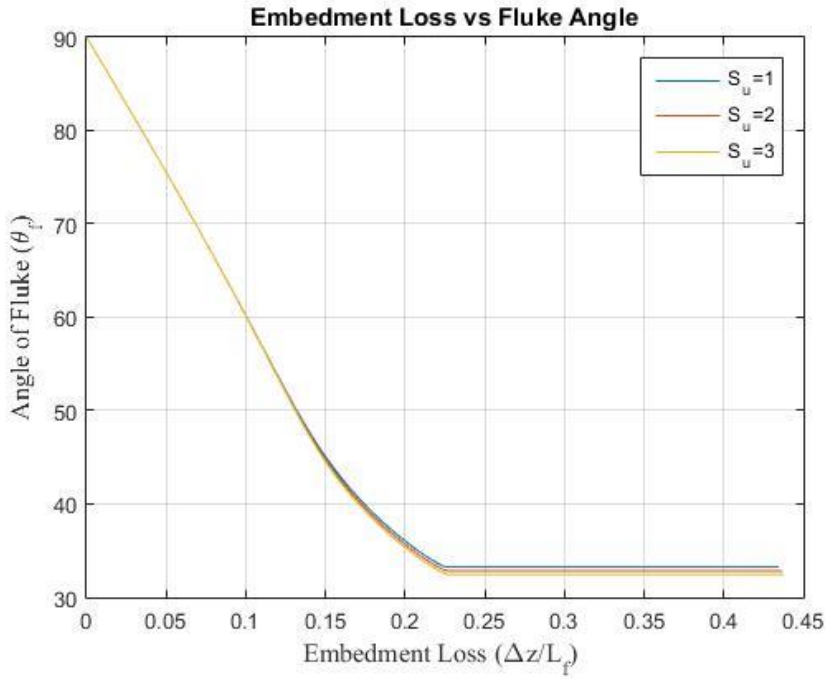

Figure 4.38 Effect of Shear Strength of Soil on the Embedment Loss

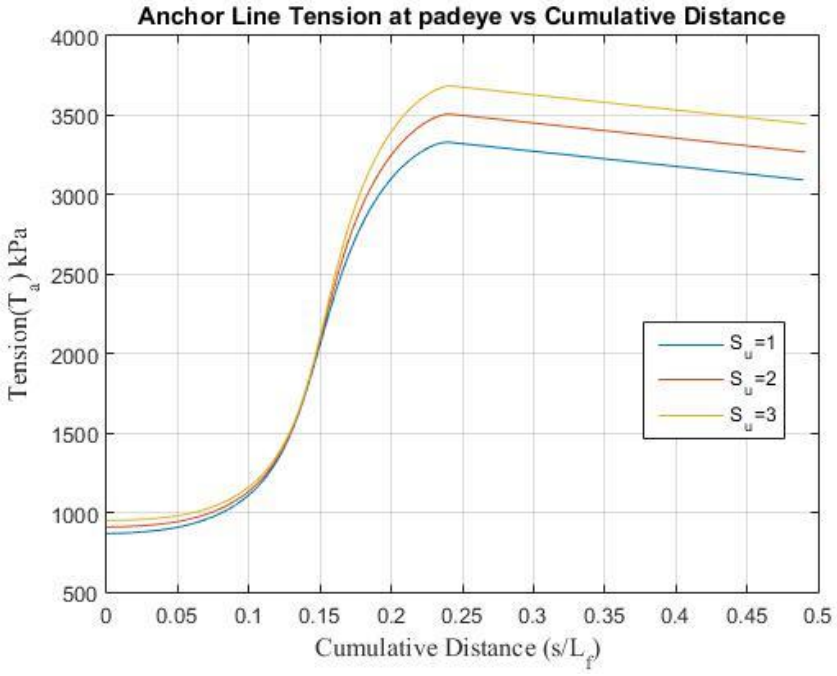

Figure 4.39 Effect of Shear Strength of Soil on the Tension Capacity

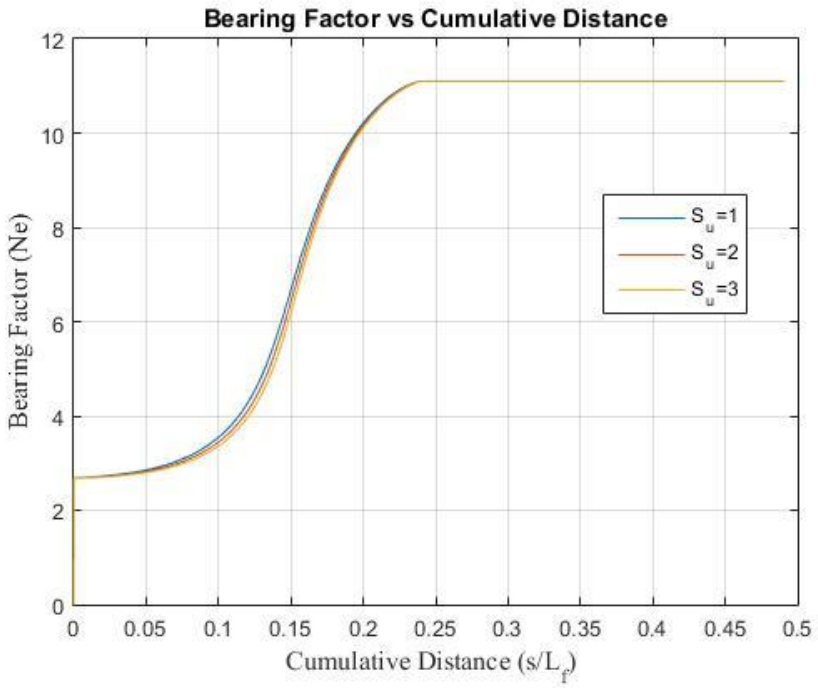

Figure 4.40 Effect of Shear Strength of Soil on the Bearing Factor

4.1.3.2.2 Strength Gradient (k)

The strength gradient of the soil also has negligible effect on the keying trajectory and the embedment loss during the keying process. The tension capacity of the anchor increases with increasing gradient as expected. The plots of keying trajectory, the embedment loss, tension at the padeye and bearing factor for different strength gradients are shown in figures 4.37-4.40.

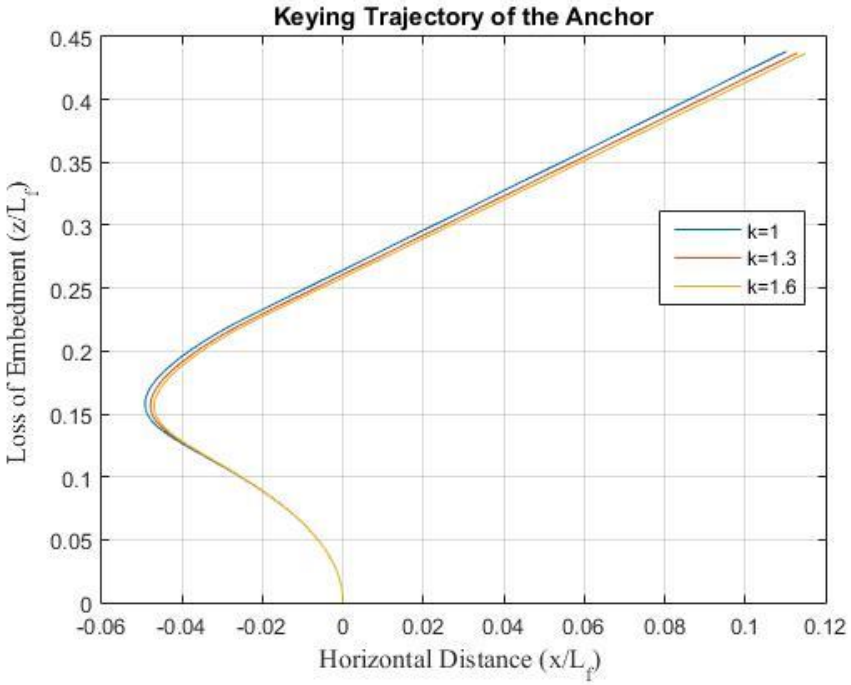

Figure 4.41 Effect of Strength Gradient of Soil on the Keying Trajectory

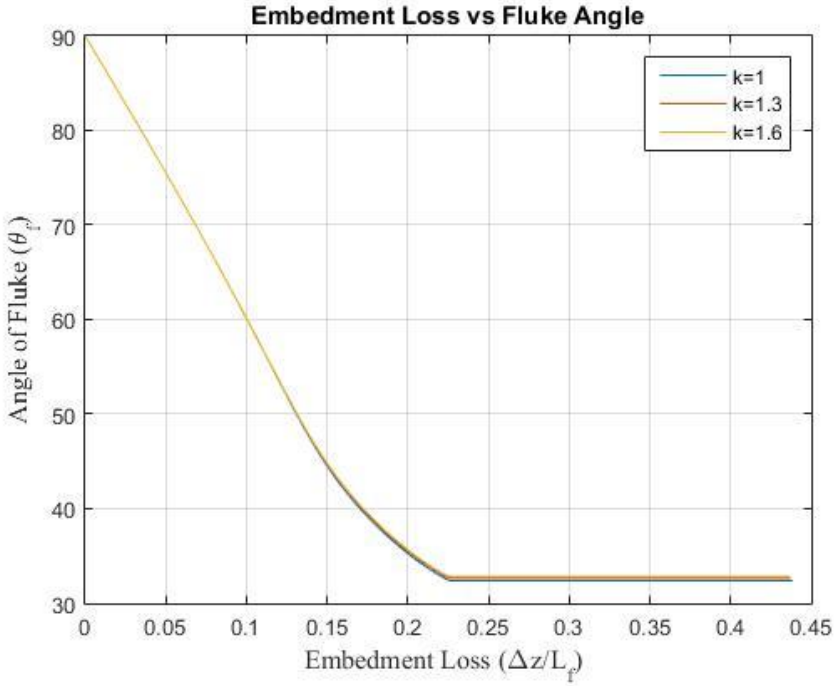

Figure 4.42 Effect of Strength Gradient of Soil on the Embedment Loss

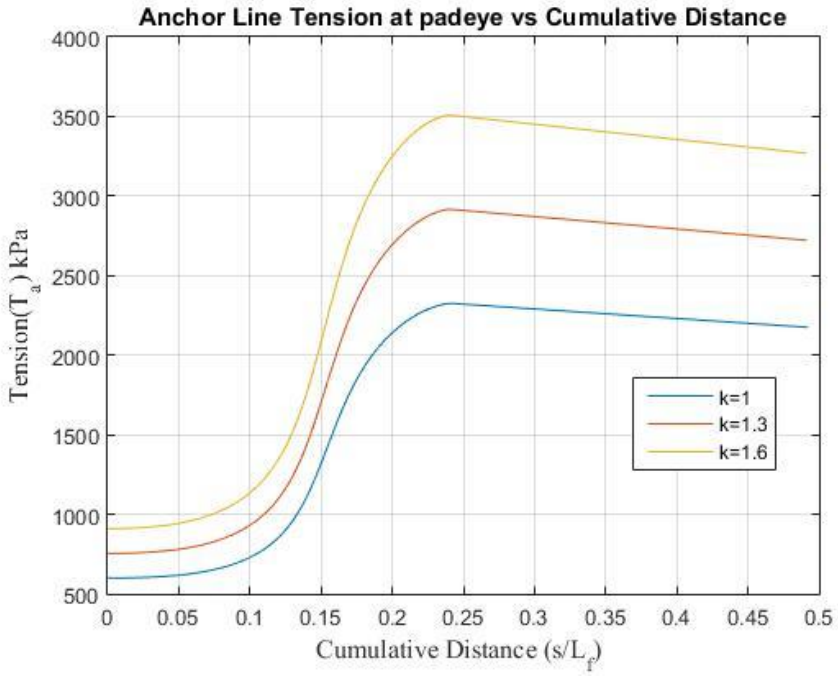

Figure 4.43 Effect of Strength Gradient of Soil on the Tension Capacity

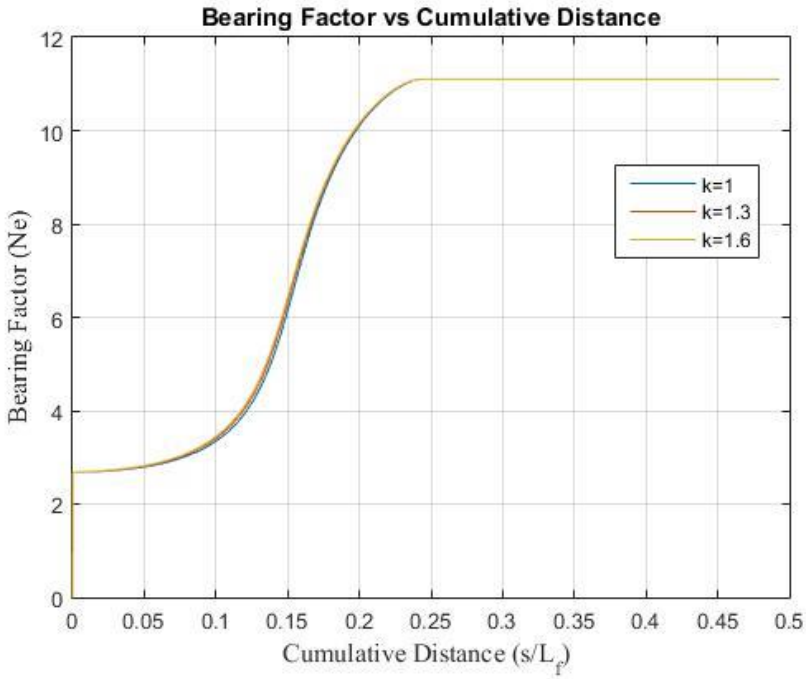

Figure 4.44 Effect of Strength Gradient of Soil on the Bearing Factor

4.1.4 Effect of Interaction Coefficients (m, n, p, and q)

The interaction coefficients are constant numbers that describes a yield surface for a particular thickness ratio and roughness factor. Finite Element methods are used to estimate the coefficients that best fit the yield surface. The existing list of interaction coefficients has been listed in Table 3.1. The table contains the interaction coefficients suggested by several studies over a wide variety of thickness, anchor geometry and roughness factor. In this study an attempt to study the effect these different coefficients on the keying process has been made. The model used for this study is a square anchor with the length of the fluke = 4m, the shank length = 2 m. The soil is assumed to have a maximum shear strength of 2 kPa and a strength gradient of 1.6 kPa/m. The anchor is tensioned at 45˚ on the surface of the water. The plots of keying trajectory, the embedment loss, tension at the padeye and bearing factor for interaction coefficients derived by different researches are shown in figures 4.41-4.44. The keying trajectory and the embedment loss varies over a wide range for different interaction coefficients. However they all follow a similar trend, the plate initially moves upward and backward and starts to move forward normally as it approaches perpendicularity with the pullout angle at the padeye. The interaction coefficients suggested by Cassidy et al, (2012) does not trace the yield surface thoroughly and provides values which completely covers the yield surface. Hence it generally overestimates the keying trajectory and the embedment loss during keying. The wide variety of results obtained by using different interaction coefficients can be attributed to the accuracy by which these terms were calculated and the thickness of the anchors used in different situations.

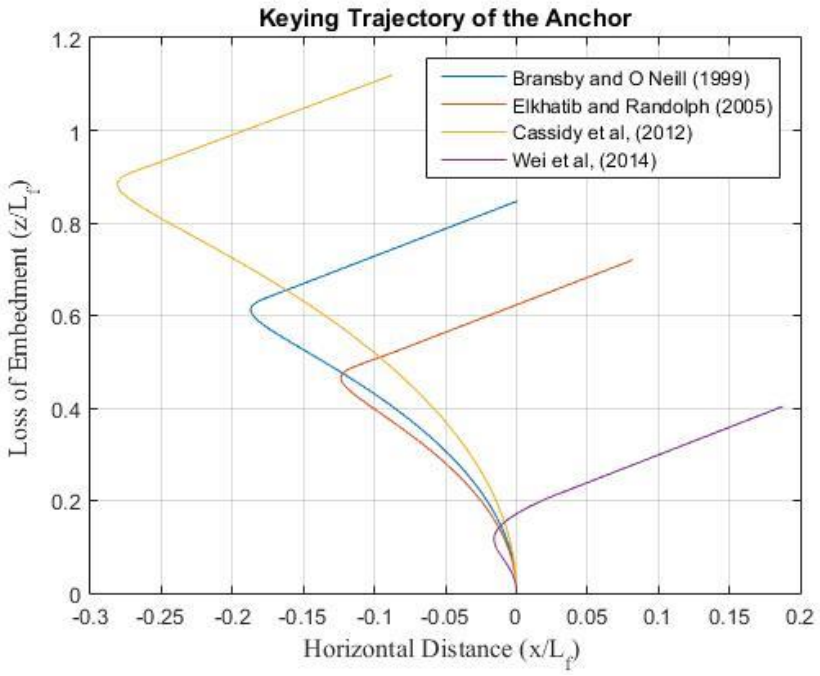

Figure 4.45 Effect of Interaction Coefficients on the Keying Trajectory

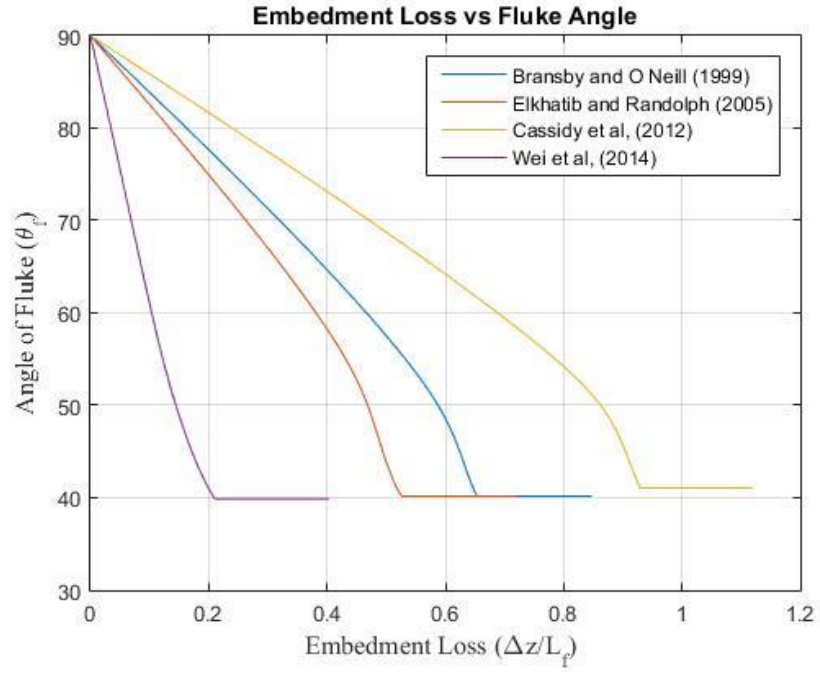

Figure 4.46 Effect of Interaction Coefficients on the Embedment Loss

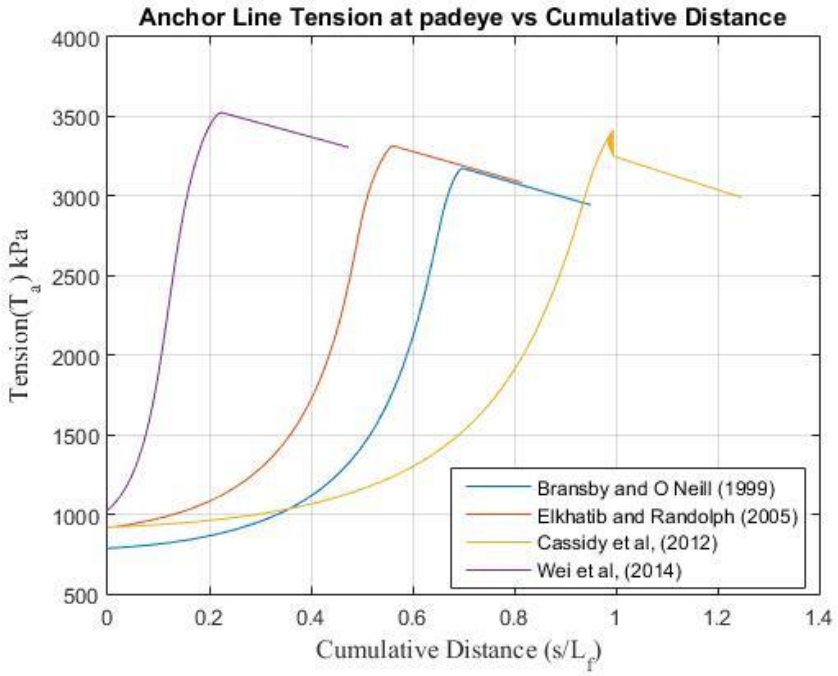

Figure 4.47 Effect of Interaction Coefficients on the Tension Capacity

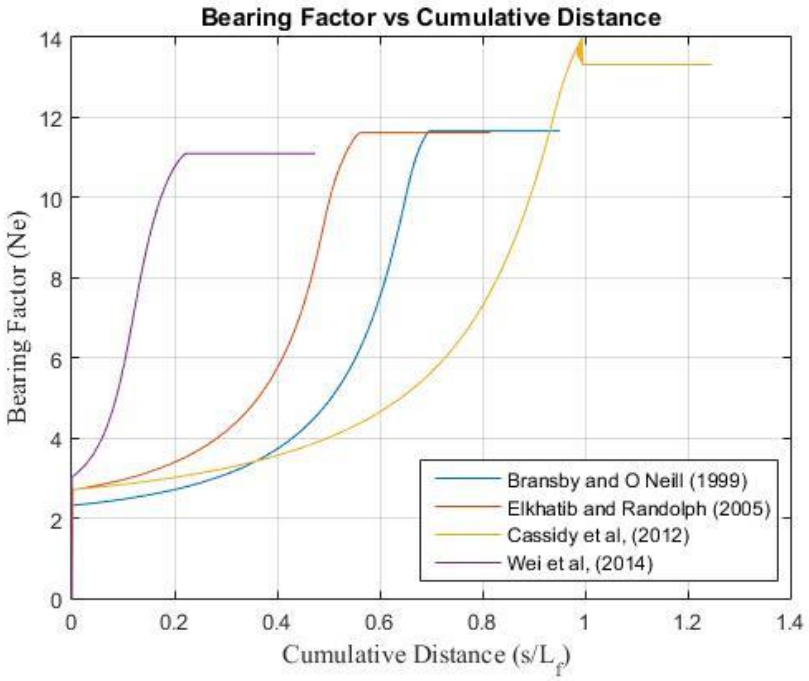

Figure 4.48 Effect of Interaction Coefficients on the Bearing Factor

CHAPTER V

VALIDATION OF THE PLASTIC MODEL

5.1 Validation of the Model

The results obtained from the current model have been compared to the available centrifuge test data and finite element (FE) modeling data. This will help ascertain the accuracy of the results obtained and also helps to modify and improve the model. Initially the prediction of the keying trajectory and the parametric study were performed based on the interaction parameters given by O'Neill et al, (1999). The results obtained by using these parameters were generally higher than the values presented by various centrifuge tests and FE modeling data. The disparity in the result was mainly due to the different anchor geometry used in these tests. In order to obtain higher accuracy, a wide range of interaction parameters derived by several researchers (Table 3.1) have been used to predict the keying process for different geometries.

5.2 Effect of the Shank Length / Padeye Eccentricity ($e_s = Ls/L_f$)

The centrifuge tests conducted by O'Laughlin et al, (2006) for a strip and square anchor for an anchor with fluke length (L_f) = 3m. The soil was found to have a uniform strength gradient of the soil was 0.7 kPa/m. The anchor was placed at a depth equal three times its fluke length and was loaded normally ($\theta_o = 90^\circ$). The test was conducted for different padeye eccentricities, which was achieved by attaching a shaft at the center of the anchor plate. The shaft behaved as the shank of the anchor to transfer the load from the mooring line to the anchor. The experimental results showed that the embedment loss

decreases considerably as the eccentricity of the pad eye is decreased. The current model predicted the rotational behaviour of the anchor with reasonable accuracy. The anchor is observed to stop rotating at a fluke angle of about 20˚ in the centrifuge test compared to completely horizontal orientation as predicted by the current model. Regardless of the different final orientations, the embedment loss predicted by the model for e_s = 0.5 and 1 agree well with the centrifuge tests. FE analyses on the effect of eccentricity have been performed by Song et al, (2010) and Wang et al, (2012) which follow similar trend observed by O'Laughlin et al, (2006). The FE analyses tried to replicate the centrifuge tests performed by O'Laughlin et al, (2006). However the anchor reaches a fully horizontal position in these studies unlike the experimental observation. The results from the current study shows excellent agreement with the results from the FE analysis by Song et al, (2010) and Wang et al, (2012) for e_s= 0.5 and it predicts slightly conservatively for e_s= 1. Wilde et al, (2001) have provided field data on the embedment loss for anchors with eccentricity e_s = 0.5. The observed the embedment loss to be in the range of 0.5-1.5 times the fluke length. The current model predicts the embedment loss to be around 0.52 times the fluke length which is within the lower limit of the field results produced by Wilde et al (2001).The results from the field tests were back calculated from the displacement of the mooring chain which will lead to certain additional displacement. But in general, the embedment loss predicted by the model is consistent with the centrifuge test, the FE analyses and the field results.

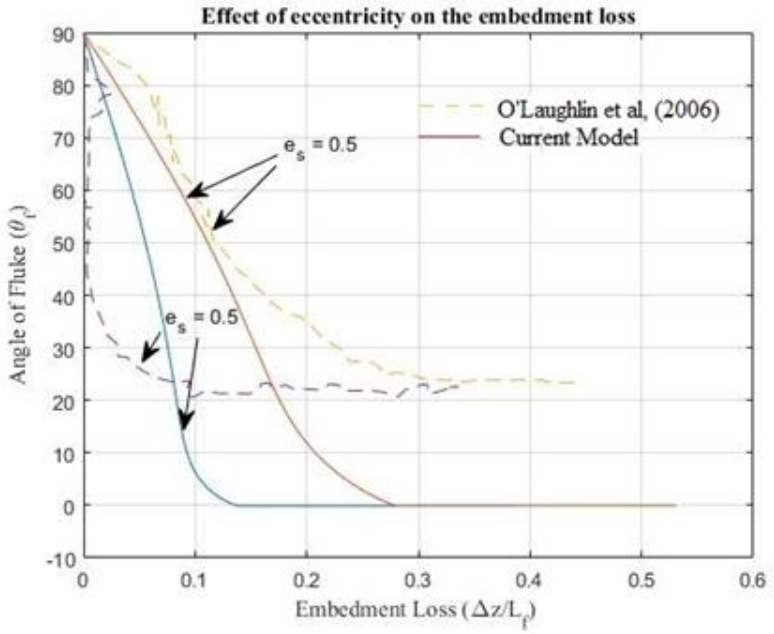

Figure 5.1 Comparison of the Effect of Eccentricity on Embedment Loss with Centrifuge Test by O'Laughlin et al (2006)

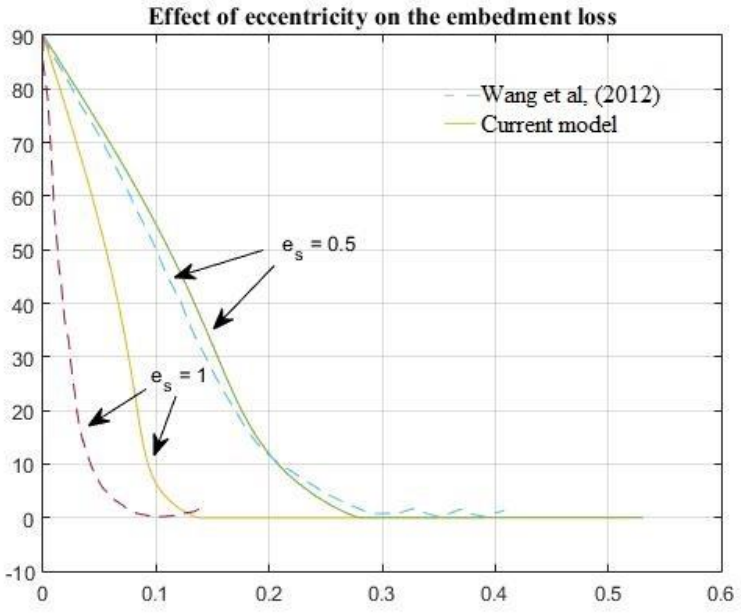

Figure 5.2 Comparison of the Effect of Eccentricity on Embedment Loss with the FE Analysis by Wang et al, (2012)

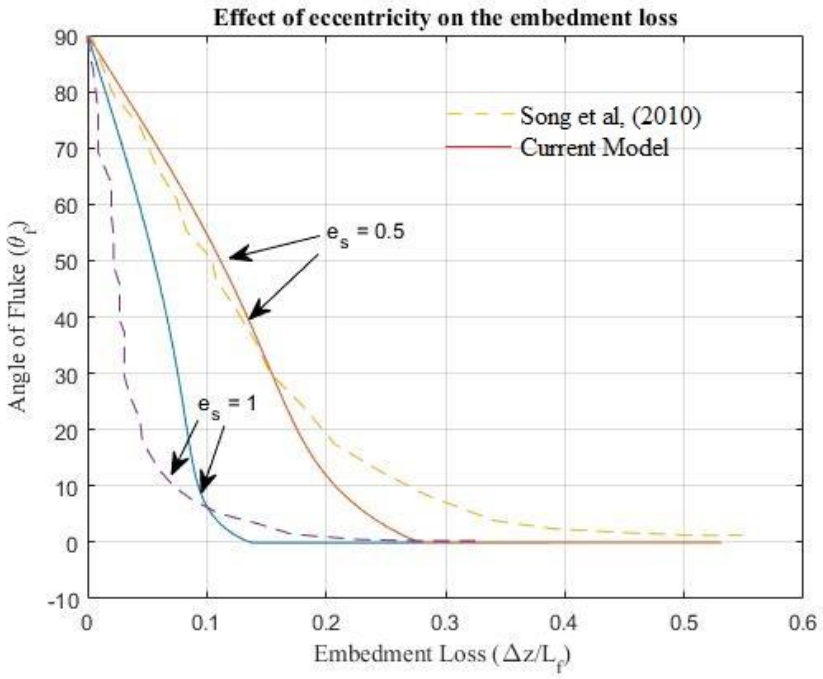

Figure 5.3 Comparison of the Effect of Eccentricity on Embedment Loss with the FE Analysis by Song et al, (2010)

5.3 Effect of Pullout Angle

Centrifuge tests have performed Gaudin et al, (2008) to study the effect of pullout angle on the keying process of the anchor. The tested a square anchor of fluke length (L_f) = 3m. They had a shaft at the center of the fluke which acted as the shank. The shank length varied from 0.75m to 3m in order to study the effect of shank length on the keying process. The test was performed in soil with constant strength gradient of 1 kPa/m. Similar to the centrifuge tests of O'Laughlin et al, (2006), the anchors did not reach completely horizontal orientation. The final plate inclination was about 10˚ to 15˚ off being normal to the loading angle. A plot of ultimate loss of embedment for padeye eccentricity (e_s) = 0.25 obtained from the centrifuge tests have been compared with the current model in figure

5.4. It is observed that the embedment loss increases as the pullout angle increases because the anchor will have to rotate more to reach the horizontal position. The embedment loss reported by Gaudin et al (2008) has two distinct patterns it remains relatively unchanged for pullout angles less than 45˚ and increases substantially for pullout angles greater than 45˚. But the embedment loss calculated by the current model has a linear relationship with the pullout angle. The model predicts higher values of embedment loss for pullout angles less than 45˚ and under predicts for pullout angles greater than 45˚. This can be due to the fact that the final orientations in the centrifuge tests were not horizontal and any small mistake in the test procedure will lead to a wide variety of variable results (Wang et al, (2012)).

FE analysis was performed for a square anchor with a fluke length of 4m and a padeye eccentricity of 0.625 times the fluke length for pullout angles θ_o =30˚, 45˚, 60˚ and 90˚ by the Song et al, (2010) to study the effect of pullout angle on the embedment loss. The current model has good agreement with the FE results presented by Song et al, (2010). The model slightly over predicts the embedment loss all the pullout angles, but follows the same trend as the FE result as seen in figure 5.5.

Wang et al, (2012) also performed FE analyses on the effect of pullout angle on the embedment loss during the keying process. A 3m square anchor with a padeye eccentricity (e_s) of 0.625 times fluke length was subjected to pullout angles of 30˚, 45˚, 60˚, 75˚ and 90˚. The anchor was assumed to be placed in a soil with uniform strength gradient of 0.7 kPa/m and moored by an anchor chain whose diameter 0.1 m and a frictional factor (μ) of 0.1. The embedment losses were normalized by the embedment loss

(Δz_{90}) at pullout angle = 90˚ and the pullout angles were normalized by 90˚. The same scenario was replicated in the current model and the embedment losses estimated were in good agreement with the FE results. Current model has predicted slightly conservative values than the FE result but in general follows the same pattern. Figure 5.6 shows the comparison of the results predicted by Wang et al (2012) and the current model.

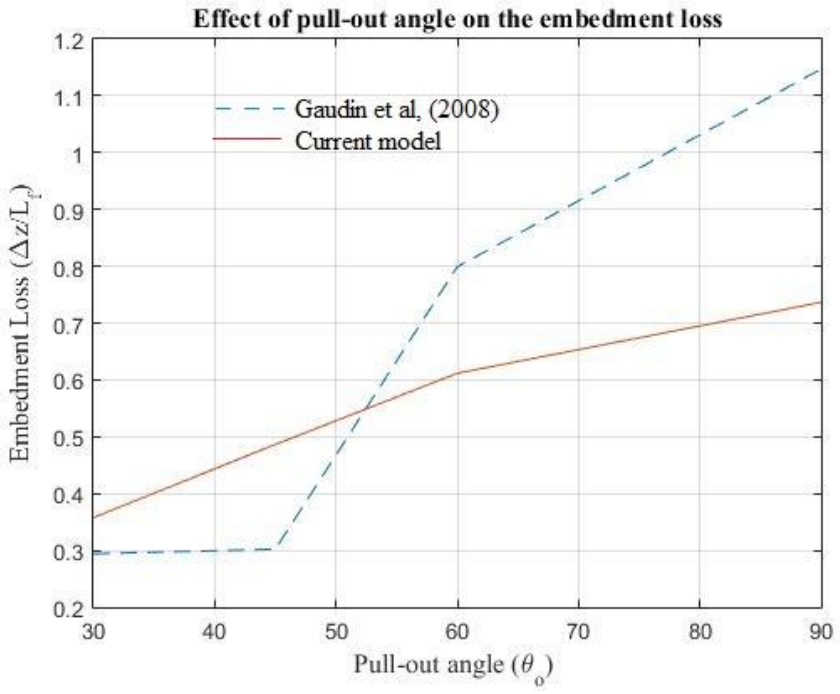

Figure 5.4 Comparison of the effect of pullout on Embedment Loss with the Centrifuge Test by Gaudin et al, (2008)

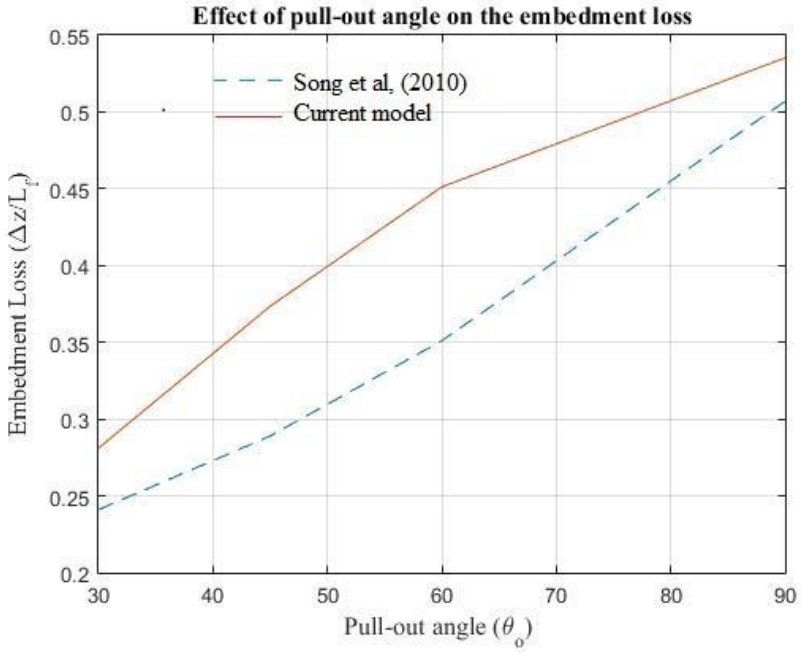

Figure 5.5 Comparison of the Effect of Pullout on Embedment Loss with the FE Analysis by Song et al, (2010)

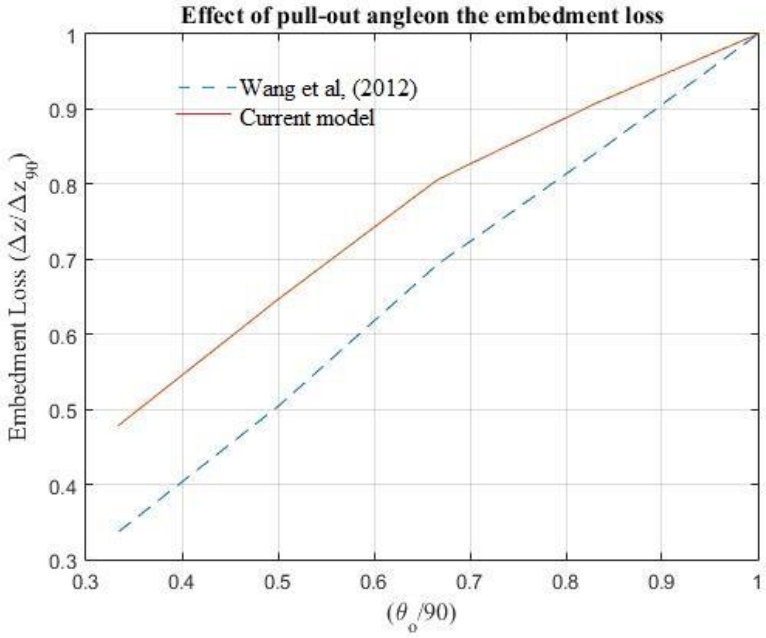

Figure 5.6 Comparison of the Effect of Pullout on Embedment Loss with the FE Analysis by Wang et al, (2012)

5.4 Performance of the Model

The current model shows good agreement with the available centrifuge tests and the FE models. The embedment loss predictions due to eccentricity have excellent agreement with the FE results and are consistent with the centrifuge test results. The model predicts the effect of pullout angle on the embedment loss slightly conservatively but is consistent with the results obtained from the centrifuge tests and the FE models. The current model can be used as a reference for future finite element studies as it predicts the performance of the anchors with good accuracy and requires very little computing power.

CHAPTER VI

CONCLUSION AND FURTHER RESEARCH

6.1 Summary

Direct embedment plate anchors can be installed by a variety of means, including suction (SEPLAs), pile-driving (PDPAs) and dynamically (DEPLAs). The cost effectiveness, ease of installation and the accuracy of the installation makes it an attractive choice for deep to ultra-deep waters. Direct embedment anchors must go through a process of keying when they are tensioned after installation. The keying process results in the loss of embedment which reduces the holding capacity of the plate anchors. A plasticity model was created to predict the keying process and to estimate the embedment loss for a plate anchor. The accuracy of the model was verified by comparing it to the existing centrifuge test data and FE modeling data. A parametric study was performed to analyze the effects of various normalized parameters on the keying process and the embedment loss.

6.2 Conclusions

1. During the process of keying, the anchor changes its orientation of being perpendicular to the horizontal to an orientation where it is normal to the angle of load application.
2. The process of keying can be broadly classified into two movements. The anchor initially rotates and moves tangentially to the loading direction. This constitutes the backward and upward and backward. As the anchor rotates and approaches normality the rotation and the tangential movement reduces and the anchor starts

to move in a direction normal to loading angle. This constitutes the upward and forward movement.

3. When the anchor is normal to the loading direction, the anchor purely translates in the normal direction without any rotation or tangential movement.
4. The embedment loss calculated by the model was compared with the centrifuge test data and FE data. The model was found have excellent agreement with the FE results and was consistent with the centrifuge test data. The model provides slightly conservative results over a wide range of parameters.
5. The parametric study helped in understanding the effect of various parameters on the keying trajectory, holding capacity and the embedment loss of the anchor.
6. Anchor geometry (L_f, w_f, t_f): The embedment loss decreases with decreasing lower aspect ratio. The anchor thickness also has a significant impact on the embedment loss. Increasing the thickness of the anchor can lead to substantial decrease in the embedment loss. So it is advisable to use anchors with low aspect ratio and high thickness to reduce the embedment loss.
7. Padeye Eccentricity ($e_s = L_s/L_f$): The embedment loss is remarkably high for lower eccentricity ($e_s<0.5$) and decreases drastically as the eccentricity is increases. The change in embedment loss starts to reduce for $e_s>0.5$ and becomes practically insignificant for $e_s>0.5$. It is advisable to use anchor with $e_s\geq1$ to have minimal embedment loss. It is also necessary to make sure that eccentricity does not fall below 0.5 ($e_s<0.5$) in order to prevent excessive embedment loss.

8. Pullout angle (θ_0): The embedment loss increases substantially with increasing pullout angle. If the pullout angle is increased, the anchor will have to rotate more to attain normality. So a low pullout angle will substantially decrease the embedment loss. It is observed that pullout angles lower than 30˚ do not involve backward movement in the keying trajectory. At these shallow pullout angles, the trajectory is dominated by tangential upward movement followed by normal upward movement. It is also observed that the padeye angle θ_a is generally higher than the pullout angle on the surface of the water (θ_o). It is advisable to load the anchor at a low pullout angle ($\theta_0 \leq 45^\circ$) to minimize the embedment loss.

9. Anchor Line: The effect of a chain and wire anchors were studied and it was found that the chain anchor has a slightly higher embedment loss compared to the wire anchor. So it is advisable to use a wire anchor line over a chain to minimize the embedment loss

10. Strength of the soil: The effect of maximum shear strength (S_u) of the soil and the strength gradient (k) were found to have minimal impact on the keying trajectory and the embedment loss of the anchor. However, the tension capacity of the soil increases with higher soil strength.

11. Soil sensitivity (S_t): Soil sensitivity is the inverse of the contact roughness between the soil and the anchor. As the sensitivity increases, the roughness of contact decreases leading to higher embedment loss. It was observed that soil sensitivity had a marked effect on the embedment loss of the anchor. The embedment loss increased dramatically with higher sensitivity. So it is necessary to make sure that

contact between the soil and the anchor plate is rough to decrease the loss of embedment.

6.3 Further Research

Although this study helps to understand the keying process of direct embedment plate anchors and the parameters affecting the keying trajectory, there is scope for future research in certain aspects of the model. The following research can help better understand the keying process

1. Incorporate the effect of flap in the model to understand the effects of flap on the keying process.
2. Finite Element modeling should be performed to better understand the effects of different parameters on the keying process and also helps validate the current model.
3. The limited availability of the interaction parameters hinders the accurate parametric study of thickness of the fluke and the sensitivity of soil on the keying process. Developing interaction coefficients as a function of thickness of the fluke and sensitivity of the soil will greatly help in solving this problem and also helps to validate the behavior observed in the current model.
4. Additional laboratory and field-scale model tests will provide a database of trajectory and load capacity measurements for a more complete validation of the plasticity-based keying model.

REFERENCES

(NCEL), N. C. (1985). Handbook for Marine Geotechnical Engineering. Hueneme: U.S. Naval Civil Engineering Laboratory.

Andersen, K. H., Murff, J. D., Randolph, M. R., Clukey, E. C., Erbrich, C., Jostad, H. P., et al. (2005). Suction Anchor for Deepwater Applications. Balkema, Perth, Australia: Proc. Int. Symp. on Frontiers in Offshore Geotechnics, ISFOG05.

Andersen, K. H., Murff, J. D., and Randolph, M. R. (2003). Deepwater Anchor Design Practice-Vertically Loaded Drag Anchors. Phase II Report to API/Deepstar, Norwegian Geotechnical Institute, Norway, Offshore Technology Research Center, USA and Centre for Offshore Foundation Systems, Australia.

Aubeny, C. P., Murff, D. J., & Roesset, J. M. (2001). Geotechnical Issues in Deep and Ultra Deep Waters. Int. J. Geomech., 10.1061/(ASCE)1532-3641(2001)1:2(225), (pp. 225-247).

Aubeny, C. P., Kim, B. M., and Murff, J. D. (2005). Proposed Upper Bound Analysis for Drag Embedment Anchors in Soft Clay. Frontiers in Offshore Geotechnics. London, Taylor and Francis Group, (pp. 179-183).

Aubeny, C. P., Murff, J. D., and Kim, B. M. (2008). Prediction of Anchor Trajectory During Drag Embedment in Soft Clay. Int. J. Offshore Polar Eng., 18(4), (pp. 314-319).

Aubeny, C., & Chi, C. M. (2010a). Mechanics of Drag Embedment Anchor in a Soft Seabed. Journal of Geotechnical and Geoenvironmental Engineering, Vol. 136(1), (pp. 57-68).

Bransby, M. F., & O'Neill, M. (1999). Drag Anchor Fluke Soil Interaction in Clays. Proc., 7th Int. Symp. on Numerical Models in Geomechanics, (pp. 489-494). Rotterdam.

Bransby, M. F., & Randolph, M. F. (1998). Combined Loading Of Skirted Foundations. Geotechnique, Vol. 48(5), (pp. 637-655).

Brown, P. R., Wong, P. C., & Audibert, J. M. (2010). SEPLA Keying Prediction Method Based on Full Scale Offshore Tests. Frontiers in Offshore Geotechnics (pp. 717-722). Perth: Taylor & Francis Group.

Cassidy, M. J., Gaudin, C., Randolph, M. F., Wong, P. C., Wang, D., & Tian, Y. (2012). A Plasticity Model to Assess the Keying of Plateanchors. Geotechnique, Vol. 62(9), (pp. 825–836).

Chen, W.-F. (2013). Limit Analysis and Soil Plasticity. Elsevier.

Chi, C. M. (2010). Plastic Limit Analysis of Offshore Foundation and Anchor. College Station: Texas A&M University .

Dove, P., Treu, H., & Wilde, B. (1998). Suction Embedded Plate Anchor (SEPLA): A New Anchoring Solution for Ultra-Deepwater Mooring. Proc. DOT Conf. New Orleans.

Elkhatib, S. (2006). The Behaviour of Drag-In Plate Anchors in Soft Cohesive Soils. Perth: Univ. of Western Australia.

Elkhatib, S., & Randolph, M. (2005). The Effect of Interface Friction on the Performance of Drag-In Plate Anchors. (pp. 171–177).

Forrest, J., Taylor, R., & Bowman, L. (1995). Design Guide for Pile-Driven Plate Anchors. Port Hueneme, California 93043-4328: Naval Facilities Engineering Service Center.

Gaudin, C., O'Loughlin, C. D., Randolph, M. F., & Lowmass, A. C. (2006). Influence of the Installation Process on the Performance of Suction Embedded Plate Anchors. Geotechnique, Vol. 56(6) , (pp. 381–391).

Gaudin, C., Tham, K. H., & Ouahsine, S. (2008). Plate Anchor Failure Mechanism During Keying Process. Proc., 18th Int. Offshore and Polar Eng. Conf.2. Cupertino: Int. Society of Offshore and Polar Engineers (ISOPE).

Jackups - . (2016). Petrowiki.org. Retrieved 29 August 2016, from http://petrowiki.org/Jackups

Maersk Drilling (2016). Retrieved 29 August 2016, from http://www.maerskdrilling.com/en/drilling-rigs/semi-submersibles

Murff. (2006). Plastic Limit Analysis in Geotechnical Engineering Class Notes. College Station: Department of Civil Engineering, Texas A&M University.

Murff, J. D. (1994). Limit Analysis of Multi-Footing Foundation Systems. Proc., 8th Int. Conf. on Computer Methods and Advances in Geomechanics, 1. Rotterdam.

Neubecker, S. R., & Randolph, M. F. (1995). Profile and Frictional Capacity of Embedded Anchor Chain. Journal of Geotechnical Engineering Division, ASCE, Vol. 121, (pp. 787-803).

Neubecker, S. R., & Randolph, M. F. (1995). Profile and Frictional Capacity of Embedded Anchor Chains. Journal of Geotechnical Engineering, (pp. 797-803).

O'Loughlin, C. D., Lowmass, A. C., Gaudin, C., & Randolph, M. F. (2006). Physical Modelling to Assess Keying Characteristics of Plate Anchors.

O'Neill, M. P., Bransby, M. F., & Randolph, M. F. Drag Anchor Fluke-Soil Interaction in Clay. Canadian Geotechnical Journal, Vol. 40, (pp. 78-94).

Offshore Moorings www.dredgingengineering.com/moorings/overview. (08/10/2016) Retrieved Sptember 04, 2016, from Offshore Moorings: http://www.dredgingengineering.com/moorings/overview/Tool%20Ibb.html

O'Loughlin, C. D., Blake, A., Richardson, M. D., Randolph, M. F., & Gaudin, C. (2014). Installation and Capacity of Dynamically Embedded Plate Anchors as Assessed Through Centrifuge Tests. Perth: University of Western Australia.

Ruinen, R. (2000). The Use Of Drag Embedment Anchors and Vertical Loaded Anchors (VLAs) for Deepwater Moorings. Continuous Advances in Mooring & Anchorings , (pp. 1-19).

RSS Content | Chevron. (2016). Investor.chevron.com. Retrieved 29 August 2016, from http://investor.chevron.com/phoenix.zhtml?c=130102&p=RssLanding&cat=news&id=2003528

Song, Z., Hu, Y., & Randolph, M. F. (2005). Pullout Behaviour of Inclined Plate Anchors in Uniform Clay. The 11th International Conference of IACMAG, (pp. 715-722).

Song, Z., Hu, Y., Wang, D., & O'Loughlin, C. D. (2006). Pullout Capacity and Rotational Behaviour of Square Anchors. Proceedings of 6th International Conference on Physical Modelling in Geomechanics, Vol. 1, (pp. 325-1).

Song, Z., Hu, Y., O'Loughlin, C., & Randolph, M. F. (2009). Loss in Anchor Embedment During Plate Anchor Keying in Clay. Journal of Geotechnical and Geoenvironmental Engineering , (pp. 1475-1485).

Wang, D., Hu, Y., & Randolph, M. F. (2011). Keying of Rectangular Plate Anchors in Normally Consolidated Clays. Journal Of Geotechnical And Geoenvironmental Engineering, Vol. 137(12), (pp. 1244-1253).

Wei, Q., Cassidy, M. J., Tian, Y., & Gaudin, a. C. (2014). Incorporating Shank Resistance into Prediction of the Keying Behavior of Suction Embedded Plate Anchors. Journal of Geotechnical and Geoenvironmental Engineering, (ISSN 1090-0241/04014080), (pp. 1-13).

Wilde, B., Treu, H., & Fulton, T. (2001). Field Testing of Suction Embedded Plate Anchors. Proc., 11th Int. Offshore and Polar Eng. Conf.,. Cupertino: ISOPE.

Yang, M., Aubeny, C. P., & Murff, J. D. (2012). Behavior of Suction Embedded Plate Anchors during Keying Process. Journal of Geotechnical and Geoenvironmental Engineering, ASCE , (pp. 174-185).